

## Radiative Transfer in Moving Atmospheres

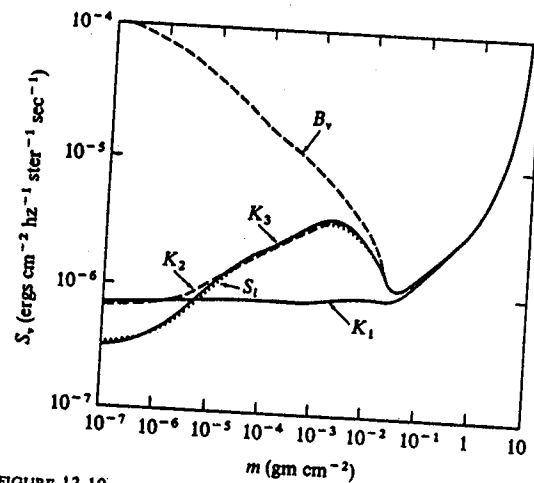


FIGURE 13-10

Depth-variation of K-line source function (for a five-level atom) and Planck function in model 1. Dashed curve: Planck function  $B_r$ . Dotted curve: complete-redistribution source-function  $S_i$  (see also Figure 12-2). The other curves show the partial-redistribution source-functions at line-center ( $K_3$ ), the emission peak ( $K_2$ ), and the profile minimum outside the peak ( $K_1$ ). Abscissa: column density  $\text{gm/cm}^2$ . From (570), by permission.

deeper in, near the minimum. This explains both the rapid increase in  $\Delta\lambda(K_1)$  as a function of  $\mu$ , and the near-constancy of  $I_K$ , predicted by CR. In contrast, the PR source function at line-center ( $K_3$ ) lies above the CR value (as a result of photon trapping as discussed previously). But at  $K_1$  the source function has an essentially coherent-scattering character, is decoupled from other frequencies, and shows a monotonic decrease outward in the atmosphere [similar results were obtained in (642)]. For this behavior of  $S_i$ , changing the point of observation from center to limb merely samples  $S_i(K_1)$  higher in the atmosphere, where it has (for PR) a lower value, and hence produces a decrease in  $I_K$ , as desired, at about the same  $\Delta\lambda$ . In short, taking partial redistribution into account yields a substantial improvement in the degree of agreement between theory and observation for the solar Ca II H- and K-lines. Similar calculations, yielding similar results, have also been made for the Mg II  $h$  and  $k$  ( $3s-3p$ ) lines for the solar atmosphere (458; 59) and for solar-type stars (455). It now appears that it is mandatory to account for partial redistribution effects in the interpretation of strong chromospheric resonance lines with strong radiation-damping wings, and further efforts in this direction will undoubtedly be amply rewarded.

The existence of macroscopic motions (i.e., nonthermal velocities that are coherent over distances much larger than a particle mean-free-path) in stellar atmospheres is well-documented by a wealth of observational evidence. These motions appear to be present on all scales, from "eddies" whose sizes are small compared to a photon mean-free-path, up to expansion of the atmosphere as a whole. Although velocity fields have but little effect on radiative transfer in the continuum, they strongly influence line-formation because even a small (Doppler) frequency shift of a line produces a major change in its absorptivity as seen by a stationary observer.

In the analysis of spectra of supergiants, Struve and Elvey (617) discovered that the Doppler widths inferred from the position of the flat part of the curve of growth (cf. §§10-3 and 10-4) were far in excess of the thermal value. They attributed this broadening to nonthermal "turbulent" velocities, presumed to have a Gaussian distribution. The geometric scale of these motions (which are called "microturbulence") is supposed to be so small that they act as additional line-broadening agents, and thus enhance the line-strength. The inferred velocities often approach or exceed the speed of sound in the material, and it is clear that astrophysical "microturbulent" velocities are not to be identified

with turbulence in the strict fluid-dynamical sense, but rather with unresolved motions.

The picture is clarified when we examine the solar spectrum. From curves of growth, or from spectra of low spatial, spectral, and temporal resolution, one again infers a significant microturbulent velocity. But high-resolution spectra have a characteristic "wiggly-line" appearance [see Figure III-2 of (20) for an excellent example], showing distinct Doppler shifts and asymmetries that fluctuate rapidly along the length of the slit, and in time. Probably a large part, or even all, of the velocity field is composed of *wave motions* of various types, scales, and periods, which (when superposed) give rise to a pattern that appears chaotic and "turbulent". However, the diagnostics are still in a primitive state, and the precise nature of the velocity field is not at all well known.

Evidence for velocity patterns on a *large scale* ("macroturbulence") was provided by Struve's observation (616) that the *widths of line profiles* in certain stars exceeded the Doppler widths obtained from the curve of growth of their spectra; here the line strength is unchanged, and one envisions areas on the stellar surface so large as to be practically independent "atmospheres" moving systematically along the line of sight. A discussion of the observations, with numerous references, can be found in (261, Chap. 8). Further, periodic Doppler shifts of the lines in some stellar spectra reveal that they are from pulsating stars. Beyond this, objects such as the WR stars, P-Cygni stars, and early-type supergiants all show characteristic line profiles, with blue-shifted absorption components and red-shifted emission components, indicative of large-scale expansion.

It is clear that a characterization of stellar velocity fields by the two extremes of "micro"- and "macro"-turbulence is an oversimplification and, in the end, we wish to know *distribution functions* describing the amplitudes and scales of the velocity patterns. Further, one would like to relate observed parameters to more fundamental quantities such as the velocities of convective motions. Finally, a truly consistent theory of stellar atmospheres will require a *dynamical* theory of the interaction of material velocities, the thermodynamic state of the matter, and the radiation field; only then will we be able fully to understand stellar chromospheres and coronae.

At the present time, however, we are far from having such a complete theoretical structure. In this chapter we shall focus almost entirely on the "kinematics" of radiative transfer in moving media; i.e., given the velocity field and the model atmosphere, compute the emergent spectrum. A variety of techniques exist to attack the problem just posed. *Observer's-frame methods* can handle complicated velocity fields and multidimensional structures (although we shall confine attention to one-dimensional problems only), but are generally restricted to velocities of the order of a few Doppler widths, and hence are not well suited to handle rapid atmospheric expansion. *Sobolev's method*, on the other hand, provides an approximate solution in the case of

rapid flow with large velocity gradients. *Comoving-frame methods* span the two extremes and provide general solutions applicable in both limits. Special techniques have been developed to treat *random* or *stochastic velocity fields*.

## 14-1 The Transfer Equation in the Observer's Frame

### FORMULATION AND SOLUTION OF THE TRANSFER EQUATION

When the material in the atmosphere moves with velocity  $\mathbf{v}(\mathbf{r})$  relative to an external observer at rest, there is a *Doppler shift* of photon frequencies between the observer's frame, and the frame of the atoms of which the material is composed. If the frequency in the observer's frame is  $v$ , then in the atom's frame the frequency at which a photon traveling in direction  $\mathbf{n}$  was emitted, or can be absorbed, is

$$v' = v - v_0(\mathbf{n} \cdot \mathbf{v}/c) \quad (14-1)$$

Thus, the opacity and emissivity of the material, as seen by a stationary observer, become *angle-dependent*. The transfer equations for a time-independent moving medium in planar geometry is then

$$\mu[\partial I(z, \mu, v)/\partial z] = \eta(z, \mu, v) - \chi(z, \mu, v)I(z, \mu, v) \quad (14-2)$$

It is convenient to measure frequency displacements from line center in units of a fiducial Doppler width  $\Delta v_D^* \equiv v_0 v_{th}^*/c$ , where  $v_{th}^*$  is a thermal velocity parameter, and to measure velocities in the same units,  $V = v/v_{th}^*$ . Then the transformation between observer's frame and atom's frame frequencies is

$$x' = x - \mu V \quad (14-3)$$

where  $x \equiv (v - v_0)/\Delta v_D^*$  and  $x'$  is defined similarly. The effects of Doppler shifts are inconsequential for continuum terms, which do not vary much over the frequency range implied by velocity shifts, so we account only for changes in line terms and write

$$\chi(z, \mu, x) = \chi_c(z) + \chi_l(z)\phi(z, \mu, x) \quad (14-4)$$

and

$$\eta(z, \mu, x) = \eta_c(z) + \eta_l(z)\phi(z, \mu, x) \quad (14-5)$$

where the normalized line-profile is defined by

$$\phi(z, \mu, x) \equiv \phi(z; x - \mu V) \quad (14-6)$$

For example, for a Doppler profile,

$$\phi(z, \mu, x) = \pi^{-\frac{1}{2}} \delta^{-1}(z) \exp\{-[x - \mu V(z)]^2/\delta^2(z)\} \quad (14-7)$$

where  $\delta$  measures the local Doppler width in units of the fiducial value; i.e.,  $\delta(z) \equiv \Delta v_D(z)/\Delta v_D^*$ . We now define line and continuum source functions  $S_l(z) \equiv \eta_l(z)/\chi_l(z)$ , and  $S_c(z) \equiv \eta_c(z)/\chi_c(z)$ ; a total source function

$$S(z, \mu, x) \equiv [\phi(z, \mu, x)S_l(z) + r(z)S_c(z)]/[\phi(z, \mu, x) + r(z)] \quad (14-8)$$

where  $r(z) \equiv \chi_c(z)/\chi_l(z)$ ; and an optical depth scale measure along a ray specified by  $\mu$ ,

$$\tau(z, \mu, x) \equiv \mu^{-1} \int_z^{z_{\max}} \chi(z, \mu, x) dz \quad (14-9)$$

where  $z_{\max}$  denotes the upper surface of the atmosphere. Then the transfer equation becomes

$$[\partial I(z, \mu, x)/\partial \tau(z, \mu, x)] = I(z, \mu, x) - S(z, \mu, x) \quad (14-10)$$

The formal solution of equation (14-10) can be written immediately as

$$\begin{aligned} I(z_{\max}, \mu, x) &= I(0, \mu, x)e^{-\tau(0, \mu, x)} + \int_0^{\tau(0, \mu, x)} S(z, \mu, x)e^{-\tau(z, \mu, x)} d\tau(z, \mu, x) \\ &= I(0, \mu, x)e^{-\tau(0, \mu, x)} \\ &\quad + \int_0^{z_{\max}} \mu^{-1} [\phi(z, \mu, x)S_l(z) + r(z)S_c(z)] e^{-\tau(z, \mu, x)} \chi_l(z) dz \end{aligned} \quad (14-11)$$

from which we can compute the emergent intensity for given source functions. (For example in LTE,  $S_c = S_l = B$ ; or we might use the values of  $S_l$  found for the line in a static atmosphere, an approximation that often is surprisingly accurate as we shall see below.) In equation (14-11) we have taken the atmosphere to be a finite slab with intensity incident at  $z = 0$ ; for a semi-infinite atmosphere, we set  $\tau(0, \mu, x) = \infty$  and omit the term in  $I(0, \mu, x)$ . The formal solution allows a direct evaluation of the effects of velocity fields on profiles by accounting for the velocity-induced shifts in the opacity and emissivity of the material.

The line source function will, in general, contain a scattering term, and therefore depend on the radiation field; thus the source function can be strongly affected by material motions. For example, an expansion at the upper surface of an atmosphere can displace a line away from a dark absorption feature, at the rest position, into the bright nearby continuum, thus raising  $J$  (and  $S_l$ ) dramatically. If we assume that photons scattered by the line are completely redistributed, then the source function for a two-level atom becomes

$$S_l(z) = \frac{1}{2}(1 - \varepsilon) \int_{-\infty}^{\infty} dx \int_{-1}^1 d\mu I(z, \mu, x) \phi(z, \mu, x) + \varepsilon B(z) \quad (14-12)$$

where  $\varepsilon$  is the usual thermalization parameter. Note that in the scattering integral we can no longer replace  $I$  with  $J$  because  $\phi$  is angle-dependent; note also that the intensity can no longer be assumed to be symmetric around the line center, hence the full profile must be considered. The approximation of complete redistribution becomes questionable for moving media, as the conditions that help validate it in static media no longer occur; a good discussion of this point is contained in (273, 87) (this is a superb paper that is highly recommended to the reader). Recently some work has been devoted to the problem of partial redistribution in moving atmospheres; it has been shown that to treat the problem in the observer's frame, the full angle-frequency dependent redistribution function must be employed. In contrast, in a comoving-frame method (see §14-3), one can employ static redistribution functions in the fluid frame, and angle-averaging again yields accurate results.

Accurate calculation of the scattering integral in equation (14-12) with a quadrature sum poses a fundamental difficulty in an observer-frame solution for two reasons. (1) The line-profile  $\phi(x - \mu V)$  is clearly shifted by an amount  $2V$  in frequency as  $\mu$  varies from  $-1$  to  $1$ . Thus, in the frequency quadrature, an amount equal to twice the maximum macroscopic flow velocity must be added to the bandwidth required to describe the static line-profile. This requirement is not severe in studies of, say, wave motions in the solar atmosphere, but becomes prohibitive for atmospheres in supersonic expansion where  $v/c \approx 0.01$ , or  $2(v_0 v/c)/\Delta v_D^* \approx 200$ . (2) The angle-quadrature scheme must employ a large number of angles. Because the argument of the profile function is  $(x - \mu V)$ , there is an inextricable coupling between the angular and frequency variations of the intensity. Thus if some maximum frequency increment  $\Delta x_{\max} (\approx \frac{1}{2})$  is required to obtain sufficient precision in the frequency quadrature, the maximum tolerable angle increment will be  $\Delta \mu_{\max} = \Delta x_{\max}/V$ , which is quite stringent! These difficulties are ameliorated by transforming to the comoving frame.

Equation (14-10) may be cast into second-order form. If the line profile is symmetric about line center, then  $\phi(-x + \mu V) = \phi(x - \mu V)$ , which suggests that we group the two pencils  $I(z, \mu, x)$  and  $I(z, -\mu, -x)$  together, for  $d\tau(z, \mu, x) = d\tau(z, -\mu, -x)$  and  $S(z, \mu, x) = S(z, -\mu, -x)$ . Thus, defining

$$u(z, \mu, x) \equiv \frac{1}{2} [I(z, \mu, x) + I(z, -\mu, -x)] \quad (14-13)$$

and  $v(z, \mu, x) \equiv \frac{1}{2} [I(z, \mu, x) - I(z, -\mu, -x)]$  (14-14)

we obtain  $[\partial^2 u(z, \mu, x)/\partial \tau(z, \mu, x)^2] = u(z, \mu, x) - S(z, \mu, x)$  (14-15)

At the upper boundary there is no incoming radiation, hence

$$[\partial u(z, \mu, x)/\partial \tau(z, \mu, x)]_{z_{\max}} = u(z_{\max}, \mu, x) \quad (14-16)$$

At the lower boundary we assume either that the incident radiation is specified, in which case

$$[\partial u(z, \mu, x)/\partial r(z, \mu, x)]_{z=0} = I(0, \mu, x) - u(0, \mu, x) \quad (14-17)$$

or that, in a semi-infinite atmosphere, the lower boundary is chosen to be so deep that the *diffusion approximation* is valid [which demands that the velocity gradient be small enough that  $\chi^{-1}(dV/dz) \ll 1$ ; i.e., there is a negligible change in the velocity over a photon mean-free-path], in which case

$$\frac{\partial u(z, \mu, x)}{\partial r(z, \mu, x)} \Big|_{z=0} = \left[ \frac{\mu}{\chi(z, \mu, x)} \left( \frac{\partial B_v}{\partial T} \right) \frac{dT}{dz} \right]_{z=c} \quad (14-18)$$

As in the static case, we introduce a discrete depth-mesh  $\{z_d\}$ , angle-mesh  $\{\mu_m\}$ , and frequency-mesh  $\{x_n\}$ , and combine angles and frequencies into a single quadrature set  $\{\mu_l, x_l\} \equiv (\mu_m, x_n)$  where  $l = m + (n - 1) M$ ; the angle-points are distributed on the interval  $[0, 1]$ , while frequencies must now span a range  $[x_{\min}, x_{\max}]$ ,  $x_{\min} < 0$  and  $x_{\max} > 0$ , large enough to contain both halves of the line profile and to allow for Doppler shifts  $\pm 2V_{\max}$ . We then replace equations (14-15) through (14-18) with difference equations and write

$$S_{dl} = S(z_d, \mu_l, x_l) = \alpha_{dl} J_d + \beta_{dl} \quad (14-19)$$

where  $\alpha$  and  $\beta$  are the appropriate combinations of  $r_d$ ,  $\phi_{dl}$ , and  $\varepsilon_d$ , and

$$J_d \equiv \sum_{l=1}^L w_l \phi_{dl} u_{dl} \quad (14-20)$$

where  $\phi_{dl} \equiv \phi(z_d, x_l - \mu_l V_d)$ . The resulting system is then of the *standard Rybicki form* [see equation (6-47)] and is solved for  $J$  as described in §6-3. An analogous integral-equation solution can also be constructed (273, 120), but in application the differential-equation method is easier to use. The whole procedure is stable and general, and quite efficient, as the computing time  $T_R = cL D^2 + c' D^3$  is only *linear* in  $L$ , the number of angles and frequencies. The depth-mesh must be chosen sufficiently fine to assure that only modest changes in  $V(z_d)$ , say  $\lesssim \frac{1}{2}$ , occur between successive depth-points; otherwise the profile function  $\phi_{dl}$  may change radically with depth and lead to inaccuracies in the optical depth increments. Except for supersonic winds, this is not a stringent requirement. Note also that the same methods can be used to construct the *formal solution*, when  $S$  is given, by solving a single tridiagonal system (at each angle-frequency point desired) of the form  $T_d u_l = S_l$ ; here the computing time required is only  $T_s = cL D$ , which is minimal.

#### LINE-FORMATION WITH SYSTEMATIC MACROSCOPIC VELOCITIES IN PLANAR ATMOSPHERES

The effects of velocity fields on line-formation in planar atmospheres have been studied by a number of authors; we shall review some typical results here. Basic insight into effects of motions can be gained by using just the formal solution. Consider, for example, a semi-infinite atmosphere with a line formed in LTE, with  $r = \text{constant}$ , and  $S_l = S_c = B_v = B_0(1 + a\tau_l)$ , where  $\tau_l$  denotes the static line optical depth. Choose a velocity field of the form  $v(\tau_l) = v_0/[1 + (\tau_l/\tau_0)]$ , taken to be positive toward the observer (i.e., toward increasing  $z$ ). Then it is easy to calculate the emergent intensity  $I(\mu, x)$  over the surface of the star, and to construct the flux  $F(x)$  by integrating over  $\mu$ ; results for models with  $a = 3 \times 10^{-2}$ ,  $r = 10^{-2}$ ,  $v_0 = (0, 1, 3, 5, 10)$ , and  $\tau_0 = (1, 10, 100)$  are displayed in Figure 14-1. There we see that the line flux profile shows an asymmetry toward the blue. Similar asymmetries result even if there is no velocity gradient and the atmosphere is assumed to expand with *constant* velocity, because of the way velocities and intensities are weighted in the flux integral (Cf. Exercises 14-1 and 14-2).

*Exercise 14-1:* (a) For a linear limb-darkening law  $\phi(\mu) = I(\mu)/I(0) = 1 + \beta\mu$ , show that the function normalized to give unit flux is  $\phi^*(\mu) = \frac{1}{2}(1 + \beta\mu)/(\frac{1}{2} + \frac{1}{3}\beta)$ . (b) Assume that a weak line is formed on the surface of an atmosphere expanding with velocity  $v_0$ , and that the line depth, as a fraction of the continuum, does not vary with  $\mu$ . Derive an expression for the radial velocity measured from observations of the flux in a spectrogram. In particular, show that for the grey-body limb-darkening law, in the Eddington approximation,  $v_{\text{obs}} = (17/24)v_0$ . What is the ratio of  $v_{\text{obs}}/v_0$  for  $\beta = 0$ ; for  $\beta = \infty$ ?

*Exercise 14-2:* Calculate the flux profile from a line, idealized as a delta-function of constant depth, on a stellar surface expanding with constant velocity  $v_0$ ; i.e., take  $I(\mu, x) = \frac{1}{2}(1 + \beta\mu)[1 - a_0 \delta(x - \mu V_0)]/(\frac{1}{2} + \frac{1}{3}\beta)$ . Derive an explicit expression for  $F(x; a_0, \beta, V_0)$ , and plot the profile in the limiting cases  $\beta = 0$ ,  $\beta = \infty$ . (b) Expand the analysis to a line with a Gaussian profile, and compute numerically a typical flux profile.

The formal solution can be used to evaluate proposed velocity-diagnostic techniques by computing profiles for given velocity fields, subjecting these profiles to the diagnostic analysis, and comparing the inferred with the originally-assumed fields. For example, the "bisector shift" technique has been examined (373) for a variety of cases. This method supposes that the displacement  $\delta x$ , from the static line-center, of the position of the point midway between two points of *equal intensity* in the line-profile, gives the Doppler shift caused by velocities in a layer at unit optical depth for a (static) line frequency  $\Delta x$ , where  $2\Delta x$  is the full distance between the two points on the profile. It is found that the inferred velocities are in *fair agreement* with

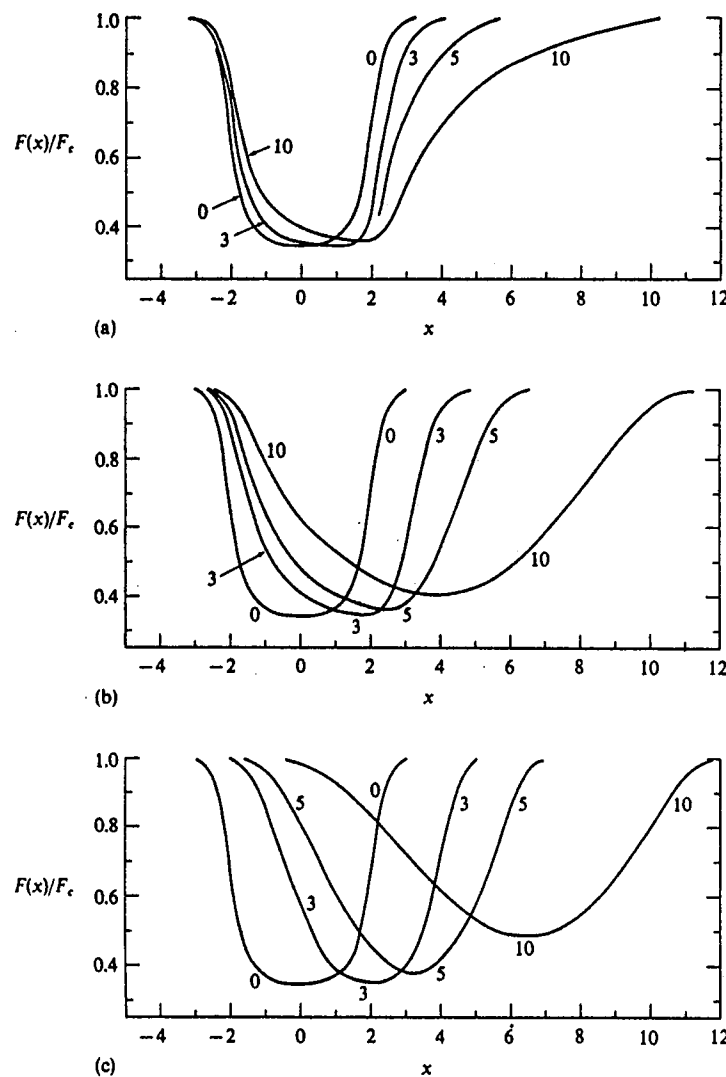


**FIGURE 14-1**  
Flux profiles from an expanding atmosphere, for a line formed in LTE, with  $B_s(\tau_i) = B_0(1 + \alpha\tau_i)$  and  $v(\tau_i) = v_0/[1 + (\tau_i/\tau_0)]$ . Ordinate: flux in units of continuum; Abscissa: frequency displacement from line center in Doppler units. Parameters are  $B_0 = 1$ ,  $\alpha = 3 \times 10^{-2}$ ,  $r = 10^{-2}$ , for all curves. Each curve is labeled with  $v_0$ . Panels (a), (b), and (c) have  $\tau_0 = 1, 10, 100$ , respectively.

the input velocities for measurements in the line-core, but that spurious velocities at great depths are inferred from the wings. It is easy to see why this is so. Suppose that the atmosphere moves with velocity  $v_0$  on the range  $0 \leq \tau_i \leq \tau_1$ , and is at rest for  $\tau_i > \tau_1$ . It is clear that the shift of the line in the upper layer forces the line-wings to be asymmetric, because opacity from the upper layer intrudes into the wing and absorbs radiation from below. By assuming that radiation at frequency displacement  $\Delta x$  from line-center arises from depths  $\tau_i \sim 1/\phi(\Delta x)$ , velocities will automatically be ascribed to these depths even if  $\tau_i > \tau_1$ . This example shows that care must be taken in inferring velocity fields!

A further example of such problems is shown in (321) where a calculation is made [using the Riccati method (544)] of the non-LTE source function of a line with  $\epsilon = 10^{-3}$  and  $r = 0$ , in a differentially expanding finite slab of total (static) optical depth  $\tau_{\max} = 50$ . The expansion is taken to be symmetric about the midpoint of the slab (assumed to be at rest) with a linear velocity law of the form  $V(\tau) = V_0 + V_1\tau_i$ ; the medium is effectively thin, and simulates an expanding nebula. Line profiles are shown in Figure 14-2. There we see that the usual central reversal arising in the material nearest the observer is blue-shifted, and thus obliterates the blue emission peak, while the red peak is enhanced because photons more easily emerge from below; the line as a whole appears red-shifted even though the average velocity of the material is zero! One cannot, therefore, immediately conclude that a small observed red shift implies a receding emitter.

To evaluate the effect of velocity fields on the source function one must solve the transfer equation self-consistently. Some of the early work on this

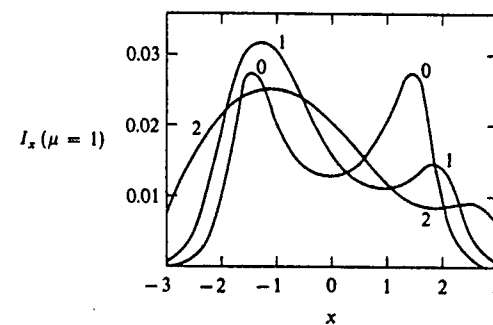


**FIGURE 14-2**  
Normally-emergent intensity from differentially expanding slab with total (static) thickness  $\tau_{\max} = 50$ , for a line with  $\epsilon = 10^{-3}$  and  $r = 0$ . Abscissa:  $x = \Delta v/\Delta v_D$ . Curves are labeled with  $v_0$ , velocity of expansion at surface; velocity law is linear in  $\tau$  and gives zero velocity at slab center. From (23, 215).

problem (370; 371) treated the case of an isothermal atmosphere with a velocity jump  $\Delta$  at a depth  $\tau_1$ , with constant velocities above and below. The transfer equation was solved in the Eddington approximation, for a two-level atom, using a discrete-ordinate method. When  $\Delta = 0$ , the static solution for the appropriate values of  $\epsilon$  and  $r$  is obtained. As  $\Delta$  becomes greater than about 4, the lines (which have Doppler profiles) in the upper and lower regions are strongly shifted with respect to one another and no longer interact. The atmosphere then acts as if it consists of two *independent* parts: (a) a finite upper layer of optical thickness  $\tau_1$ , and (b) an underlying semi-infinite atmosphere in which  $\tau = 0$  at the depth,  $\tau_1$ , of the velocity jump. In this limit, the source functions in the two layers both achieve their respective *static* limits. Thus for  $\Delta = 0$  and  $\Delta \rightarrow \infty$ , one recovers profiles identical to those computed from *static* source functions, the major effect just being the Doppler shift of the line-center in the formal solution. This result is strengthened when there is an appreciable background continuum [see also (372)]. For  $\Delta$  on the range of 2 to 3, the two layers interact strongly and a full solution must be found.

A more realistic problem (273, 120) is presented by an atmosphere with a "chromospheric" Planck-function rise at the surface (see Figure 14-3a) and with velocity laws of the form  $V(\tau_i) = 10/[1 + (\tau_i/\tau_0)]$ , where  $\tau_i$  is the static optical depth in the line. The resulting source functions for a line with  $r = 10^{-4}$  and  $\epsilon = 10^{-2}$  and various values of  $\tau_0$  are shown in Figure 14-3a, while emergent intensity profiles are shown in Figure 14-3b, and flux profiles in Figure 14-3c. The striking result seen in Figure 14-3a is that the line source function is only *weakly* affected by the velocity field, even though the profiles' show *drastic* changes. The basic reason for this result is that photon-escape through the outer layers is *increased* in the red wing, but *decreased* in the violet wing—and, to a large measure, these effects nearly cancel [see also (18, 53)]. On the whole, the photon-escape probability is slightly enhanced by the atmospheric expansion, which explains why  $S_l$  tends to lie *below* its static value for  $1 \lesssim \tau_i \lesssim 10^2$ . In the case  $\tau_0 = 10$ , the value of  $S_l$  increases for  $\tau_i \lesssim 10$  because the line intercepts underlying continuum radiation while it is optically fairly thin, which leads to an increase in  $J$ ; for larger values of  $\tau_0$ , the line becomes optically thick above the velocity rise, and the effect vanishes. When  $\tau_0 \gtrsim 10^3$ , the point of the velocity rise already lies below the thermalization depth of the line; line-formation in the upper (effectively thick) layer then proceeds as if the atmosphere were static, and the static value of  $S_l$  is recovered very closely. The flux profiles for  $\tau_0 = 10^2$  to  $10^3$  show "P-Cygni" features with red emission components and violet-shifted absorption. Here the emission, however, arises from the assumed temperature rise, and not from the geometrical effects that occur in extended atmospheres. To a high degree of approximation, one would find the same profiles from a velocity-dependent formal solution using static source functions.

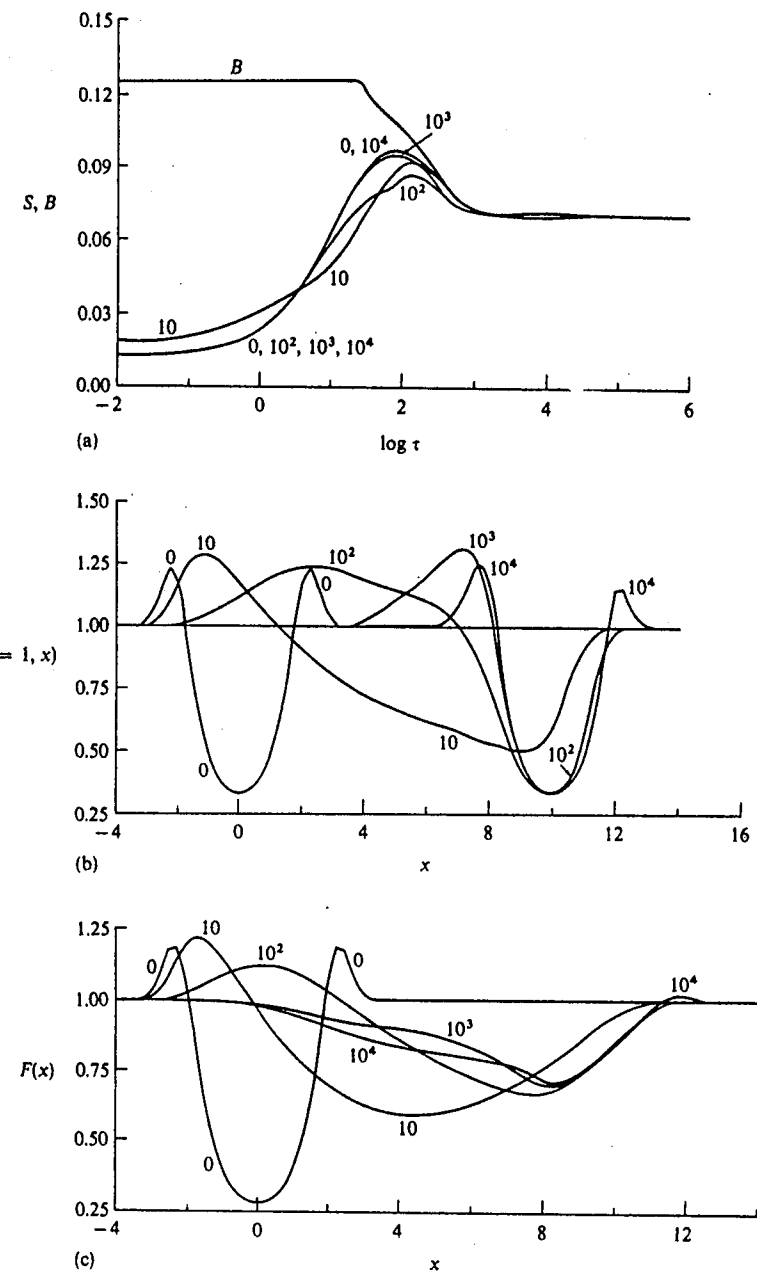


FIGURE 14-3  
 (a) Planck function and source function in an expanding atmosphere, for a line with  $\epsilon = 10^{-2}$  and  $r = 10^{-4}$ . Abscissa: static line optical depth. (b) Normally-emergent intensity. Abscissa:  $x \equiv \Delta v / \Delta v_D$ . (c) Flux profiles. Curves are labeled with value of  $\tau_0$  in velocity law  $V(\tau) = 10/\tau_0 + (\tau_i/\tau_0)$ . From (273, 120).

The results described above apply to *expansion*, where an increased escape probability in one wing can be compensated by a decrease in the other. In fluctuating velocity fields, however, the coherence of shifts from one point in the atmosphere to another is lost, and effects similar to a marked depth-variation of the line profile are produced. The effects of fluctuating mesoscale velocity fields on line-formation have been studied (568) for sinusoidal waves with  $V(\tau, t) = \beta \sin[2\pi(\lambda^{-1} \log_{10}\tau + t)]$ , and for "sawtooth" waves; the latter simulate steepened shock-like structures. Using the Rybicki-type method described earlier, the transfer equation was solved at times spaced equally over a period, and time-averaged profiles were found for various values of  $\beta$  and  $\lambda$ . The limit  $\lambda \rightarrow 0$  corresponds to a "microturbulent" regime, while  $\lambda \rightarrow \infty$  yields a "macroturbulent" limit. For a given source function (e.g.,  $S_i \equiv B_v$ ), the line profiles for finite  $\lambda$  invariably lie between those given by the two extremes  $\lambda = 0$  and  $\lambda = \infty$ . The lines computed with a given  $\beta$  and  $\lambda = 0$  are always stronger than those for  $\lambda = \infty$ , as expected. When non-LTE cases are considered, the source functions are modified by the velocity field; characteristically,  $S_i$  shows ripples as a function of  $\tau$ , and the departure of the results for finite  $\lambda$  from the microscopic limit ( $\lambda = 0$ ) are larger at smaller values of  $\epsilon$ . The primary result found for non-LTE isothermal atmospheres is a significant rise in the core intensity of the time-averaged profile for finite  $\lambda$ ; the profile lies between the limiting ( $\lambda = 0$ ,  $\lambda = \infty$ ) profiles only in the wings, and is much brighter than both in the core (by a factor of 2.5 for  $\beta = 2.5$  and  $\lambda = 4$ ). The same behavior of the line core is also found in computations using the HSRA, and substantial changes in the source function occur. In particular, even though a collision-dominated source function is used,  $S_i$  rises above  $B_v$  (as it can for photoionization-dominated lines), because velocity shifts allow the line to intercept bright continuum radiation. The brightening of the line core appears to improve greatly the agreement between the observed and computed solar Na I D-lines at disk center, without recourse to unusually high densities as hitherto required; this result may also offer an explanation for similar discrepancies observed in the solar Ca I and Fe I lines. Further work in this area will be quite rewarding.

The results discussed above take no account of possible effects of the velocity field on the state of the gas. Recently a study has been made (291) of effects of acoustic pulses on formation of the solar Ca II lines, allowing for the temperature and density changes the pulses produce in the gas. These computations show that, if changes in the physical variables are ignored, the velocity field alone produces little change in the source function, and the correct profile is predicted using the static source function in a velocity-dependent formal solution; a similar conclusion was reached in (185). In contrast, the changes in  $T$  and  $N$  produced by the pulses have major effects on  $S_i$  and hence on the profiles. In particular, both  $T$  and  $n_e$  increase together,

and increase the local coupling of  $S_i$  to  $B_v$ ; this, in turn, leads to substantial increases first in the violet, and then the red, emission peaks of the doubly-reversed profile. These results again point to the need for a dynamical theory for the velocity fields.

#### SPHERICAL ATMOSPHERES: LOW-VELOCITY REGIME

Observer's frame calculations in the low-velocity regime have been carried out for radially expanding spherical atmospheres (375). Such an approach can be useful in studying line formation in the deeper layers of expanding atmospheres, but for the large-velocity regime a comoving-frame formulation is preferable. The method is similar to that described in §7-6 for static atmospheres, and carries out a ray-by-ray solution in the same  $(p, z)$  coordinate system. The transfer equation along the ray is

$$[\partial J^\pm(z, p, x)/\partial z] = \eta(z, p, x) - \chi(z, p, x)J^\pm(z, p, x) \quad (14-21)$$

where  $\chi(z, p, x) \equiv \chi_c(r) + \chi_i(r)\phi(z, p, x)$ , and a similar expression defines  $\eta(z, p, x)$ ; we use the relations  $r(z, p) = (z^2 + p^2)^{1/2}$  and  $\mu(z, p) = z/(z^2 + p^2)^{1/2}$ . The profile is defined as  $\phi(z, p, x) \equiv \phi[r(z, p); x - \mu(z, p)V(r)]$ . The velocity  $V(r)$  is positive in the direction of increasing  $r$ . Introducing the optical depth along the ray

$$\tau(z, p, x) \equiv \int_z^{z_{\max}} \chi(z', p, x) dz' \quad (14-22)$$

$$\text{and defining } u(z, p, x) \equiv \frac{1}{2} [I^+(z, p, x) + I^-(z, p, -x)] \quad (14-23)$$

$$\text{and } v(z, p, x) \equiv \frac{1}{2} [I^+(z, p, x) - I^-(z, p, -x)] \quad (14-24)$$

we may rewrite equation (14.21) in second-order form:

$$[\partial^2 u(z, p, x)/\partial \tau(z, p, x)^2] = u(z, p, x) - S(z, p, x) \quad (14-25)$$

where  $S(z, p, x) \equiv \eta(z, p, x)/\chi(z, p, x)$  has the general form  $S(z, p, x) = \alpha(z, p, x)J[r(z, p)] + \beta(z, p, x)$ . Here  $\alpha$  and  $\beta$  contain combinations of the line parameters  $\epsilon$  and  $r_0 \equiv \chi_c/\chi_i$ , and the profile function  $\phi(z, p, x)$ , while

$$J(r) = \int_{-x_{\max}}^{x_{\max}} dx \int_0^1 d\mu \phi[r; x - \mu V(r)] u[z(r, \mu), p(r, \mu), x] \quad (14-26)$$

In formulating the boundary conditions a difficulty arises. On the axis  $z = 0$  we can no longer write  $v(0, p, x) = 0$  because two frequencies ( $\pm x$ ) of radiation are involved. We may circumvent this problem by following the ray for its entire length—i.e., we consider the whole interval  $[-z_{\max}, z_{\max}]$ . The lower

and upper boundary conditions for rays that do not intersect the core then become

$$[\partial u(z, p, x)/\partial z](z, p, x)|_{z=\pm z_{\max}} = \pm u(z, p, x)|_{z=\pm z_{\max}} \quad (14-27)$$

For rays that intersect the core,  $p \leq r_c$ , we either (a) apply a *diffusion approximation* at an *opaque core* (stellar surface), which yields  $v(z_{\min}, p, x)$  directly, or (b) for a *hollow core* (nebular case), apply equation (14-25) at  $z_{\min}$  (forcing the points at  $\pm z_{\min}$  to be identical), and equation (14-27) at the ends of the ray.

To solve the system we introduce the same discrete meshes  $\{r_d\}$  and  $\{p_i\}$  used in §7-6 to solve the static problem. The frequency mesh now includes the *whole profile*  $\{x_n\}$ ,  $n = \pm 1, \dots, \pm N$ , with  $x_{-n} = -x_n$ ; we shall, however, be able to eliminate half of these (see below). We again obtain equations of the form of (6-27) and (6-48), and hence can apply the Rybicki method to obtain  $J$ . Because  $J(r_d)$  need be defined only for  $\{r_d\}$ ,  $1 \leq d \leq D$ , while  $u_{din} = u(z_d, p_i, x_n)$  is defined on a mesh  $\{z_{d_i}\}$ ,  $d_i = 1, \dots, D_i$ , which runs the whole length of the ray, it now turns out that, while the tridiagonal T-matrix is square, the U-matrix is *rectangular*, and is a *chevron matrix*. Solution of these systems for each choice of  $(i, n)$  yields an expression of the form

$$u_{in} = A_{in}J + B_{in} \quad (14-28)$$

Equation (14-26) defining  $J$  can be written in the discrete form

$$J(r_d) = \sum_{n=-N}^N w_n \sum_{i=1}^{D_i} a_{di} \phi[r_d; x_n - \mu(r_d, p_i) V(r_d)] u_{din} \quad (14-29)$$

But, from the spherical symmetry of the problem,  $I^\pm(z, p, x) \equiv I^\mp(-z, p, x)$ , and thus  $u(z, p, -x) \equiv u(-z, p, x)$ , and  $v(z, p, -x) \equiv -v(-z, p, x)$ ; these relations allow elimination of the values of  $u$  at negative  $x$  and positive  $z$ , in equation (14-29), in terms of  $u$  at positive  $x$  and negative  $z$ . Thus

$$J = \sum_{n=1}^N w_n \sum_{i=1}^{D_i} a_{di} \{\phi[r_d; x_n - \mu_{di} V_d] u_{din} + \phi[r_d; x_n + \mu_{di} V_d] u_{d'in}\} \quad (14-30)$$

where  $d' = D_i + 1 - d$ . Equation (14-30), when used in the Rybicki method, yields V-matrices that are rectangular chevron matrices. Using equations (14-28) for all values of  $i$  and  $n$  in equation (14-30), we obtain a final system for  $J$ , which is then solved. The computing time required for the solution scales as  $T_R \approx cN D^3 + c' D^3$ ; this is less favorable than the result for the planar case, because now there are about as many angles (i.e., impact parameters) as there are depths. The method is stable and easy to use for small velocities (i.e., a few times thermal). For larger velocities, the number of depth-points required to resolve the velocity field becomes large, and the

computing time is prohibitive; in this case one may use a comoving-frame method. An advantage of the observer-frame method is that it can be used for *arbitrary* variations in the velocity field (e.g., nonmonotone flows), which is *not* true for comoving-frame methods, as currently formulated.

*Exercise 14-3:* (a) Verify the symmetry relations quoted above for  $I^\pm$ ,  $u$ , and  $v$ , and the reduction of (14-29) to (14-30). (b) Sketch the form of the rectangular chevron matrices  $U_{in}$  and  $V_{in}$  in the Rybicki scheme, and show that the dimensions of the matrices mesh in the correct way to allow a solution.

The method described above has been applied (375) to highly idealized spherical atmospheres with power-law opacities and linear velocity laws of the form  $V(r) = V(R)(r - r_c)/(R - r_c)$ . Calculations were made in extended isothermal models with  $R/r_c = 30$ , for a line with  $\epsilon = 10^{-2}$  and  $10^{-4}$  and zero background continuum, with  $V(R) = 0, 1$ , and  $2$ . The results include the following. (a) The source function is more strongly affected by extension than by small velocity fields; to a first approximation, one may use the *static* spherical source-function in a velocity-dependent profile computation. (b) The effects of extension and velocities are more significant for smaller values of  $\epsilon$ . (c) The dominant effect of the velocity field is to reduce photon trapping, and hence to increase the photon escape probability. (d) The line profiles become skewed to the *red* as the central absorption feature obliterates the violet emission peak [true also in planar geometry, cf. Figure (14-2)]. In a second sequence of models, the maximum velocity was held fixed,  $V(R) = 2$ , and  $R/r_c$  was chosen to be 3, 10, and 30;  $B = r^{-2}$ ,  $\epsilon = 10^{-4}$ ,  $\chi_e/\chi_i = 10^{-4}$ , and  $\chi_i = Cr^{-2}$ . The effects of velocities on the source function are small compared to the changes produced by spherical geometry, and the relative departure from static results increases as  $R$  decreases, probably because the velocity gradient increases. The emergent profiles all show a strong P-Cygni character. A final calculation worthy of mention is a case in which the velocity is constant throughout the atmosphere; i.e.,  $V(r) \equiv V_0$ . For a *planar* medium the source function would, of course, be unchanged (though the flux profile computed by averaging over the surface of a star changes; recall Exercise 14-1). For a *spherical* medium however, the radii diverge from the center, leading to a *transverse velocity gradient* that decreases photon trapping; as a result, the escape probability increases, and the source function decreases. Even a modest constant velocity of expansion has quite dramatic effects on emergent flux profiles.

#### EFFECTS OF LINES ON ENERGY BALANCE IN MOVING MEDIA

The energy balance in the outer layers of an atmosphere can be dominated by spectral-line contributions. Hence Doppler shifts, which may move a line away from its rest position and allow it to interact with the continuum (in

which the intensity can be markedly different), can significantly alter the temperature distribution. Qualitatively, we can expect three effects to be present, over and above the usual boundary-temperature change and backwarming that occur in static media. (1) Lines Doppler-shifted away from their rest frequencies can intercept continuum photons from deeper layers; we may call this the *irradiation effect*. The absorbed continuum flux provides additional energy input to the gas and, because the color temperature of the flux exceeds the ambient temperature locally, irradiation will lead to a net *heating* of the outer layer. The effectiveness of the input is determined by the strength of the coupling of the lines to the thermal pool; thus heating will be greatest when  $\epsilon = 1$ , and should be negligible for  $\epsilon \rightarrow 0$ . (2) As the lines shift away from their rest positions, photons that would have been trapped in the deeper layers by overlying line absorption now encounter only continuum opacity, and hence may diffuse freely to the surface and escape; we may refer to this effect as *escape-enhancement*. In general, an increase in photon escapes will lead to a *cooling* of deeper layers. (3) A velocity gradient in the atmosphere smears the lines over a larger bandwidth, thus impeding the free flow of photons; we may call this the *bandwidth-constriction effect*. At depth in the atmosphere, where the diffusion approximation is valid, a velocity gradient causes little, if any, change in the temperature structure when the scale of the velocity variation is large compared to a photon mean-free-path. But if a velocity shift of the order of a Doppler width occurs in a mean-free-path, then bandwidth constriction leads to a decrease in the effective radiation-diffusion coefficient, and hence to increased backwarming. In the extreme limit of an abrupt velocity step near the surface, photons emerging from lower layers in formerly-open continuum bands encounter opaque material, and have their escape impeded; this might more appropriately be termed a "backscattering" or "reflector" effect.

Studies of the influence of line-shifts on energy balance have been made for highly schematic picket-fence models, in planar geometry with an abrupt velocity jump (428), and in spherical expanding atmospheres (445). The velocity-step can be regarded as a caricature of a shock front. The escape-enhancement and irradiation effects show very clearly for the velocity-jump, where the layers above the jump heat markedly (one case gives  $\Delta T \sim 1100^{\circ}\text{K}$  for  $T_{\text{eff}} = 10,000^{\circ}\text{K}$ ), and a cooling of a few hundred degrees occurs immediately below. For the expanding spherical atmospheres one obtains large irradiation-effect rises at the surface, and substantial backwarming below. The irradiation-effect temperature rise is larger for extended models than for nearly-planar models; this is because the discrepancy between the color temperature of the flux, and the ambient temperature characteristic of the local energy density, becomes larger as atmospheric size increases. For one extreme case, the velocity field produces a change  $\Delta B/B \approx 3$ , which implies  $\Delta T/T \approx 0.33$ , or  $\Delta T \sim 10,000^{\circ}\text{K}$  for an O-star.

Even though the models upon which the results quoted above are based are very schematic, it is clear that velocity-field effects on line-absorption can lead to very substantial changes in the energy balance of the outer layers of stellar atmospheres. These changes could, in principle, influence the hydrodynamics of the flow. Thus, in a pulsating atmosphere, energy deposition in the lines produces a kind of radiative precursor that could affect shock propagation; for expanding atmospheres, significant energy deposition could occur in the transsonic flow region, which might alter the nature of the stellar wind. It is also possible that velocity-dependent line-absorption contributions to energy balance could affect the flow-dynamics of novae, supernovae, and mass-exchange in binaries. Much further work remains to be done on this subject.

#### LINE-FORMATION IN TURBULENT ATMOSPHERES

As mentioned earlier, the dichotomy of velocity-field effects on spectrum line-formation into the "microturbulent" and "macroturbulent" limits is obviously oversimplified. In these two extreme limits, the effects of the velocity field upon line strengths and profiles may be predicted from simple phenomenological arguments. To study the influence of velocity fields that have a scale which is neither zero, nor infinite, with respect to a photon mean-free-path, a detailed computation must be made. One could, in principle, specify a particular run of the velocity, solve the equation of transfer, and average over as many realizations of the velocity field as are necessary to embrace the possible ranges of its inherent degrees of freedom. Such an approach, however, would be costly, and would not yield direct insight into the problem. An attractive alternative (motivated by the expectation that in stellar atmospheres the velocity field is *chaotic*, and possibly even *turbulent* in the hydrodynamic sense) is to assume that the velocity is a *random variable*, described locally by a *probability distribution for the amplitude*, and nonlocally by a *characteristic correlation length*.

Considerable progress in solving the transfer equation in turbulent media has recently been made with two distinct approaches. One formulation, developed by the Heidelberg group (70, 325; 234; 235; 236; 557), employs the *joint probability*  $P(z; v, I)$  that, at point  $z$ , the velocity lies in the range  $(v, v + dv)$ , and the intensity in the range  $(I, I + dI)$ , for Markov-process variations of  $v$  and  $I$ .  $P$ , or some other suitable distribution function derived from  $P$ , is found by solving a Fokker-Planck equation. This method is powerful and general, and allows the treatment of velocity fields that are *continuous* functions of depth. However, the resulting partial differential equations are difficult to solve, and a succinct description of the method would presume considerable familiarity of the reader with the mathematical methods for treating Markov processes. A rather different formulation has

been developed by the Nice group (49; 226; 227). The flow is conceived as consisting of turbulent eddies or cells. The velocity is taken to be uniform within each cell, and to jump discontinuously at sharp boundaries that separate the cell from neighboring cells with uncorrelated velocities; this description is called a *Kubo–Anderson process*. Although the discontinuity of the velocity structure is unphysical and introduces some artificial high-order correlations in the field (49; 70, 325), this approach nevertheless has the advantages of yielding exact analytical results in certain limits, and of expository simplicity. We shall therefore describe the Nice method here, but quote results from both bodies of work.

We assume that the cell boundaries, at which the velocity changes, are located at random continuum optical depths  $\{\tau_n\}$ , distributed according to a *Poisson law* characterized by an *eddy density*  $n(\tau)$ , which gives the reciprocal of the correlation length  $l$  (in continuum optical depth units) of the velocity field. The probability that no jump has occurred on the interval  $(\tau', \tau)$  is given by  $\exp[-\int_{\tau'}^{\tau} n(\tau'') d\tau'']$ . Let  $v_h(\tau)$  denote the hydrodynamic velocity of the cell at  $\tau$ ; these velocities are *independently* distributed according to a probability distribution function  $P(v_h)$ , which we shall take to be Gaussian. Let  $v_{th}(\tau)$  denote the thermal velocity of the line-forming atoms at  $\tau$ , and measure all velocities in thermal units,  $u_h(\tau) \equiv v_h(\tau)/v_{th}(\tau)$ , and frequencies from line center in units of the corresponding Doppler widths,  $x \equiv \Delta\nu/\Delta\nu_D(\tau)$ . Characterize the turbulent field by a dispersion  $\xi$  (in thermal units); then

$$P(u_h) = \exp(-u_h^2/\xi^2)/(\pi^{1/2}\xi) \quad (14-31)$$

The transfer equation to be solved in

$$\mu[\partial I(z, \mu, x)/\partial z] = -(\chi_c + \chi_l \phi_x)I(z, \mu, x) + \chi_c S_c + \chi_l S_l \quad (14-32)$$

where  $\phi_x(\tau) \equiv \phi[x - \mu u_h(\tau)]$ . Equation (14-32) is a *stochastic equation*—i.e., the coefficients in the equation are *random variables*. We now assume that the turbulent velocity field influences *only* the line absorption coefficient via Doppler shifts; fluctuations in the continuous opacity, source functions, and occupation numbers are expected to be of secondary importance, and are ignored here. We adopt LTE and ignore scattering, so that  $S_l = S_c = B_v(\tau)$ , and employ a Voigt line-profile so that

$$[\chi_l(\tau)\phi_x(\tau)]/\chi_c(\tau) = \beta(\tau)H[a(\tau), x - \mu u_h(\tau)] \quad (14-33)$$

$$\text{where } \beta(\tau) \equiv (\pi^{1/2}e^2/mc)[f_{ij}n_i(\tau)(1 - e^{-hv/kT})]/[\chi_c(\tau)\Delta\nu_D(\tau)] \quad (14-34)$$

$$\text{and } a(\tau) \equiv \Gamma/4\pi\Delta\nu_D(\tau) \quad (14-35)$$

Here  $\Gamma$  is the damping width, and  $n_i$  denotes the occupation number of the lower level of the transition.

We may obtain an analytical solution of the problem if we introduce the following additional assumptions: (1) set  $B_v(\tau) = B_0(1 + \alpha\tau)$ ; (2) use a Milne–Eddington model—i.e.,  $\beta = \text{constant}$ ,  $a = \text{constant}$ ,  $\Delta\nu_D = \text{constant}$ ; (3) adopt a constant eddy density  $n(\tau) \equiv n$ . All of these assumptions may be relaxed if the problem is solved numerically (49; 226). To simplify the treatment still further, we consider the intensity emergent at disk-center, and set  $\mu \equiv 1$ . The transfer equation thus becomes

$$[\partial I(\tau, x)/\partial \tau] = [1 + \beta H_x(\tau)][I(\tau, x) - B_0(1 + \alpha\tau)] \quad (14-36)$$

where  $H_x(\tau)$  denotes  $H[a, x - u_h(\tau)]$  and is constant between successive jump-points. If we define

$$q_x(\tau) \equiv \exp\left\{-\int_0^\tau [1 + \beta H_x(\tau')] d\tau'\right\} \quad (14-37)$$

then the *emergent intensities* in the continuum and the line are

$$I_c = \int_0^\infty B_0(1 + \alpha\tau)e^{-\tau} d\tau \quad (14-38)$$

$$\text{and } I(0, x) = \int_0^\infty B_0(1 + \alpha\tau)q_x(\tau)[1 + \beta H_x(\tau)] d\tau \quad (14-39)$$

It is easy to show that  $I_c = B_0(1 + \alpha)$ , and that the intensity in a line of infinite strength ( $\beta \rightarrow \infty$ ) is  $B_0$ ; the absorption depth of such a line will be  $A_0 = \alpha/(1 + \alpha)$ . Then, in general, the line absorption depth  $a_x \equiv [I_c - I(0, x)]/I_c$  can be written

$$(a_x/A_0) = 1 - \int_0^\infty q_x(\tau) d\tau \quad (14-40)$$

The *ensemble average* of the line profile over all possible realizations of the velocity field is thus

$$\langle a_x \rangle/A_0 = 1 - \int_0^\infty \langle q_x(\tau) \rangle d\tau \quad (14-41)$$

while the average of the reduced equivalent width is

$$\langle W^* \rangle \equiv \langle W/A_0 \Delta\nu_D \rangle = A_0^{-1} \int_{-\infty}^\infty \langle a_x \rangle dx \quad (14-42)$$

Thus the crux of the problem is the calculation of  $\langle q_x(\tau) \rangle$ .

The function  $\langle q_x(\tau) \rangle$  can be found from the solution of an integral equation, which is obtained by the following arguments. First, at a given point  $\tau$ , the probability that no jump has occurred on  $(0, \tau)$  is  $\exp(-n\tau)$ ; the corresponding contribution to  $\langle q_x(\tau) \rangle$  is then  $\exp(-n\tau)\langle q_x(\tau) \rangle_s$ , where the

static average is

$$\langle q_x(\tau) \rangle_s = \langle \exp[-(1 + \beta H_x)\tau] \rangle \\ = \int_{-\infty}^{\infty} \exp\{-[1 + \beta H(a, x - u_h)]\tau\} P(u_h) du_h \quad (14-43)$$

Here  $u_h$  (and hence  $H_x$ ) is constant over the entire interval  $(0, \tau)$ . On the other hand, suppose that one or more jumps have occurred on the interval  $(0, \tau)$ , and let  $\tau' (< \tau)$  denote the last jump point. On the interval  $(\tau', \tau)$ ,  $H_x$  will be constant, hence

$$q_x(\tau) = \exp[-(\tau - \tau')(1 + \beta H_x)] q_x(\tau') \quad (14-44)$$

The probability that the last jump, at  $\tau'$ , occurs between  $\tau'$  and  $\tau' + dt'$  is  $\exp[-n(\tau - \tau')]n dt'$ ; thus averaging (14-44), and summing over all  $\tau'$ , we obtain the contribution to  $\langle q_x(\tau) \rangle$  from jumps on  $(0, \tau)$ , namely

$$\langle q_x(\tau) \rangle_{\text{jump}} = \int_0^\tau \langle \exp[-(\tau - \tau')(1 + \beta H_x)] q_x(\tau') \rangle \exp[-n(\tau - \tau')]n dt' \quad (14-45)$$

Now all steps in  $H_x(\tau'')$  on the interval  $0 < \tau'' < \tau'$  are independent of the value of  $H_x$  on the interval  $(\tau', \tau)$ , hence

$$\begin{aligned} \langle \exp[-(\tau - \tau')(1 + \beta H_x)] q_x(\tau') \rangle &= \langle \exp[-(\tau - \tau')(1 + \beta H_x)] \rangle \langle q_x(\tau') \rangle \\ &= \langle q_x(\tau - \tau') \rangle_s \langle q_x(\tau') \rangle \end{aligned} \quad (14-46)$$

Adding the static and jump contributions we have, finally,

$$\langle q_x(\tau) \rangle = e^{-n\tau} \langle q_x(\tau) \rangle_s + \int_0^\tau \langle q_x(\tau') \rangle \langle q_x(\tau - \tau') \rangle_s e^{-n(\tau - \tau')} n d\tau' \quad (14-47)$$

Because we have taken  $n$  to be depth-independent, the integral in equation (14-47) is a convolution integral, and we may apply a Laplace transformation to obtain the solution. Thus let

$$Q_x(s) \equiv \int_0^\infty e^{-st} \langle q_x(\tau) \rangle d\tau \quad (14-48)$$

and

$$\begin{aligned} S_x(s) &\equiv \int_0^\infty e^{-st} \langle q_x(\tau) \rangle_s d\tau = \int_{-\infty}^\infty du_h P(u_h) \int_0^\infty \exp[-(1 + \beta H_x)\tau] e^{-st} d\tau \\ &= \langle [s + (1 + \beta H_x)]^{-1} \rangle \end{aligned} \quad (14-49)$$

Then from equation (14-47) we find

$$Q_x(s) = S_x(s + n) / [1 - nS_x(s + n)] \quad (14-50)$$

*Exercise 14-4:* Derive equation (14-50).

We do not require the inverse transform of  $Q_x$  because, as can be seen by comparison of equations (14-48) and (14-41), the residual intensity can be expressed entirely in terms of  $Q_x(0)$ . Thus we have the general result that

$$\langle a_x \rangle / A_0 = 1 - \langle (n + 1 + \beta H_x)^{-1} \rangle [1 - n \langle (n + 1 + \beta H_x)^{-1} \rangle]^{-1} \quad (14-51)$$

We can recover the *macroturbulent limit* by taking the correlation length  $l = \infty$ , or  $n = 0$ , so that the entire atmosphere along the ray moves with constant velocity. From equation (14-51) we find

$$\langle a_x(\beta) \rangle_{\text{macro}} = A_0 \langle \beta H_x / (1 + \beta H_x) \rangle \quad (14-52)$$

This result agrees with our intuitive expectations when we recognize that the argument in the bracket is just the emergent residual intensity of a line in the Milne-Eddington model (cf. §10-3), shifted bodily by a velocity  $u_h$ , and then averaged over the probability distribution of  $u_h$ . We may express the general result in terms of the macroturbulent limit as

$$\langle a_x(\beta) \rangle = (n + 1) \langle a_x[\beta/(n + 1)] \rangle_{\text{macro}} [1 + n A_0^{-1} \langle a_x[\beta/(n + 1)] \rangle_{\text{macro}}]^{-1} \quad (14-53)$$

To obtain the *microturbulent limit*, we let  $n \rightarrow \infty$ . First, note that for  $\beta \rightarrow 0$ , equation (14-52) can be expanded as  $\langle a_x(\beta) \rangle_{\text{macro}} \approx A_0 (\beta \langle H \rangle - \beta^2 \langle H^2 \rangle)$ , which yields

$$A_0^{-1} \langle a_x(\beta) \rangle_{\text{micro}} = \beta \langle H(a, x) \rangle / [1 + \beta \langle H(a, x) \rangle] \quad (14-54)$$

$$\text{where } \langle H(a, x) \rangle \equiv (\pi^{1/2} \xi)^{-1} \int_{-\infty}^{\infty} H(a, x - u_h) \exp(-u_h^2/\xi^2) du_h \quad (14-55)$$

Because the Voigt function is a convolution of a Lorentz profile with a Gaussian [cf. equation (9-34)], we obtain, from an interchange of the order of integration,

$$\langle H(a, x) \rangle = (1 + \xi^2)^{-1/2} H[a(1 + \xi^2)^{-1/2}, x(1 + \xi^2)^{-1/2}] \quad (14-56)$$

That is, in the microturbulent limit the Doppler width  $\Delta v_D$  is increased by a factor of  $(1 + \xi^2)^{1/2}$ .

In the limit of zero turbulence the standard Milne-Eddington curve of growth is given by [cf. equation (10-38)]

$$W_0^*(a, \beta) = \int_{-\infty}^{\infty} \frac{dx}{v} \beta H(a, x) [1 + \beta H(a, x)]^{-1} dx \quad (14-57)$$

Now, substituting equation (14-52) into (14-42) and interchanging the order of integration, we find  $W_{\text{macro}}^*(a, \beta) = \langle W_0^*(a, \beta) \rangle \equiv W_0^*(a, \beta)$ ; i.e., in the macroturbulent limit the curve of growth is unchanged—which, of course,

is the expected result. In the microturbulent limit, by substitution of equations (14-54) and (14-56) into (14-42), we obtain immediately

$$W_{\text{micro}}^*(a, \beta) = (1 + \xi^2)^{\frac{1}{2}} W_0^*[a/(1 + \xi^2)^{\frac{1}{2}}, \beta/(1 + \xi^2)^{\frac{1}{2}}]$$

This shows that the linear and damping parts of the curve are unaffected, while the flat part rises by a factor of  $(1 + \xi^2)^{\frac{1}{2}}$ . Between these limits the curve of growth is found by numerical integration of equation (14-42), using equation (14-53). In addition to expressions for  $\langle a_x \rangle$  and  $W^*$ , it is possible to derive an expression for  $\sigma_x$ , the rms fluctuation in the residual intensity that would be seen along the slit in a spectrogram of perfect resolution; i.e.,  $\sigma_x \equiv A_0^{-1}(\langle a_x^2 \rangle - \langle a_x \rangle^2)^{\frac{1}{2}}$  [see (49)].

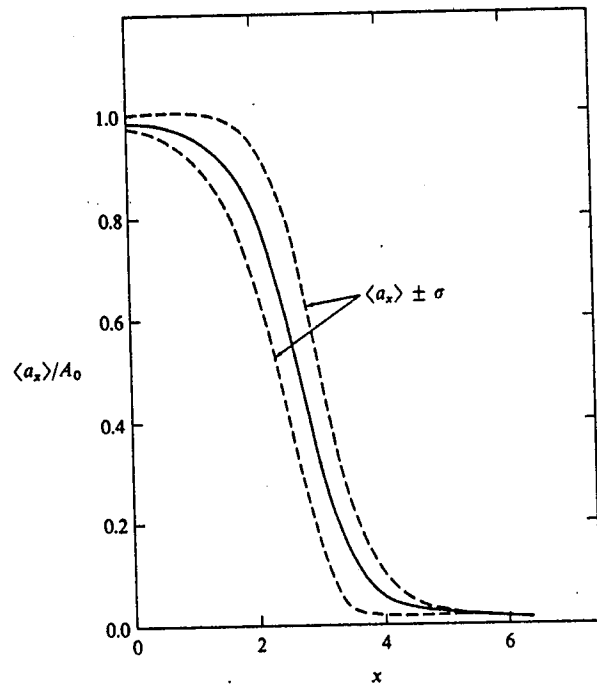


FIGURE 14-4  
Absorption depth in line with  $\beta = 100$ , in a turbulent atmosphere with turbulent velocity  $\xi = 1$ , and eddy-density  $n = 10$ . Abscissa:  $x \equiv \Delta v / \Delta v_p$ . Solid curve: average profile from all realizations of velocity distribution. Dashed curves: average profile  $\pm$  the rms fluctuation seen by spectrograph of perfect resolution. From (49), by permission.

Results for the average depth, and its dispersion, of a strong line in an atmosphere with the turbulent-velocity parameter  $\xi$  equal to the thermal velocity, and a density of 10 "eddies" per unit continuum optical depth, are shown in Figure 14-4. Curves of growth for  $\xi = 1$  are shown in Figure 14-5. There we see that the dependence of the theoretical curve upon the eddy density,  $n$ , implies that a comparison of an observed curve to a theoretical curve with  $\xi = 0$  cannot lead to a unique value for  $\xi$ . In general, the value of  $\xi$  deduced in the microturbulent limit will be a lower bound on the actual value. Note that this effect is opposite to that produced by departures from LTE—which, typically, raise the flat part of the curve of growth even when no velocities are present (cf. §11-4).

Detailed calculations, using a realistic solar atmosphere, have been made for the O I  $\lambda\lambda 7771, 7774, 7775$  lines, and the Fe I  $\lambda\lambda 5576, 5934, 6200$  lines (235); an excellent fit to observed profiles is achieved. In the fitting procedure, the loci of points in the  $(\xi, l)$  plane [ $l \equiv 1/n$  (km)] that match the observed

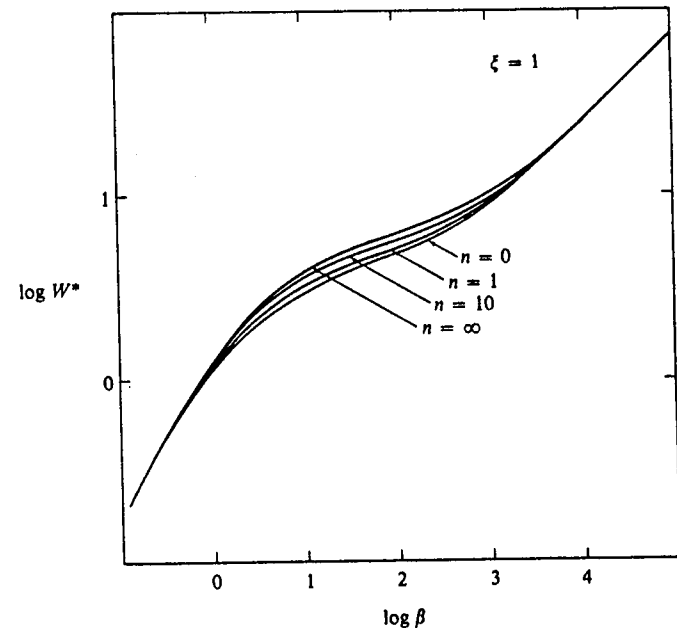


FIGURE 14-5  
Curves of growth in turbulent atmospheres with  $\xi = 1$ . Ordinate: Logarithm of reduced equivalent width  $W^* \equiv (W_p / A_0 \Delta v_p)$ . Abscissa: Logarithm of line-strength  $\beta = \chi_p / \chi_c$ . Curves are labeled with depth-independent eddy density. From (49), by permission.

intensities at several values of  $\Delta\lambda$  from line center, as well as the equivalent width, intersect at almost a unique point. Thus it proves possible to determine both  $\xi$  and  $l = 1/n$  (km) uniquely; numerically  $\xi \approx 2.2 \text{ km s}^{-1}$ , and  $l \approx 150 \text{ km}$ . The velocity is *larger* than that usually adopted as a microturbulent velocity; the correlation length is of the same order as the photospheric scale height. It would be of interest to ascertain whether the apparent near-equality of the correlation length with the scale height has hydrodynamic significance, or is mere coincidence.

Allowance for a finite scale in the velocity structure also has important implications for the interpretation of the center-to-limb variation of solar line profiles. A long-standing problem has been that the profiles at disk center have a characteristic V-shaped appearance, suggestive of macroturbulence, while those at the limb have a U-shaped appearance, suggestive of microturbulence. Moreover, the microturbulent velocities derived from limb profiles are typically larger than those derived from the same lines at disk center.

This result has been advanced as evidence for *anisotropic* turbulence (a situation difficult to understand hydrodynamically). Both of these effects can be understood, at least qualitatively, in terms of a finite eddy density for the velocity field (226). If  $n_0(\tau)$  gives the eddy density at  $\mu = 1$ , then the appropriate density at other values of  $\mu$  is  $n_0(\tau)/\mu$ ; this follows from the requirement that the turbulence be isotropic, so that we encounter the same eddy density per unit path-length *along the ray*. If the density is *depth-independent*, equation (14-53) is unaltered except that we replace  $n$  with  $n_0$ , and now  $A_0 = \alpha\mu(1 + \alpha\mu)^{-1}$ . In general,  $n_0(\tau)$  must vary with  $\tau$ . Suppose we demand that the eddies have constant *geometrical size L*; then  $n_0(\tau) = [\chi_c(\tau)L]^{-1}$ . For the HSRA  $\chi_c(\tau) \propto \tau$ , hence  $n_0(\tau) \propto \tau^{-1}$ . Thus the eddy density pertinent to observations near the limb must be higher than at disk center, and this result provides at least a qualitative explanation of the center-to-limb effects mentioned above. An analysis of the Mg I  $\lambda 4571$  line has been performed (226) using the HSRA. A good fit to the profiles is obtained with *isotropic* turbulence characterized by  $\xi = 1.2 \text{ km s}^{-1}$  and  $l \approx 70 \text{ km}$ . The smaller value for  $l$  quoted here, compared to the results for O I and Fe I mentioned earlier, may reflect the fact that this analysis is based on a Kubo–Anderson discontinuous velocity field while the other uses a continuous field. It turns out that for a *given*  $\xi$ , a given line-strength is always achieved at a *smaller* value of  $l$  in the discontinuous case (237).

Non-LTE effects produce line profiles that are deeper in the core, and approach the LTE profile in the wing (227; 236). The deviations of the non-LTE profiles from their LTE counterparts become larger as the turbulent velocity parameter  $\xi$  increases, and as the correlation length  $l$  decreases. Much useful information about the nature of velocity fields in stellar atmospheres will undoubtedly emerge from further detailed application of the methods described above to the analysis of the solar spectrum, and to stellar spectra where possible.

## 14-2 Sobolev Theory

The existence of large-scale, rapid (sometimes violent) *expansion* in stellar atmospheres is well established observationally. Probably the first objects in which such motions were unequivocally recognized were the *novae* (and later the *supernovae*). In their spectra, after the explosive increase in the star's luminosity, one observes absorption lines strongly violet-shifted from their rest positions, indicating material flowing rapidly toward the observer. These lines are accompanied by extensive red-shifted emission features, resulting in characteristic *P-Cygni profiles* resembling those in Figure 14-6. In nova spectra these features are transients, and indicate episodes of violent ejection of the outer layers of the star. In other objects [the *classical P-Cygni stars* (79; 366)], these lines, though variable, are more-or-less permanently present in the spectrum, and indicate persistent outflow of material. Beals first recognized (75; 77) that the great breadths of lines in WR spectra (indicating velocities of the order of  $3000 \text{ km s}^{-1}$ ) could be interpreted in terms of rapid outflow of material. He suggested that the flow was driven by radiation pressure, a conclusion supported by current dynamical models. Similar conclusions can be reached for the Of stars. We know today that in the WR and Of stars, and in many early-type supergiants, there are *transsonic stellar*

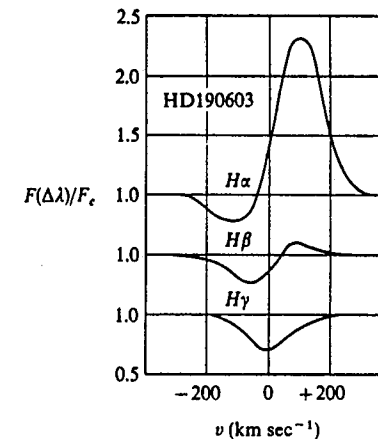


FIGURE 14-6  
P-Cygni profiles of the hydrogen lines in the spectrum of HD 190603 as observed by Beals (79). Ordinate: observed flux in units of the continuum (successive profiles are displaced for clarity). Abscissa: displacement from line center in velocity units—i.e.,  $v = c \Delta\lambda/\lambda$ .

winds (cf. §15-4), that have vanishingly-small outward velocities in the deeper layers, and a large outward acceleration producing very large velocities ( $v/c \approx 0.01$ ) at great distances from the star.

The solution of the transfer equation in a spherical expanding medium is difficult, and in the early work by Beals (75; 76; 77; 78), Chandrasekhar (149), Gerasimović (243), and Wilson (674) it was assumed that the material was *optically thin* so that transfer effects could be ignored. This approach, while obviously oversimplified, has nevertheless contributed a good deal to our basic picture of the physical situation. A major advance occurred with the brilliant realization by Sobolev (590; 591; 15, Chap. 28) that the presence of the velocity gradient in an expanding medium actually simplifies line-transfer problems, for it dominates the photon *escape and thermalization process*, and implies a *geometric localization of the source function* not present in static problems. In Sobolev's theory the solution of the transfer problem is, in effect, replaced by the calculation of *escape probabilities*; the basic theory has been refined and extended by Castor (134), and has been applied to fairly realistic calculations of spectra from multilevel atoms in WR envelopes (139; 140).

#### SURFACES OF CONSTANT RADIAL VELOCITY

Consider a spherically-symmetric, radially-expanding envelope surrounding a star with a fairly well-defined photospheric surface, as sketched in Figure 14-7. With this basic model we can explain qualitatively the main features of P-Cygni profiles such as those in Figure 14-6. For the discussion in this subsection, we shall assume that the envelope is essentially transparent, so that every photon emitted towards an external observer can be received. This approach yields insight, and results that will be useful later. Throughout the discussion we make use of the fact that most of the line emission (or absorption) occurs at line center; thus radiation from a given region, as received by an external observer, appears mainly at the line-center frequency, Doppler-shifted by an amount corresponding to the velocity of the material along the line of sight.

The material behind the stellar disk is in an *occulted region*, and cannot be seen by an external observer. The matter projected on the stellar disk can either (a) simply emit radiation without significant reabsorption as occurs in, e.g., a forbidden line in a nebula or in a thermally excited medium where  $T_e \gg T_c$  (the color temperature of the radiation from the underlying photosphere), or (b) absorb the incident photospheric radiation and scatter it out of the line of sight. From this material, in case (a) we would obtain a violet-shifted emission feature, while in (b) we obtain a violet-shifted absorption dip characteristic of P-Cygni profiles. From the matter in the emission

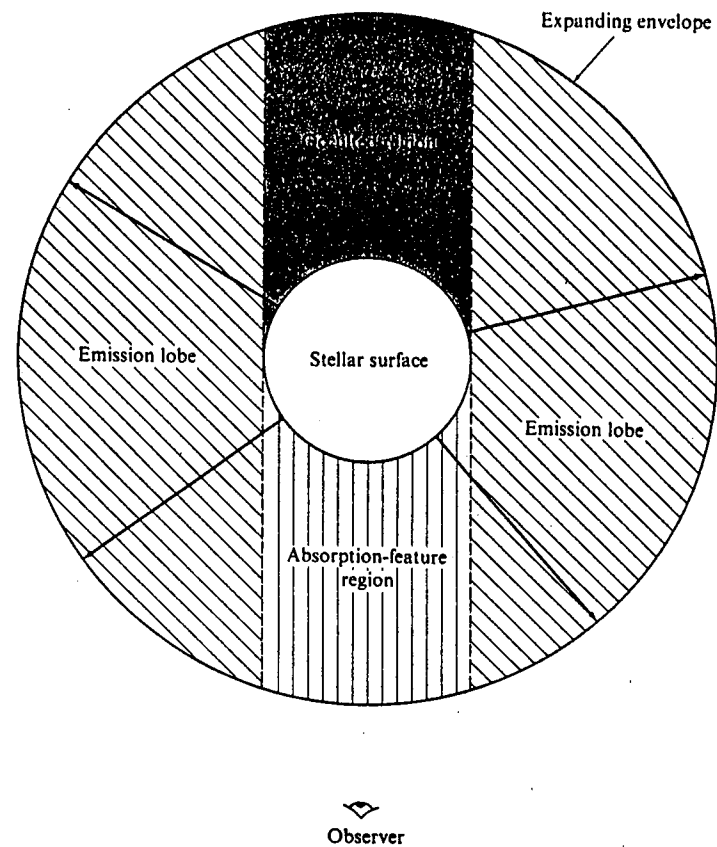


FIGURE 14-7

Schematic diagram of expanding envelope surrounding a stellar surface. The material in the *occulted region* is blocked from view by the stellar disk, and cannot be seen by an external observer.

lobes to the sides of the disk, we receive photons either emitted thermally or scattered from both the stellar and diffuse (from the envelope itself) radiation fields. The velocities along the line of sight in the emission-lobe material range from positive through negative values, and produce a symmetric emission feature extending from a wavelength to the violet of the rest-wavelength, to redder wavelengths. Because material is occulted by the star, the maximum redshifts that could be produced will not be observed, and, in general, we expect to derive information about the *maximum flow*

velocities from the position of the *blueward edge* of the absorption feature (or emission feature if no absorption is present). The volume of the emitting region can be enormous compared to that of the star, and the integrated contributions to the observed emission line from this volume may far outweigh the amount of energy received from the stellar disk. As a result, the peak intensities in strong emission lines may be several times the background continuum value (see Figures 14-6 and 14-9). Also, when the size of the stellar disk is much smaller than that of the emission region, occultation effects become unimportant. Finally, some lines are much more opaque than others and may, therefore, have a larger effective volume for emission; thus in Figure 14-6 we see a transition from quite strong emission at  $H\alpha$ , to practically no emission at  $H\gamma$ , where we see essentially the photospheric  $H\gamma$  absorption-line.

To make these notions more quantitative, we can compute the energy received at frequency  $v$  by an external observer as

$$E_v = \int_V \eta(r, v) d^3r \quad (14-58)$$

where the integration is carried out over the entire unocculted volume. In performing the integration we may use, as was done in our earlier work in spherical geometry, either  $(r, \theta)$  coordinates with the axis of symmetry from the center of the star through the observer, or  $(p, z)$  coordinates (see Figure 7-27). Equation (14-58) can be made more explicit if we write  $\eta(r, v) = \tilde{\eta}(r)\phi[v - v_0(1 + \mu v_r/c)]$ , which accounts for the shift of line center, as seen by an external observer, to  $v_0(1 + v_z/c)$ , where  $v_z = \mu v$ , is the velocity along the line of sight resulting from the expansion velocity  $v_r$ . If we suppose that  $\tilde{\eta}(r) = \eta_0(\rho/\rho_0)^\alpha$ , (where reasonable values for  $\alpha$  lie in the range  $0 \leq \alpha \leq 2$ ) and, further, assume  $v = v_0(r/r_0)^\alpha$ , then from the requirement of continuity,  $\rho v r^2 = \rho_0 v_0 r_0^{-2}$ , we obtain finally  $\tilde{\eta}(r) = \eta_0(r/r_0)^{-(n+2)\alpha}$ . Choose units such that  $r_0 = v_0 = 1$  (these quantities referring to values at the photospheric surface), and measure frequency displacements from line center in units  $x = (v - v_0)/\Delta v_D$ , where  $\Delta v_D \equiv v_0 v_0/c$ . Then

$$E_x = \eta_0 \int_V \phi[x - \mu v(r)] r^{-(n+2)\alpha} d^3r \quad (14-59)$$

In principle  $V$  refers to the entire unocculted volume; in actuality the volume of integration can be defined more precisely.

Most of the emission observed at frequency  $x$  will arise from regions where the line center frequency, after Doppler shifting, is at the observed value. The observed flow velocities (up to  $3000 \text{ km s}^{-1}$ ) in WR and Of atmospheres vastly exceed the thermal velocity ( $\sim 30 \text{ km s}^{-1}$ ). Therefore the geometrical region from which the emission at any one frequency arises must be a very

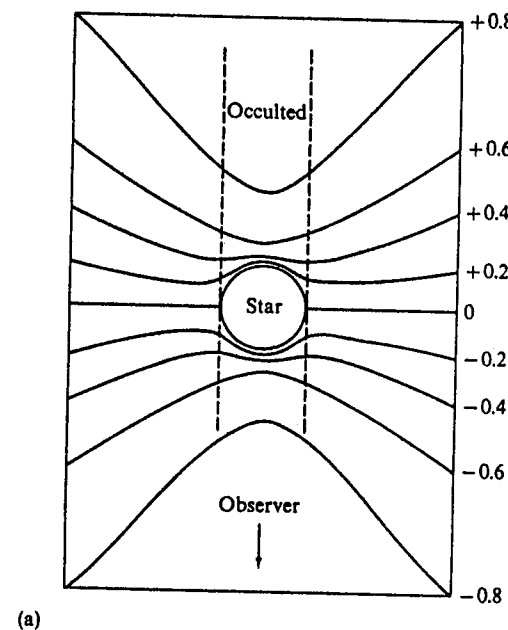
thin zone, centered on a *surface of constant radial velocity* such that  $v_z = \mu v_r = x$ . (NOTE: here the term "radial velocity" has the usual astronomical meaning of velocity *along the line of sight*, not the more fundamental meaning of the velocity  $v_r$  measured from the center of the star.) In the idealized limit that the width of the line profile is negligible (because  $v_{\text{thermal}} \ll v_{\text{flow}}$ ), the zones degenerate to the radial velocity surfaces themselves, which therefore play a basic role in the theory.

The shape of these surfaces depends upon the nature of the velocity field—which, ultimately, must be obtained from *dynamical* calculations. We can gain insight, however, by consideration of some simple velocity laws of the form  $v = r^n$  (in units  $v_0 = r_0 = 1$ ). (a) Suppose  $v_r = \text{constant}$ . This law could apply to a thin spherical shell (e.g., a planetary nebula at large distance from the star), or in high-velocity flows nearing terminal velocity [see (c) below]. (b) Suppose  $v = r$ . This law could apply in the case of an explosive ejection that started at some time  $t_0$  such that  $(t - t_0) = r/v$ ; here the faster-moving particles outrun the slower ones, giving the linear relation of  $v$  with  $r$ . (c) Suppose the gas leaves the star with velocities greater than escape velocity. We then can write  $v = v_\infty(1 - r_c/r)^\frac{1}{2}$ , which provides a crude simulation of a transsonic wind; the flow accelerates everywhere on the range  $r_c \leq r \leq \infty$ . (d) If the material is ejected with just the escape velocity and is decelerated by gravity, we may take  $v = r^{-\frac{1}{2}}$ . Each of these laws has a distinctive set of constant radial-velocity surfaces.

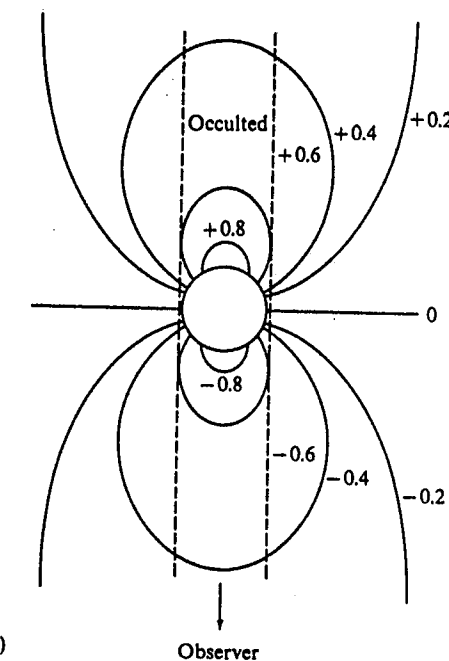
*Exercise 14-5:* Show that the surfaces  $v_z = \text{constant}$  for cases (a) and (b) are the cones  $\theta = \cos^{-1} \mu = \text{constant}$ , and the planes  $z = \text{constant}$ , respectively, in the usual  $(r, \theta)$  and  $(p, z)$  coordinate systems.

The constant-radial-velocity surfaces for laws of the form (c) and (d) are shown in Figure 14-8 (a and b).

From what has been said above, some far-reaching conclusions can be drawn. The fact that the surfaces of constant radial velocity extend over large regions (infinite if the flow is not decelerating) implies a complete breakdown of the *Eddington-Barbier relation* for expanding atmospheres. We can no longer associate a given frequency in the line profile with a specific position  $r$  in the envelope, but only with a wide range of values  $(r, r + \Delta r)$ . From the viewpoint of an outside observer, geometric localization occurs only if variations in total particle density and ionization-excitation equilibria confine the region of high emissivity. What is worse, this conclusion is independent of the intrinsic line-strength (317). So we can no longer, in principle, obtain a depth-analysis of atmospheric structure, with a precision better than the characteristic  $\Delta r$  defined above, by examining weak and strong lines. Clearly these considerations imply severe modeling and diagnostic



(a)



(b)

FIGURE 14-8

Surfaces of constant radial velocity,  $v_z = \text{constant}$ .

(a)  $v(r) = v_x(1 - 1/r)^{\frac{1}{2}}$ . Curves are labeled with  $v_z/v_x$ .

(b)  $v(r) = r^{-\frac{1}{2}}$ . From (366), by permission.

problems for expanding atmospheres. The problems are even more severe in the case of decelerating flows where, as can be seen in Figure 14-8b, a particular line of sight may intersect a surface of constant radial velocity at two distinct points; hence two regions, which may have vastly different physical properties, contribute to the information received by the observer. Furthermore, in this case these two distinct regions can also interact radiatively, and the Sobolev method to be described below requires reformulation.

Taking into account the geometry of the surfaces of constant radial velocity, equation (14-59) can be applied to calculate observable line profiles. For instance, as Beals first showed (75; 76; 77; 78), if we can ignore occultation, then the profile from an optically thin shell expanding with  $v = \text{constant}$  is *flat-topped*; an example of such a profile appears in Figure 14-9, where the  $\lambda 5696$  line of C III and the  $\lambda 5808$  line of C IV in the spectrum of the hot WR star HD 165763 are shown. The rounded profile for the C IV line indicates it is *optically thick* (see below). Beals's result can be seen by inspection of equation (14-59) using an  $(r, \theta)$  coordinate system. We note that radiation at each value of  $v_z$  (and hence of  $x$  in the line profile) is contributed by a conical volume element centered on  $\mu \equiv \cos \theta = x$ , in a range  $d\mu$ ; the volumes of all such elements are manifestly identical. Results for other velocity laws may easily be derived so long as the line is *optically thin*; this approximation will *not* be true in general, and the need for it is overcome by Sobolev's method.

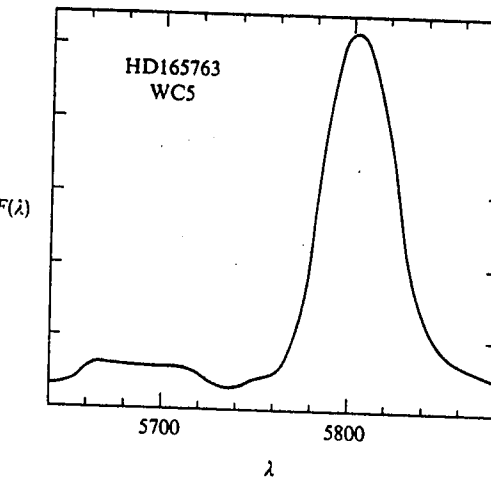


FIGURE 14-9

Observed profiles of C III  $\lambda 5696$  and C IV  $\lambda 5808$  in the WC5 star HD 165763. Notice the flat-topped profile for the transparent  $\lambda 5696$  line, and the rounded profile for the optically-thick  $\lambda 5808$  line. From (369), by permission.

**Exercise 14-6:** (a) Suppose that the intrinsic line profile is  $\phi(x) = \delta(x)$ . Consider an envelope for which  $v \equiv v_0 = 1$ . Ignoring occultation, show that  $E_x = E_0 = \text{constant}$  for  $-1 \leq x \leq 1$ , and  $E_x = 0$  for  $|x| > 1$ . Derive expressions for  $E_0$  from equation (14-59), and show that different results are obtained for  $\alpha < 1.5$ ,  $\alpha = 1.5$ , and  $\alpha > 1.5$ . Show that for  $\alpha \leq 1.5$  the envelope must be bounded,  $r \leq R$ , but that no restriction is required for  $\alpha > 1.5$ . Accounting for occultation, show that  $E_x = 0$  for  $x < x_{\min}$ , where  $x_{\min} = -(1 - R^{-2})^{\frac{1}{2}}$ , and write an expression for  $E_x$  on the range  $x_{\min} \leq x \leq 0$ . (b) Perform a similar analysis for  $v = r$ ; determine  $E_0$  for appropriate ranges of  $\alpha$ , and derive analytical expressions for the profiles of  $E_x/E_0$ , including occultation effects.

#### ESCAPE AND THERMALIZATION IN AN EXPANDING MEDIUM

Consider now the formation of a line in an optically-thick expanding envelope surrounding an opaque core of radius  $r_c$ ; assume that the effects of a background continuum can be ignored. If we now transform to a coordinate system at rest with respect to a particular fluid element, and inquire what happens as we look along a given ray, it is clear that (as a result of the velocity gradient) there will be a differential Doppler shift of each successive sample-point along the ray relative to the test-point. Eventually this shift becomes so large that no line photon emitted within the effective bounds of the line profile (assumed to be limited by some  $\pm x_{\max}$ ) can interact with the line profile at the test point. The velocity field has introduced an *intrinsic escape mechanism* for photons; beyond the interaction limit (measured from the point of emission) they no longer can be absorbed by the material (even if it is of infinite extent!) but escape freely to infinity. Thus there is a definite limit to the size of the region within which photons emitted, or scattered, can have any effect upon the intensity within the line at the test-point. In the limit of large velocity gradients the *interaction region* will be small, and may, therefore, be presumed to be *nearly homogeneous* in its physical properties (temperature, density, ionization state, etc.). The theory then can be formulated in terms of *local quantities*, and a parameter  $\beta$  that gives the *probability of photon escape* summed over all directions and line-frequencies. In the limit of negligible transfer effects, we can therefore write

$$J(r) = (1 - \beta)S(r) + \beta_c I_c \quad (14-60)$$

The first term is derived from the value that  $J$  would have in the limit of no escapes, namely  $J = S$ , corrected for velocity-induced escapes. The parameter  $\beta_c$  measures the probability of penetration (summed over frequency and angle) of the specific intensity  $I_c$ , emitted from the core, to the test-point. We must now calculate  $\beta$  and  $\beta_c$ .

As was done earlier, we measure velocities in units of a thermal velocity [i.e.,  $V(r) = v(r)/v_{th}$ ] and frequency displacements from line center in Doppler units, [i.e.,  $x \equiv (v - v_0)/\Delta\nu_D$ , where  $\Delta\nu_D \equiv v_0 v_{th}/c$ ]. The optical depth along a ray to an observer at infinity can then be written [cf. equation (14-22)]

$$\tau(z, p, x) = \int_z^\infty \chi(z', p, x) dz' = \int_z^\infty \chi_i(r') \phi(x') dz' \quad (14-61)$$

where  $r' \equiv (z'^2 + p^2)^{\frac{1}{2}}$ ,  $\mu' \equiv (z'/r')$ , and

$$x' = x'(z', p, x) \equiv x - V_z(z') = x - \mu' V(r') \quad (14-62)$$

The main contribution to the integral in equation (14-61) must come from the region where  $x' = 0$ —i.e., from  $z' = z_0(p, x)$ , where  $z_0$  is chosen such that  $z_0 r_0^{-1} V(r_0) = x$ ; here  $r_0 \equiv (z_0^2 + p^2)^{\frac{1}{2}}$ . The surface  $z_0(p, x)$  is, of course, just a surface of constant radial velocity. To a good approximation, we can then replace  $\chi_i(r')$  with  $\chi_i(r_0)$ , and remove this factor from the integral. We now change the variable of integration from  $z'$  to  $x'$ ; in view of equation (14-62) the transformation is

$$\begin{aligned} -(\partial x'/\partial z)_p &= (\partial V_z/\partial z)_p = (\partial \{\mu(z, p)V[r(z, p)]\}/\partial z)_p \\ &= \mu^2(\partial V/\partial r) + (1 - \mu^2)(V/r) \equiv Q(r, \mu) \end{aligned} \quad (14-63)$$

where  $\mu$  and  $r$  are again understood to be functions of  $z$  and  $p$ . If the interaction region is small, the transformation coefficient written above may be assumed to be essentially constant and may be evaluated at the resonance point  $z = z_0(p, x)$ . Then if we define

$$\Phi(x) \equiv \int_{-\infty}^x \phi(\xi') d\xi' \quad (14-64)$$

where clearly  $\Phi(-\infty) = 0$ , and  $\Phi(\infty) = 1$ , we can rewrite equation (14-61) as

$$\tau(z, p, x) = \tau(-\infty, p, x)\Phi[x'(z, p, x)] \quad (14-65)$$

where  $x'(z, p, x)$  is defined by equation (14-62) and

$$\tau(-\infty, p, x) = \chi_i(r_0)/Q(r_0, \mu_0) \equiv \tau_0(r_0)/\{1 + \mu^2[(d \ln V/d \ln r) - 1]\}_0 \quad (14-66)$$

Here  $\chi_i(r_0) = (\pi e^2/mc)f_{ij}[n_i(r_0) - (g_i/g_j)n_j(r_0)]/\Delta\nu_D$  (14-67)

and  $\tau_0(r_0) \equiv \chi_i(r_0)/(V/r)_0$  (14-68)

In equations (14-66) through (14-68) it should be borne in mind that  $r_0$  and  $\mu_0$  are functions of  $p$  and  $x$ , i.e.,  $r_0 = r_0[z_0(p, x), p]$  and  $\mu_0 = \mu_0[z_0(p, x), p]$ .

Let us now choose a fixed value of  $r$  and calculate  $\beta(r)$ ; because of spherical symmetry, integration over  $\mu$  can be effected by using the above results for various values of  $p$ . The escape probability along any ray is just  $\exp(-\Delta\tau_\infty)$  where  $\Delta\tau_\infty$  denotes the optical path length from the test-point to infinity. Thus, summing over angle and frequency, we have

$$\beta(r) = \frac{1}{2} \int_{-1}^1 d\mu \int_{-\infty}^{\infty} dx \phi[x'(z, p, x)] \exp\{-\tau[z(r, \mu), p(r, \mu), x]\} \quad (14-69)$$

Here we have assumed that photons that hit the opaque core are absorbed and hence lost. To evaluate equation (14-69), we use equations (14-64) through (14-67), and assume that the material in the interaction region is sufficiently homogeneous that the distinction between  $r_0$  and  $r$  may be ignored. Then

$$\begin{aligned} \beta(r) &= \frac{1}{2} \int_{-1}^1 d\mu \int_0^1 d\Phi \exp[-\chi_i(r)\Phi/Q(r, \mu)] \\ &= \chi_i^{-1}(r) \int_0^1 \{1 - \exp[-\chi_i(r)/Q(r, \mu)]\} Q(r, \mu) d\mu \end{aligned} \quad (14-70)$$

For the special case that  $V = kr$ ,  $Q(r, \mu) \equiv k$ , and equation (14-70) reduces considerably to

$$\beta(r) = \{1 - \exp[-\tau_0(r)]\}/\tau_0(r) \quad (14-71)$$

where now  $\tau_0(r) \equiv k^{-1} \chi_i(r)$ . The same result is obtained if the angle-dependent terms in equation (14-63) are merely ignored.

To calculate  $\beta_c$ , assume that the test point is relatively far from the core (i.e., that the surface of the core is at  $-\infty$ ). Then, from its physical meaning,  $\beta_c$  can be written

$$\begin{aligned} \beta_c(r) &= \frac{1}{2} \int_{-1}^{-\mu_c} d\mu \int_0^1 d\Phi \exp[-\chi_i(r)\Phi/Q(r, \mu)] \\ &= \chi_i^{-1}(r) \frac{1}{2} \int_{\mu_c}^1 \{1 - \exp[-\chi_i(r)/Q(r, \mu)]\} Q(r, \mu) d\mu \end{aligned} \quad (14-72)$$

where  $\mu_c \equiv [1 - (r_c/r)^2]^\frac{1}{2}$ . Again, for the special case of a linear velocity law we obtain a considerable reduction, namely  $\beta_c(r) = W\beta(r)$ , where  $W$  is the usual dilution factor given by equation (5-36). The result just quoted is what would be expected physically, because  $W$  is the fraction of the full sphere contained in the solid angle subtended by the disk, while  $\beta$  measures the probability of penetration from the disk to the test point.

Note that both  $\beta$  and  $\beta_c$  are defined essentially in terms of local quantities: the local opacity and velocity gradient. Given these values, one can compute  $J$  from equation (14-60) without actually solving a transfer equation; thus we see the enormous simplification that has been achieved. For the particular case of a two-level atom, where the source function (assuming complete redistribution) is given by  $S = (1 - \varepsilon)J + \varepsilon B$ , we may use equation (14-60) to write

$$S = [(1 - \varepsilon)\beta_c I_c + \varepsilon B]/[(1 - \varepsilon)\beta + \varepsilon] \quad (14-73)$$

which shows that knowledge of  $\beta$  and  $\beta_c$  is sufficient to determine  $S$ . Further, if we ignore the continuum contribution ( $\beta_c I_c = 0$ ), equation (14-60) allows us to write the net radiative bracket for each line of a multilevel atom immediately, namely  $Z_{ji} \equiv \beta_{ij}$ ; we shall exploit this result in the discussion of multilevel atoms.

It is very instructive to consider a uniformly expanding plane-parallel atmosphere, for then we can obtain expressions that show the effects of the velocity gradient on the thermalization of the source function in a particularly transparent way [see (273, 87) and (406)]. Let  $\tau$  denote the integrated line optical depth defined for a medium at rest; assume the velocity gradient  $\gamma = \partial V/\partial t$  is everywhere constant. The specific intensity at a test point  $\tau$  in direction  $\mu$  is

$$I(\tau, \mu, x) = \int_{\tau}^{\infty} S(\tau') \exp\left[-\mu^{-1} \int_0^{(\tau' - \tau)} \phi(x + \gamma\mu t) dt\right] \phi[x + \gamma\mu(\tau' - \tau)] d\tau'/\mu \quad (14-74)$$

Thus the source function for a two-level atom is given by the integral equation

$$S(\tau) = (1 - \varepsilon)J(\tau) + \varepsilon B(\tau) = (1 - \varepsilon) \int_{-\infty}^{\infty} K_{\beta} |\tau' - \tau| S(\tau') d\tau' + \varepsilon B(\tau) \quad (14-75)$$

where the kernel function

$$K_{\beta}(s) \equiv \frac{1}{2} \int_{-\infty}^{\infty} dx \int_0^1 d\mu \mu^{-1} \phi(x) \phi(x + \gamma\mu s) \exp\left[-\mu^{-1} \int_0^s \phi(x + \gamma\mu t) dt\right] \quad (14-76)$$

It is easy to show that, unlike the static case where the kernel is normalized to unity, in the present case the effects of escapes lead to

$$\int_{-\infty}^{\infty} K_{\beta} |\tau| d\tau = 1 - \beta \quad (14-77)$$

where  $\beta$  is the planar-atmosphere escape probability that follows from equations (14-70) and (14-63) in the limit that  $1/r \rightarrow 0$ , namely

$$\beta = |\gamma| \int_0^1 \{1 - \exp[-1/(|\gamma| \mu^2)]\} \mu^2 d\mu \quad (14-78)$$

*Exercise 14-7:* Verify equations (14-77) and (14-78).

Equation (14-75) may be cast into the standard form for a two-level atom by renormalizing the kernel to  $K^*(\tau) = K_p(\tau)/(1 - \beta)$ , and defining  $1 - \varepsilon^* = (1 - \beta)(1 - \varepsilon)$  and  $B^*(\tau) \equiv \varepsilon B(\tau)/\varepsilon^*$ . Then

$$S(\tau) = (1 - \varepsilon^*) \int_{-\infty}^{\infty} K^* |\tau' - \tau| S(\tau') d\tau' + \varepsilon^* B^*(\tau) \quad (14-79)$$

When thermalization is achieved,  $S$  varies slowly and may be removed from under the integral to yield  $S(\tau) = B^*(\tau) = \varepsilon B(\tau)/(\varepsilon + \beta - \varepsilon\beta)$ . For  $\varepsilon \gg \beta$ ,  $S(\tau) \rightarrow B(\tau)$ , as expected. But for  $\beta \gg \varepsilon$ , escapes dominate and  $S(\tau) \rightarrow \varepsilon B(\tau)/\beta$ , showing that  $S$  decreases to the local creation rate  $\varepsilon B$  as  $\beta \rightarrow 1$ , which is reasonable on physical grounds. If the medium has a boundary surface and  $B$  is constant, then [cf. (406)]

$$S(0) = (\varepsilon^*)^{\frac{1}{2}} B^* = \varepsilon B / (\varepsilon^*)^{\frac{1}{2}} \quad (14-80)$$

Thus when  $\varepsilon \gg \beta$  we recover the usual static result  $S(0) = \varepsilon^{\frac{1}{2}} B$ , while for  $\beta \gg \varepsilon$ , we find  $S(0) = \varepsilon B / \beta^{\frac{1}{2}} = \beta^{\frac{1}{2}} S_{\infty}$ , where  $S_{\infty}$  denotes the asymptotic value for  $S$  at depth.

#### LINE PROFILES

Let us now derive expressions for the line profiles seen by an external observer. The flux emergent at frequency  $x$  is proportional to

$$\begin{aligned} F_x &= 2\pi \int_0^{\infty} I(\infty, p, x) p dp \\ &= 2\pi \int_{r_c}^{\infty} S(r_0) \{1 - \exp[-\tau(-\infty, p, x)]\} p dp \\ &\quad + 2\pi \int_0^{r_c} S(r_0) \{1 - \exp[-\tau(-\infty, p, x)\Phi(x_c)]\} p dp \\ &\quad + 2\pi I_c \int_0^{r_c} \exp[-\tau(-\infty, p, x)\Phi(x_c)] p dp \end{aligned} \quad (14-81)$$

where, as above,  $r_0$  denotes the value of  $r$  at the surface of constant radial velocity specified by  $x$ , and  $x_c$  is the value of  $x'$  given by equation (14-62) at  $r' = r_c$  and  $\mu' = [1 - (p/r_c)^2]^{\frac{1}{2}}$ . The first term gives the emission from the part of the envelope seen outside the disk (i.e.,  $p > r_c$ ). The second term

gives the emission from the part of the envelope superposed on the core, the factor  $\Phi(x_c)$  correcting for occultation of material by the core. Note that, for an expanding atmosphere,  $\Phi(x_c)$  equals zero for  $x < 0$  and will be essentially unity for  $x > 0$ , showing immediately the effect of core occultation on the red wing of the profile. The last term gives the continuum contribution from the core; in view of the properties of  $\Phi(x_c)$  just mentioned, we see that it is unattenuated in the red wing, and more or less heavily attenuated in the blue wing of the line. The flux in the continuum outside the line is proportional to

$$F_c = 2\pi I_c \int_0^{r_c} p dp = \pi r_c^2 I_c \quad (14-82)$$

Transforming the variable of integration from  $p$  to  $r$  on surfaces  $(z/r)V(r) = x$ , equations (14-81) and (14-82) can be combined to yield an expression for the line profile  $R_x \equiv (F_x - F_c)/F_c$ , namely

$$\begin{aligned} R_x &= 2(r_c^2 I_c)^{-1} \int_{r_{\min}(x)}^{\infty} S(r) [\tau_0(r)/\tau(-\infty, p, x)] \{1 - \exp[-\tau(-\infty, p, x)]\} r dr \\ &\quad - 2(r_c^2 I_c)^{-1} \int_0^{r_c} S(r_c) \{\exp[-\tau(-\infty, p, x)\Phi(x_c)] \\ &\quad - \exp[-\tau(-\infty, p, x)]\} p dp \\ &\quad - 2r_c^{-2} \int_0^{r_c} \{1 - \exp[-\tau(-\infty, p, x)\Phi(x_c)]\} p dp \end{aligned} \quad (14-83)$$

where  $r_{\min}(x)$  is the radius at which  $V(r) = x$ , and  $p$  is regarded as  $p(r, x)$ . Note the change in sign convention [relative to equation (8-2)] that has been made to give positive numbers for emission lines. Each term in equation (14-83) can be interpreted in parallel with terms in equation (14-81).

If we ignore the last two terms, from the core, in equation (14-83), we consider a two-level atom for which the envelope is so thick that the source function achieves its asymptotic value  $S = \varepsilon B/\beta$ , and we replace  $\tau(-\infty, p, x)$  with  $\tau_0$ , then, in view of equation (14-71), we may write

$$R_x \approx \frac{\langle \varepsilon B \tau_0 \rangle}{I_c} \int_{r_c}^{\infty} \frac{\varepsilon B \tau_0}{\langle \varepsilon B \tau_0 \rangle} \frac{2r dr}{r_c^2} = \frac{A \langle \varepsilon B \tau_0 \rangle}{I_c} \quad (14-84)$$

where  $\langle \varepsilon B \tau_0 \rangle$  is a typical value of  $\varepsilon B \tau_0$ ; here the quantity  $A$  denotes the effective emitting area measured in core units. For sufficiently large effective emitting areas, the line can become quite bright relative to the continuum. In fact, most strong emission lines result largely from this geometrical effect.

Another interesting result follows easily from equation (14-81) [see, e.g., (15, Chap. 28)]. Consider an envelope with constant velocity of expansion  $V$ ; then  $Q(r, \mu) = (V/r) \sin^2 \theta$ , and the surfaces of constant radial velocity are given by  $\cos \theta = (x/V) = \text{constant}$ . The transformation from  $p$  to  $r$  is

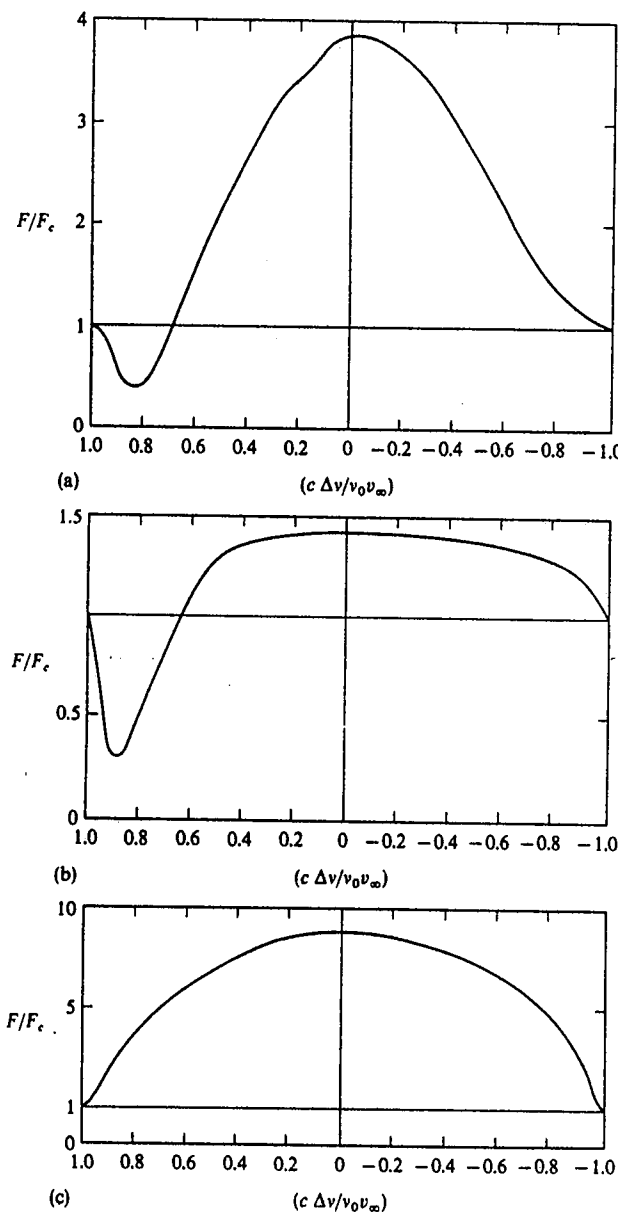


FIGURE 14-10  
Calculated line profiles in expanding spherical atmospheres.  
(a)  $\epsilon = 0.0092$  and  $\tau_0(\max) \approx 15$ . (b)  $\epsilon = 0.002$  and  $\tau_0(\max) \approx 0.5$ .  
(c)  $\epsilon = 0.021$  and  $\tau_0(\max) \approx 2$ . From (134), by permission.

$p = r \sin \theta$ , and in the limit that we can neglect the contribution from the core,

$$F_x = 2\pi \sin^2 \theta \int_0^\infty S(r) \{1 - \exp[-\chi_l(r)r/(V \sin^2 \theta)]\} r dr \quad (14-85)$$

If the envelope is *opaque*, the exponential term vanishes, and the integral becomes a constant, so that  $F_x = C \sin^2 \theta = C[1 - (x/V)^2]$ ; the line profile in this case is *rounded* (specifically, it is parabolic). This conclusion is of importance because it shows that rounded profiles occur naturally, as a result of optical-depth effects, even if the velocity is constant. In contrast, an interpretation based upon an analysis that assumes the lines are optically thin would necessarily have involved an accelerating, or decelerating, velocity field (which would, of course, have quite different dynamical implications). We thus see that the spectroscopic diagnostic procedure must be carried out with care, and to a high degree of consistency, if physically meaningful results are to be derived.

Detailed calculations of flux profiles, using equation (14-83), have been made (134) using the two-level-atom source function of equation (14-73), along with assumed distributions of  $V(r)$ ,  $\tau_0(r)$ , and the constants  $\epsilon$  and  $B/I_c$  (the latter chosen always to have the numerical value 5). The velocity law was taken to be of the form  $V(r) = V_\infty(1 - r_c/r)^\frac{1}{2}$ . The adopted distributions of  $\tau_0(r)$  all are characterized by a maximum on the range  $1.1 \leq (r/r_c) \leq 4$ . If monotone decreasing distributions are used, very asymmetric profiles (not observed) result. Presumably this indicates that the lines observed in real stars arise in shell-like zones, produced by variations in the ionization equilibrium that yield a dominance of a particular ion in a definite range of radii. A wide variety of profiles can be produced by suitable choices of the parameters. Three characteristic types of profiles, similar to those observed in WR stars, are shown in Figure 14-10: (a) rounded emission with violet absorption, such as observed in the C III  $\lambda 4650$  and N III  $\lambda 6438$  lines; (b) flat-topped emission with violet absorption, such as seen in the He I lines; (c) very intense rounded emission with no absorption, such as observed in the He II lines. In each case the intensity of the emission is proportional to  $A \langle \epsilon B \tau_0 \rangle / I_c$  as expected from equation (14-84); note that the flat-topped profile results from an optically thin line.

#### MULTILEVEL ATOMS: APPLICATION TO WOLF-RAYET STARS

In the spectra of Wolf-Rayet stars, extensive series of extremely strong emission lines can be observed. The spectra fall into two broad classes: WC, in which lines of C and O are prominent while those of N seem to be practically absent; and WN, which have prominent lines of N and essentially no lines of C. The He II Pickering series ( $n = 4 \rightarrow n'$ ) is very strong and, by

comparison of lines with odd  $n'$  (not overlapped by a hydrogen line) and even  $n'$  (blended with a hydrogen Balmer line), it is found that the hydrogen emission is weak, and hence we conclude that the hydrogen to helium ratio must be significantly less than unity. To derive quantitative information about these interesting abundance anomalies, as well as about the physical structure of the envelope, it is necessary to carry out a complete multilevel analysis of the spectrum. At present it is not possible to specify the atmospheric structure in detail, and studies (139; 140) have been carried out in the spirit of a coarse analysis (making a fair number of approximations), with the goal of obtaining estimates of the physical properties at a single typical point in the envelope.

The statistical equilibrium equations are of the form  $\mathcal{R}_i + \mathcal{C}_i = 0$  where  $\mathcal{R}_i$  and  $\mathcal{C}_i$  are, respectively, the net rates at which level  $i$  is populated by radiative and collisional processes. We have one such equation for each level of the ion under consideration, plus one additional equation specifying a total abundance for the chemical species. The net collision rate can be written (cf. §5-4)

$$\mathcal{C}_i = \sum_{j < i} [n_j - (n_j/n_i)*n_i] C_{ji} + \sum_{j > i} [(n_i/n_j)*n_j - n_i] C_{ij} + (n_i^* - n_i) C_{ik} \quad (14-86)$$

while the net radiative rate is

$$\begin{aligned} \mathcal{R}_i = & \sum_{j > i} [n_j(A_{ji} + B_{ji}J_{ij}) - n_iB_{ij}J_{ij}] + \sum_{j < i} [n_jB_{ji}J_{ji} - n_i(A_{ij} + B_{ij}J_{ji})] \\ & + n_i^* 4\pi \int_{v_i}^{\infty} \alpha_{ik}(v)(hv)^{-1} B_v(T_e) [1 - \exp(-hv/kT_e)] dv \\ & - n_i 4\pi \int_{v_i}^{\infty} \alpha_{ik}(v)(hv)^{-1} J_v [1 - b_i^{-1} \exp(-hv/kT_e)] dv \end{aligned} \quad (14-87)$$

Here  $T_e$  denotes the envelope temperature, and  $n_i^* \equiv n_k n_e \Phi_{ik}(T_e)$  [cf. equation (5-14)] where  $n_k$  is the actual ion density. The expression for  $\mathcal{C}_i$  is useful as written, for a given value of  $T_e$  and  $n_e$ , but that for  $\mathcal{R}_i$  must be rewritten. To simplify the bound-bound rates we use equation (14-60) to obtain

$$n_j(A_{ji} + B_{ji}J_{ij}) - n_iB_{ij}J_{ij} = [n_jA_{ji} - (n_iB_{ij} - n_jB_{ji})WB_v(T_e)]\beta_{ij} \quad (14-88)$$

where  $\beta_{ij}$  is given by equation (14-71), and  $\tau_{ij}$  (called  $\tau_0$  there) is given by equations (14-67) and (14-68); in equation (14-88) we have used the approximate result  $\beta_e \approx WB$ , and have parameterized  $I_e$  in terms of a radiation temperature  $T_e$ . The bound-free terms are somewhat harder to reduce, because the Doppler shifts produced by expansion scarcely affect continuum formation, and no essential simplification is introduced by intrinsic escapes, as it is for lines; in fact, a solution of the static transfer problem is, in principle,

required. To circumvent the need for a detailed solution, write  $J_v = J_v^c + J_v^d$ , where  $J_v^c$  represents the radiation emitted by the stellar core, and  $J_v^d$  is the diffuse field from the envelope. Allowing for absorption, we adopt

$$J_v^c \approx WB_v(T_e)e^{-\tau_v} \quad (14-89)$$

where a representative optical depth between the test-point ( $R$ ) and the core ( $r_c$ ) is taken to be

$$\tau_v = n_i \alpha_{ik}(v) [1 - b_i^{-1} \exp(-hv/kT_e)] (R - r_c) \quad (14-90)$$

Further, if we assume that (a) the envelope is homogeneous, and (b) the optical depth from the test point to the boundary in any direction is  $\tau_v$ , we then may adopt

$$J_v^d \approx S_{ik}(v) (1 - e^{-\tau_v}) \quad (14-91)$$

where  $S_{ik}(v) = (2hv^3/c^2)[b_i \exp(hv/kT_e) - 1]^{-1}$ . With these approximations we have rate equations of the form  $\mathcal{A}n = \mathcal{B}$  where  $\mathcal{A}$  and  $\mathcal{B}$  contain rate coefficients, line escape probabilities, and analogous continuum quantities. To solve the system, the parameters that must be specified are  $T_e$ ,  $r_c$ ,  $R$ ,  $v(R)$ ,  $T_e$ ,  $n_e$ , and the total number density  $n_{atom}$  of the species under consideration. Most of these quantities can be specified from independent considerations, and typically only  $T_e$ ,  $n_e$ , and  $n_{atom}$  are free parameters to be determined from model-fitting. The system of statistical equilibrium equations is nonlinear because the optical depths  $\tau_{ij}$ ,  $\tau_v$ , and the departure coefficients  $b_i$  in the continuum terms, depend upon the solution; it is necessary, therefore, to solve the system iteratively. The iteration may be effected using a Newton-Raphson procedure, which yields swift convergence.

To compute line-strengths we use equation (14-83) and, in the spirit of coarse analysis, we assume that  $S_{ij}$  and  $\tau_{ij}$  are constant for  $r_c \leq r \leq R$ , and ignore angular factors. Then the three contributions to the line profile are constant, and are equal to (a)  $R_e = (R^2/r_c^2)[S_{ij}/B_v(T_e)](1 - e^{-\tau_v})$  from the emission component; (b)  $R_o = -[S_{ij}/B_v(T_e)](1 - e^{-\tau_v})$  from the occulted material; and (c)  $R_a = -(1 - e^{-\tau_v})$  from the absorption component. The blue half and red half of the line profile each has a width, in wavelength units, of  $\Delta\lambda = \lambda v(R)/c$ . Thus the equivalent width (taken positive for emission) is

$$W_\lambda = (\lambda v/c)(1 - e^{-\tau_v}) \{[(2R^2/r_c^2) - 1][S_{ij}/B_v(T_e)] - 1\} \quad (14-92)$$

If occultation and absorption effects are ignored, the two terms involving “-1” in the above formula are suppressed. Equation (14-92) is only approximate, because of the assumption of homogeneity of the envelope, and could be in error by as much as a factor of two. The above results can be used to

compute intensities and line strengths if  $S_{ij}$  and  $\tau_{ij}$  (i.e., the level-populations) are known, or, alternatively, may be used in diagnostics to determine these quantities.

The methodology developed in this section has been applied (140) in a thorough analysis of the He II spectrum of two WN6 stars: HD 192163 and HD 191765. As a first step, the total line intensities (which show neither absorption components nor occultation effects) are used to establish the level populations empirically. For the line ( $u \rightarrow l$ ) the total intensity is

$$\begin{aligned} I_{ul} &\propto \int A_{ul} h v_u n_u(r) \beta_{ul}(r) dV \propto \int \eta_{ul}(r) \beta_{ul}(r) dV \\ &\propto \int S_{ul}(r) [v_0 v(r)/c] \{1 - \exp[-\tau_{lu}(r)]\} dV \end{aligned} \quad (14-93)$$

where equation (14-71) was used for  $\beta_{ul}$ , and equations (14-67) and (14-68) for  $\tau_{lu}$ . Therefore, assuming homogeneity,

$$(I_{ul}/v_{ul})^4 = K \{1 - \exp[-\tau_{lu}(R)]\} / [(g_u n_l/g_l n_u) - 1] \quad (14-94)$$

where  $K$  is the same for all lines. For any line that is optically thick, we can set the exponential term to zero; this is expected to be true for  $\lambda 4686$  ( $n = 3 \rightarrow n = 4$ ). From the observed intensities, the "reduced intensities" (relative to  $\lambda 4686$ )  $\mathcal{I}_{ul} \equiv (I_{ul}/v_{ul})^4 / (I_{43}/v_{43})^4$  can be formed. From equation (14-94),

$$\mathcal{I}_{ul} = [1 - \exp(-\tau_{lu})] [(g_4 n_3/g_3 n_4) - 1] / [(g_u n_l/g_l n_u) - 1] \quad (14-95)$$

where we have set  $\exp(-\tau_{34}) = 0$ . Further, we can write

$$\tau_{lu} = A [(n_l/g_l) - (n_u/g_u)] (g_l f_{lu} \lambda) / (n_4/g_4) \quad (14-96)$$

where  $A \equiv (\pi e^2/mc)(n_4/g_4)[R/v(R)]$  (14-97)

If we now assume that both the  $\lambda 3203$  ( $5 \rightarrow 3$ ) and the  $\lambda 10124$  ( $5 \rightarrow 4$ ) lines are also opaque, we may solve for the numerical value of  $(g_4 n_3/g_3 n_4) = \mathcal{I}_{54}(1 - \mathcal{I}_{53})/\mathcal{I}_{53}$ , and  $S_{43}$  in each star. The three lines considered thus far are, in fact, opaque, but this need not be true for higher series members which have much smaller  $f$ -values. Suppose, however, we presume that all Pickering-series line are opaque; then from equation (14-95) we can obtain empirical values for  $(g_4 n_u/g_u n_4)$ . At reasonable values of  $n_e$  and  $T_e$ , the upper levels of the  $\text{He}^+$  ion should become dominated by collisions, and their occupation numbers should have the LTE values

$$(n_u/g_u) = n_{\text{ion}} n_e \frac{1}{2} (h^2/2\pi m k T_e)^{\frac{1}{2}} \exp(\chi_u/k T_e) \quad (14-98)$$

for  $u \gtrsim 10$ . Because  $\chi_u/k T_e \ll 1$  for  $u \gg 1$ ,  $(n_u/g_u)$  should approach a constant value. This, however, is not found for the empirical values just obtained; but rather  $(n_u/g_u) \propto (f\lambda)_{4u}$ , as expected for optically thin lines because of the factor  $[1 - \exp(-\tau_{4u})] \approx \tau_{4u} \propto (f\lambda)_{4u}$  for  $\tau_{4u} \ll 1$ . We thus conclude that the upper Pickering-series lines are optically thin; this implies an upper bound on the parameter  $A$  defined in equation (14-97). By imposing the physically reasonable requirements that  $(n_u/g_u)$  (a) be a monotone decreasing function of  $u$  (i.e., no population inversions), and (b) become constant for  $u > 10$ , we may set limits on  $A$ ; the results are  $3 \lesssim A \lesssim 6$  for HD 192163, and  $2 \lesssim A \lesssim 8$  for HD 191765.

As a next step, one may use the known absolute magnitude  $M_v$  to obtain, from standard relations, the absolute continuum flux at  $\lambda 5500 \text{ \AA}$ ; if we adopt  $T_c \approx 40,000^\circ\text{K}$ , as indicated observationally, we can then deduce  $r_c \approx 13 R_\odot$ . Using the observed ratio  $F_c(\lambda 4686)/F_c(\lambda 5500)$ , we find  $F_c(\lambda 4686)$ ; then using the observed value of the emission line strength  $R_e(\lambda 4686)$  we can find  $R^2 S_{43}$ . This in turn yields  $R \approx 70 R_\odot$  because  $S_{43}$  is already known. The ratio  $(R/r_c) \approx 5-6$  is in agreement with direct interferometer measures for the WC star  $\gamma^2 \text{ Vel}$ , and also explains the absence of any occultation effects in the profiles. If we adopt  $v(R) = 1000 \text{ km s}^{-1}$  from the observed linewidths, and use the known values of  $A$  and  $R$  in equation (14-97), we deduce a numerical value for  $(n_u/g_u)$ , and hence for all  $(n_u/g_u)$ , from the empirically determined ratios  $(g_4 n_u/g_u n_4)$ . If these values are used in the Saha equation (14-98) for  $u \gtrsim 10$ , and if we adopt  $T_e \sim 10^5^\circ\text{K}$  and set  $n_e = 2n_i$  (i.e., a completely ionized atmosphere of helium), we find  $n_e \approx 5 \times 10^{11} \text{ cm}^{-3}$ , which implies that the optical depth of the envelope in electron scattering is  $\tau_e \approx n_e \sigma_e R = 1.5$ . Finally, knowing that the upper lines are optically thin, the observed excess emission in  $Pi\ 14$  (which is blended with  $H\ 7$ ) relative to  $Pi\ 15$  can be used to estimate  $n(\text{H}^+)/n(\text{He}^{++}) \approx n(\text{H})/n(\text{He}) \lesssim 0.5$ ; in these stars the helium-to-hydrogen ratio is thus enhanced by a factor of 20!

Having fixed  $r_c$ ,  $T_c$ ,  $R$ ,  $v(R)$ , and  $n_e$ , the rate equations can be solved for various assumed values of  $T_e$  and  $n(\text{He})$ ; the results yield theoretical values of  $A$  and  $(n_i/g_i)$ . Calculations (140) were done for a 30-level atom. Good agreement with the empirical results are obtained for  $n(\text{He}) \approx 2.5 \times 10^{11} \text{ cm}^{-3}$  and  $T_e \approx 10^5^\circ\text{K}$  (the fit is not unique). The calculations show that the upper levels are indeed collision dominated, and that  $b_u \rightarrow 1$  for  $u \gg 1$ . Further, because  $T_e > T_c$ , it appears that a nonradiative source of energy input is required to maintain the excitation of the envelope.

A second application of the methods described above has been made in an analysis of the C III line strengths (in the ultraviolet, visible, and infrared) observed in the WC 8 star  $\gamma^2 \text{ Vel}$  (139). In this work, independent estimates could be made of the parameters  $r_c$ ,  $T_c$ ,  $R$ , and  $v(R)$ . The values of  $T_e$ ,  $n_e$ , and  $n(\text{C}^{++})$  were determined by fitting the observed equivalent widths for

10 lines to theoretical widths obtained from equation (14-92), using occupation numbers from a model atom consisting of the lowest 14 terms of  $C^{++}$ . Transitions to higher levels and to the continuum were ignored; this compromises somewhat the accuracy of the upper-state populations. Good agreement with observations was obtained for

$$T_e = 22,000^\circ\text{K}, \quad n_e = 4 \times 10^{11} \text{ cm}^{-3}, \quad \text{and} \quad n(C^{++}) = 1 \times 10^9 \text{ cm}^{-3}$$

[having adopted  $T_c = 30,000^\circ\text{K}$ ,  $(R/r_c) = 3.6$ , and  $v(R) = 900 \text{ km s}^{-1}$ ]. The lowest four excited states are found to have a Boltzmannian distribution relative to the ground state, while the higher levels are underpopulated. Assuming that *all* the carbon is in the form  $C^{++}$ , and that all the electrons come from hydrogen, a lower bound is found for the ratio  $n(\text{C})/n(\text{H})$ —namely,  $2.5 \times 10^{-3}$ . This value exceeds the normal cosmic abundance by a factor of 8, and suggests that the carbon abundance in WC stars is indeed enhanced, and that the prominence of the carbon lines in the spectrum is a result of this enhancement. Allowing for other ions of carbon and for electrons from other sources (e.g., He) would raise the lower limit mentioned above. For  $\gamma^2 \text{ Vel}$ ,  $T_e < T_c$ , which does not present a compelling argument for nonradiative energy deposition, and even offers the possibility that the envelope may be in radiative equilibrium.

### 14-3 The Transfer Equation in the Fluid Frame

The formulations of the transfer equation discussed in the preceding sections of this chapter are all based in the stationary frame of the observer, who views the stellar material as moving. As we have seen, the complication in this approach is that the opacity and emissivity of the material become angle-dependent, owing to the effects of Doppler shifts and aberration of light. There results an inextricable coupling between angle and frequency that presents severe difficulties in the calculation of scattering terms with a discrete quadrature sum. It then becomes attractive to treat the transfer problem in a frame comoving with the fluid.

There are two strong motivations for working in the moving frame of the material. (1) From the point of view of the transfer equation itself, there is the advantage that both the opacity and the emissivity are *isotropic* in the comoving frame. Further, in problems involving partial redistribution effects, we may use the standard *static* redistribution functions. In addition, in the calculation of scattering integrals we need consider only a frequency bandwidth broad enough to contain fully the line profile; this bandwidth is *independent* of the fluid velocity. Finally, the angle quadrature may be chosen on the basis of the *angular* distribution of the radiation alone. (2) Dynamical

calculations in spherical flows (e.g., pulsation, expansion) can be handled accurately in a *Lagrangian coordinate system* (i.e., the comoving frame). The Lagrangian equations of gas dynamics are easy to formulate, and offer many physical and computational advantages. Obviously it is desirable to be able to treat the radiation field in a closely parallel way. On the other hand, a disadvantage of the comoving-frame formulation is that present methods of solution work only for relatively simple velocity fields; otherwise it becomes too difficult to pose boundary conditions on the problem (cf. Exercise 14-12 below).

In the comoving frame we shall develop both (1) the *monochromatic equation of transfer*, used for calculating, e.g., line profiles, and (2) *frequency-integrated moment equations*, which specify the total radiative contributions to the energy, momentum, and pressure of the gas-plus-radiation fluid.

To obtain expressions describing how the relevant physical variables change between the rest and the comoving frames, Lorentz transformations are applied. Here we encounter a problem: strictly speaking, a Lorentz transformation applies only when the velocity  $v$  of one frame relative to the other is *uniform* and *constant*. But in stellar atmospheres we are concerned with situations where  $v = v(r, t)$ , and hence the fluid frame is *not an inertial frame*. We must then imagine transformations taking place from uniformly-moving frames that *instantaneously* coincide with the moving fluid. Actually, the difficulty just mentioned introduces considerable complication into the analysis. It is easy to show that the form of the transfer equation is the same in two *uniformly* moving frames (i.e., the transfer equation is *covariant*), providing we account for the effects of Doppler shifts and aberration of photons when we calculate atomic properties. Further, it is straightforward to derive the behavior under transformation of the atomic properties themselves. But for *unsteady* or *steady differential flows*, new terms appear in the equations that account, in effect, for changes in the Lorentz transformation from one point in the medium to another; these terms can be derived by application of the differential operator  $(c^{-1} \partial/\partial t + \mathbf{n} \cdot \nabla)$  in the transfer equation to the transformation coefficient of the specific intensity.

#### THE LOCAL FREQUENCY TRANSFORMATION

Before discussing the details of transformation of the physical variables in the transfer equation, it is worthwhile to extract the essential physical flavor of the problem in simplest possible terms. A velocity field produces a *Doppler shift* and *aberration* of photons, and gives rise to *advection* terms describing the “sweeping up” of radiation by the moving fluid. Formally, these terms are all of order  $(v/c)$ . However, in the case of line-profiles, the effect of a frequency shift  $\Delta\nu$  becomes important not when  $\Delta\nu/v = v/c$  is significant,

but rather when  $\Delta v/\Delta v_D = (v/v_{th})$  is significant (i.e., of order unity); in essence, velocity-field Doppler effects are *amplified* a factor of  $(c/v_{th})$  by the swift variation of the line profile with frequency. To a first approximation, then, it is sufficient to consider *only Doppler shifts* and to ignore aberration and advection.

If  $v$  is a frequency seen in the observer's frame, then  $v_0 = v(1 - \mu v/c)$  is the corresponding comoving-frame frequency. The differential operator  $\mu(\partial/\partial z)$  in the observer's frame (for a time-independent, planar atmosphere) is evaluated at constant frequency  $v$ ; but if we move a distance  $\Delta z$ , holding  $v$  fixed,  $v_0 = v_0(v, z)$  will change because  $v$  changes. Thus  $(\partial/\partial z)_v \rightarrow (\partial/\partial z)_{v_0} + (\partial v_0/\partial z)_v (\partial/\partial v_0)_{z_0}$ . Clearly  $(\partial v_0/\partial z)_v = -(v_0 \mu_0/c)(\partial v/\partial z)$ , to order  $(v/c)$ . Substituting into the transfer equation we thus obtain

$$\begin{aligned} \mu_0 [\partial I^0(z, \mu_0, v_0)/\partial z] - [(\mu_0^2 v_0/c)(\partial v/\partial z)] [\partial I^0(z, \mu_0, v_0)/\partial v_0] \\ = \eta^0(z, v_0) - \chi^0(z, v_0) I^0(z, \mu_0, v_0) \end{aligned} \quad (14-99)$$

The corresponding result for spherical geometry is

$$\begin{aligned} \mu_0 \frac{\partial I^0(r, \mu_0, v_0)}{\partial r} + \frac{(1 - \mu_0^2)}{r} \frac{\partial I^0(r, \mu_0, v_0)}{\partial \mu_0} - \left( \frac{v_0 v}{cr} \right) \left[ (1 - \mu_0^2) + \mu_0^2 \left( \frac{d \ln v}{d \ln r} \right) \right] \\ \times \frac{\partial I^0(r, \mu_0, v_0)}{\partial v_0} = \eta^0(r, v_0) - \chi^0(r, v_0) I^0(r, \mu_0, v_0). \end{aligned} \quad (14-100)$$

*Exercise 14-8:* Derive equation (14-100).

Several points should be noticed about equations (14-99) and (14-100). (1) The variables  $I$ ,  $\mu$ , and  $v$  are now all in the *comoving* frame, and in that frame  $\chi$  and  $\eta$  are *isotropic*. (2) It is clear that any scattering terms need be evaluated only on a (small) definite range of  $v_0$ . (3) The transfer equation is now a *partial* differential equation. The frequency derivative accounts for the *change, with position, of a given photon frequency  $v_0$  in the comoving frame, as seen by an external observer*—or, equivalently, for the *frequency shift of photons as seen in the comoving frame*. In particular, suppose the atmosphere is *expanding* so that  $\partial v/\partial z$  (or  $\partial v/\partial r$ ) is greater than zero; we then see that photons are always systematically *redshifted* as they transfer from one point in the atmosphere to another, as expected intuitively. Note that in planar geometry only *velocity gradients* matter; in spherical geometry a net effect occurs even when  $v(r) = \text{constant}$ , because divergence of the rays still implies a *transverse velocity gradient* in this case. (4) From a mathematical point of view, equations (14-99) and (14-100) yield a *hyperbolic system of equations* [cf. (181, Chap. 5; 530, Chaps. 9 and 12; 462, Chap. 4)], and pose an *initial-boundary-value problem* requiring boundary conditions in the spatial coordinate and initial conditions in frequency to effect their

solution. We shall discuss a numerical method for solving these equations below.

Equations (14-99) and (14-100) contain all the *essential* physics of the *transfer* problem, but there are additional angle-dependent terms that have been omitted by our neglect of aberration and advection; to obtain these terms (which are important for the *fluid equations*), we must now develop the transformation properties of the relevant variables.

#### LORENTZ TRANSFORMATION OF THE TRANSFER EQUATION

We consider here transformations between the *rest system*, specified by the four coordinates  $(x^1, x^2, x^3, x^4) = (x, y, z, ict_0)$ , and the *fluid system*  $(x_0, y_0, z_0, ict_0)$ , moving relative to the rest system with a constant velocity  $v$  in the  $z$ -direction. This choice for  $v$  is the one most physically important to our work, and simplifies the calculation; generalizations for an arbitrary orientation of  $v$  are given in (621). Changes from one system to the other are effected by means of a *Lorentz transformation*, which corresponds to a *proper rotation* in four-dimensional space-time. Physically the Lorentz transformation is chosen in such a way that the equation for the wavefront of a light wave is of the *same form (covariant)* in both systems (i.e., such that the velocity of light is always  $\equiv c$  in both reference frames).

The mathematical form of the transformation is  $x_0^\alpha = L_\beta^\alpha x^\beta$  ( $\alpha = 1, \dots, 4$ ) where the Einstein convention of summing over repeated indices is employed. The transformation can be represented [cf., e.g., (392, 29; 253, 191)] by the matrix

$$L = \begin{pmatrix} 1 & 0 & 0 & 0 \\ 0 & 1 & 0 & 0 \\ 0 & 0 & \gamma & i\beta\gamma \\ 0 & 0 & -i\beta\gamma & \gamma \end{pmatrix} \quad (14-101)$$

where  $\gamma \equiv (1 - v^2/c^2)^{-\frac{1}{2}}$  and  $\beta \equiv (v/c)$ . Note that  $L$  is *Hermitian*; i.e.,  $L = L^\dagger$  where “ $^\dagger$ ” denotes the *adjoint* (i.e., conjugate transpose). Note also that  $L^{-1} = L^T$  where “ $T$ ” denotes the ordinary transpose. In matrix notation,  $x_0 = Lx$ , where  $x_0$  and  $x$  are *column vectors*. Clearly  $x = L^{-1}x_0 = L^T x_0$ ; equivalently,  $x^\alpha = (L^{-1})_\beta^\alpha x_0^\beta$ .

The Lorentz transformation can be applied to arbitrary four-vectors and to four-tensors of rank two. The transformation rules of tensor analysis assure that these quantities are covariant under the Lorentz transformation (because it is a proper rotation in four space); hence *physical laws written in terms of four-vectors and four-tensors are automatically covariant*. The transformation of an arbitrary *contravariant* four-vector  $A$  [e.g., a space-time increment  $(\Delta x, \Delta y, \Delta z, ic\Delta t)^T$ ] is defined such that  $A_0^\alpha = (\partial x_0^\alpha / \partial x^\beta) A^\beta = L_\beta^\alpha A^\beta$ , or, in matrix notation,  $A_0 = LA$ ,  $A = L^{-1}A_0$ . The transformation

of a covariant four-vector  $\mathbf{B}$  (e.g., the gradient operator  $[\partial/\partial x, \partial/\partial y, \partial/\partial z, (ic)^{-1} \partial/\partial t]^T$ ) is defined such that  $(B_0)_\alpha = (\partial x^\beta/\partial x_0^\alpha) B_\beta = (L^{-1})_\alpha^\beta B_\beta$ —which, in matrix notation, is equivalent to  $B_0^T = B^T L^{-1}$  or, transposing,  $B_0 = (L^{-1})^T B = LB$ ; also,  $B = L^{-1} B_0$ . Finally, the transformation of  $C^{\alpha\beta}$ , a contravariant tensor of rank two, is defined such that  $C_0^{\alpha\beta} = L_\gamma^\alpha L_\delta^\beta C^{\gamma\delta}$ , which (in matrix notation) is equivalent to  $C_0 = LCL^T = LCL^{-1}$  (i.e., the transformation is a similarity transformation); also we have  $C = L^T C_0 L = L^{-1} C_0 L$ . (NOTE: The word *covariant* describing the four-vector  $\mathbf{B}$  is used in a different sense from that used two sentences earlier in relation to physical laws, where it meant “of the same form”; this double meaning, however deplorable, is standard usage.)

Equipped with the transformation rules given above, we can now derive a number of important results. First, applying the transformation to the coordinates themselves it is easy to show that the measurement of intervals perpendicular to the  $z$ -axis is unaffected by the relative motion of the two frames—i.e.,  $\Delta x_0 = \Delta x$  and  $\Delta y_0 = \Delta y$ . But an object of length  $\Delta z$  at rest in the fixed frame will be measured by an observer in the moving frame to have a length

$$\Delta z_0 = \gamma^{-1} \Delta z \quad (14-102a)$$

This result is the celebrated *Lorentz–Fitzgerald contraction effect*. Likewise a time-interval  $\Delta t$  measured in the fixed frame will be measured by an observer in the moving frame to be

$$\Delta t_0 = \gamma \Delta t \quad (14-102b)$$

This is the *time-dilation effect*. From these results we conclude that a space-time volume element is *invariant*; i.e.,

$$dV dt = dV_0 dt_0 \quad (14-103)$$

a result we shall use repeatedly below. Next, applying the Lorentz transformation to the four-gradient (a covariant vector), we obtain

$$\left( \frac{\partial}{\partial x}, \frac{\partial}{\partial y}, \frac{\partial}{\partial z}, \frac{1}{ic} \frac{\partial}{\partial t} \right) = \left[ \frac{\partial}{\partial x_0}, \frac{\partial}{\partial y_0}, \gamma \left( \frac{\partial}{\partial z_0} - \frac{\beta}{c} \frac{\partial}{\partial t_0} \right), \frac{\gamma}{ic} \left( \frac{\partial}{\partial t_0} - c\beta \frac{\partial}{\partial z_0} \right) \right] \quad (14-104)$$

Let us now turn to the transformation of the radiation field and transfer-related variables [further discussion can be found in (521; 551; 621)]. For any particle, the four-momentum is  $P^\alpha = (p_x, p_y, p_z, iE/c)^T$ , where  $p_j$  is the  $j$ th component of the ordinary momentum, and  $E$  is the *total energy* of the particle. If the particle has rest mass  $m_0$ , then  $p^2 c^2 + (m_0 c^2)^2 = E^2$ , where  $p^2 = p_x^2 + p_y^2 + p_z^2$ . Photons have  $m_0 = 0$  and  $E = h\nu$ , hence  $p = h\nu/c$ , and

$$P^\alpha = (h\nu/c)(n_x, n_y, n_z, i)^T = (h\nu/c)(\mathbf{n}, i)^T \quad (14-105)$$

Here  $\mathbf{n}$  is the direction of photon propagation, and  $(n_x, n_y, n_z) = (\sin \theta \cos \phi, \sin \theta \sin \phi, \cos \theta)$ . Applying a Lorentz transformation to equation (14-105) we find

$$(v_0 n_x^0, v_0 n_y^0, v_0 n_z^0, iv_0) = [vn_x, vn_y, v\gamma(n_z - \beta), iv\gamma(1 - n_z\beta)] \quad (14-106)$$

which is equivalent to

$$\begin{aligned} [\phi_0; (1 - \mu_0^2)^{\frac{1}{2}}; \mu_0; v_0] \\ = [\phi; \gamma^{-1}(1 - \mu^2)^{\frac{1}{2}}/(1 - \mu\beta); (\mu - \beta)/(1 - \mu\beta); v\gamma(1 - \mu\beta)] \end{aligned} \quad (14-107)$$

The inverse transformation gives

$$[(1 - \mu^2)^{\frac{1}{2}}; \mu; v] = [\gamma^{-1}(1 - \mu_0^2)^{\frac{1}{2}}/(1 + \mu_0\beta); (\mu_0 + \beta)/(1 + \mu_0\beta); v_0\gamma(1 + \mu_0\beta)] \quad (14-108)$$

Equations (14-106) through (14-108) contain the familiar results for Doppler-shift and aberration; the classical results can be derived by keeping only terms of  $O(v/c)$ , (i.e., by setting  $\gamma \equiv 1$ ). From equations (14-107) and (14-108), it is easily seen that  $dv_0 = (v_0/v) dv$  and  $d\mu_0 = (v/v_0)^2 d\mu$ ; hence, using  $d\omega = \sin \theta d\theta d\phi = d\mu d\phi$ , we find

$$v dv d\omega = v_0 dv_0 d\omega_0 \quad (14-109)$$

To establish the transformation properties of the specific intensity we calculate (621) the *number* of photons passing through an area  $dS$  oriented perpendicular to the  $z$ -axis, in frequency interval  $dv$ , into solid angle  $d\omega$ , propagating at angle  $\theta = \cos^{-1} \mu$  to the  $z$ -axis, in a time  $dt$ . We suppose that  $dS$  is stationary in the rest frame; then  $N = [I(\mu, v)/hv] dw dv dS \cos \theta dt$ . This must be the same number that would be counted passing through the same surface element by an observer in the comoving frame, namely  $N_0 = [I^0(\mu_0, v_0)/hv_0] dw_0 dv_0 \times (dS \cos \theta_0 dt_0 + c^{-1} dS v dt_0)$ ; here the first term gives the number that would have been counted if  $dS$  had been stationary in the comoving frame, and the second gives the density of photons ( $I^0/hv_0 c$ ) times the volume ( $dS v dt_0$ ) swept out by  $dS$  in a time  $dt_0$ . Using equations (14-102), (14-108), and (14-109), we find

$$I(\mu, v) = (v/v_0)^3 I^0(\mu_0, v_0) \quad (14-110)$$

Next, consider the emissivity. The *number* of photons emitted from a given volume, into a specified solid angle and frequency-interval, in a definite time interval, must be the same in both frames, hence

$$(\eta_v dw dv dV dt)/hv = (\eta_v^0 dw_0 dv_0 dV_0 dt_0)/hv_0,$$

which implies that

$$\eta(\mu, v) = (v/v_0)^2 \eta^0(v_0) \quad (14-111)$$

(where we have noted explicitly that  $\eta$  is isotropic in the fluid frame). To be able to establish energy balance in any frame, we must be able to balance emission losses with absorptions; hence, from equations (14-110) and (14-111), we conclude that

$$\chi(\mu, v) = (v_0/v)\chi^0(v_0). \quad (14-112)$$

Finally, between two frames moving *uniformly* with respect to one another, the differential operator in the transfer equation transforms, using equation (14-104) and (14-106), to

$$c^{-1}(\partial/\partial t) + (\mathbf{n} \cdot \nabla) = (v_0/v)[c^{-1}(\partial/\partial t_0) + (\mathbf{n}^0 \cdot \nabla^0)] \quad (14-113)$$

We can now show that the transfer equation is, in fact, covariant, for we see from equations (14-110) through (14-113) that

$$c^{-1}(\partial I_v / \partial t) + (\mathbf{n} \cdot \nabla) I_v = \eta_v - \chi_v I_v \quad (14-114a)$$

transforms to

$$\begin{aligned} (v_0/v)[c^{-1}(\partial/\partial t_0) + (\mathbf{n}^0 \cdot \nabla^0)][(v/v_0)^3 I^0(\mu_0, v_0)] \\ = (v/v_0)^2[\eta^0(v_0) - \chi^0(v_0)I^0(\mu_0, v_0)] \end{aligned}$$

which, if  $(v/v_0)$  is a *constant*—as it will be if the two frames are in *uniform* motion with respect to one another (and *only* then)—can be written as

$$[c^{-1}(\partial/\partial t_0) + (\mathbf{n}^0 \cdot \nabla^0)]I^0(\mu_0, v_0) = \eta^0(v_0) - \chi^0(v_0)I^0(\mu_0, v_0) \quad (14-114b)$$

Obviously equations (14-114a) and (14-114b) are of the same form. Two points must be stressed. (a) Despite the similar form of the two equations, equation (14-114b) (at rest relative to the fluid) is actually much simpler because of the isotropy of  $\eta^0(v_0)$  and  $\chi^0(v_0)$ . (b) The reduction of equation (14-114a) to equation (14-114b) is *not valid if the two frames do not move uniformly with respect to each other*; i.e., this equation does not apply in, say, an expanding or pulsating atmosphere.

One approach to coping with the shortcoming mentioned above is to leave the streaming terms described by the differential operator, and the radiation field itself, in the observer's frame, but to use first-order expansions to write the source-sink terms in the comoving frame (521, Chap. 6). Thus, using equations (14-111), (14-112), and (14-107) we can write

$$\begin{aligned} [c^{-1}(\partial/\partial t) + (\mathbf{n} \cdot \nabla)]I(\mu, v) = \eta^0(v) - \chi^0(v)I(\mu, v) \\ + (\mathbf{n} \cdot \mathbf{v}/c)\{2\eta^0(v) - v(\partial\eta^0/\partial v) + [\chi^0(v) + v(\partial\chi^0/\partial v)]I(\mu, v)\} \quad (14-115) \end{aligned}$$

This approach may be adequate for *continua*, where the frequency derivatives are well defined and nearly constant, but will not be accurate enough for *lines*

where the changes in  $\eta_v$  and  $\chi_v$  are so swift that a first-order expansion is not sufficient. A complication in application of equation (14-115) is that both even and odd terms in  $\mu$  appear on the righthand side, so that the usual reduction to a second-order transfer equation is not possible; a satisfactory numerical scheme can, nevertheless, be devised using a staggered mesh [see, e.g., (460)].

#### TRANSFORMATION OF MOMENTS OF THE RADIATION FIELD

The total energy density, energy flux, and radiation pressure in the field are specified by the frequency-integrated quantities [cf. equations (1-7), (1-19), (1-28)]

$$E_R(r, t) \equiv c^{-1} \int_0^\infty dv \oint d\omega I(r, \mathbf{n}, v, t) \quad (14-116a)$$

$$\mathcal{F}(r, t) \equiv \int_0^\infty dv \oint d\omega I(r, \mathbf{n}, v, t)\mathbf{n} \quad (14-116b)$$

$$\text{and } P(r, t) \equiv c^{-1} \int_0^\infty dv \oint d\omega I(r, \mathbf{n}, v, t)\mathbf{n}\mathbf{n} \quad (14-116c)$$

These are related by the frequency-integrated moment equations [cf. equations (2-75) and (2-68)]

$$c^{-2}(\partial \mathcal{F} / \partial t) + \nabla \cdot P = c^{-1} \int_0^\infty dv \oint d\omega [\eta(r, v, t) - \chi(r, v, t)I(r, v, t)]\mathbf{n} \quad (14-117a)$$

and

$$(\partial E_R / \partial t) + \nabla \cdot \mathcal{F} = \int_0^\infty dv \oint d\omega [\eta(r, v, t) - \chi(r, v, t)I(r, v, t)] \quad (14-117b)$$

As written, equations (14-117) are already covariant. One way this may easily be seen is to exploit the results of electromagnetic theory in which one finds [see, e.g., (331, Chap. 12; 386, Chap. 4; or 494, Chap. 21)] that the momentum-energy conservation laws of electrodynamics can be written in the covariant form

$$\partial T^{\alpha\beta} / \partial x^\beta = -f^\alpha \quad (14-118)$$

Here  $T^{\alpha\beta}$  is the *stress-energy tensor* of the electromagnetic field, and  $f^\alpha$  is a four-vector giving, per unit volume, the three components of the *Lorentz forces* of the field on charged matter, and  $(i/c)$  times the rate of work done by the field on charges and currents. The stress-energy tensor is a contravariant four-tensor of rank two, namely

$$T = \begin{pmatrix} -T^M & icG \\ icG & -W \end{pmatrix} \quad (14-119)$$

where  $T^M$  is the Maxwell stress tensor (cf. §1-5),  $G$  is the momentum density, and  $W$  is the energy density of the field.

We have seen in Chapter 1 that a one-to-one correspondence between electromagnetic field quantities and moments of the radiation field can be made; specifically,  $T^M = -P$ ,  $G = c^{-2}\mathcal{F}$ , and  $W = E_R$ . We thus conclude that the stress-energy tensor of the radiation field must be

$$R = \begin{pmatrix} P & ic^{-1}\mathcal{F} \\ ic^{-1}\mathcal{F} & -E_R \end{pmatrix} = c^{-1} \begin{pmatrix} \int dv \oint d\omega I_{nn} & i \int dv \oint d\omega I_n \\ i \int dv \oint d\omega I_n & - \int dv \oint d\omega I \end{pmatrix} \quad (14-120)$$

We can see by inspection that  $R$  is actually a four-tensor merely by noting that it is formed from the outer product of the four-vector  $(vn, iv)$  [recall equation (14-105)] with itself, times the invariant [see equations (14-109) and (14-110)]  $(I dv d\omega/v^2)$ , integrated over all angles and frequencies. Similarly, the Lorentz force can be identified with the rate at which momentum is transferred from radiation to matter, and the rate of work with the rate of energy input of the radiation into the matter. Thus we conclude that we can write

$$g_R = c^{-1} \left[ \int dv \oint d\omega (\chi I - \eta)n, i \int dv \oint d\omega (\chi I - \eta) \right] \quad (14-121)$$

as a four-vector. This can again be seen to be the case, for  $g_R$  is composed of the four-vector  $(vn, iv)$  times the invariants  $(\chi I dv d\omega)/v$  or  $(\eta dv d\omega)/v$ . The four-divergence of a four-tensor is automatically a four-vector, hence

$$\partial R^{\alpha\beta}/\partial x^\beta = -g_R^\alpha \quad (14-122)$$

is, in fact, a covariant representation of the conservation relations for the radiation field. One can see immediately that equation (14-122) produces equations (14-117a) and (14-117b), when the latter is multiplied by  $(-ic)$ , and that these equations are, therefore, covariant between frames moving uniformly with respect to one another; for nonuniform motion, additional terms will appear in the comoving-frame moment equations.

In working with the equations of radiation hydrodynamics (§15-3), it will be useful to have transformations accurate to  $O(v/c)$  of  $E_R$ ,  $\mathcal{F}$ , and  $P$  (or, equivalently,  $J$ ,  $H$ , and  $K$ ) between the fixed and comoving frames. These are most easily obtained by using equations (14-109), (14-110), and (14-107), and expanding to first order in  $(v/c)$ . Thus, setting  $\gamma \equiv 1$ , we find readily that  $I_v^0 dv_0 d\omega_0 = (v_0/v)^2 I_v dv d\omega \approx (1 - 2\beta\mu)I_v dv d\omega$ , from which it follows that

$$J^0 = J - 2\beta H \quad (14-123a)$$

Similarly,  $I_v^0 \mu_0 dv_0 d\omega_0 = (\mu - \beta)(1 - \mu\beta)I_v dv d\omega \approx [\mu - \beta(1 + \mu^2)]I_v dv d\omega$ , and  $I_v^0 \mu_0^2 dv_0 d\omega_0 = (\mu - \beta)^2 I_v dv d\omega \approx (\mu^2 - 2\mu\beta)I_v dv d\omega$ , from which

it follows that

$$H^0 = H - \beta(J + K) \quad (14-123b)$$

and

$$K^0 = K - 2\beta H \quad (14-123c)$$

The inverse transformations yield

$$(J, H, K) = [J^0 + 2\beta H^0, H^0 + \beta(J^0 + K^0), K^0 + 2\beta H^0] \quad (14-124)$$

Notice that these transformations are valid only for the frequency-integrated moments.

*Exercise 14-9:* Derive equations (14-123) and (14-124) by applying a Lorentz transformation to the stress-energy tensor [equation (14-120)] and expanding the result to  $O(v/c)$ .

#### THE COMOVING-FRAME EQUATION OF TRANSFER

The full transformation of the equation of transfer (including the differential operator) for a nonuniform velocity field can be done rigorously using covariant differentiation (399; 135; 278); however this approach requires considerable familiarity with tensor calculus. We shall instead use a simple first-order expansion method that yields results correct to  $O(v/c)$ . The equations of transfer that we consider are (in planar and spherical geometry, respectively)

$$[c^{-1}(\partial/\partial t) + \mu(\partial/\partial r)][(v/v_0)^3 I^0(r_0, \mu_0, v_0, t_0)] = (v/v_0)^2 [\eta^0(v_0) - \chi^0(v_0)I^0(r_0, \mu_0, v_0, t_0)] \quad (14-125a)$$

$$\text{and } [c^{-1}(\partial/\partial t) + \mu(\partial/\partial r) + r^{-1}(1 - \mu^2)(\partial/\partial \mu)][(v/v_0)^3 I^0(r_0, \mu_0, v_0, t_0)] = (v/v_0)^2 [\eta^0(v_0) - \chi^0(v_0)I^0(r_0, \mu_0, v_0, t_0)] \quad (14-125b)$$

We consider one-dimensional flows, and apply a local Lorentz transformation to a frame that instantaneously coincides with the moving fluid. We shall ignore terms of  $O(v^2/c^2)$ , and set  $\gamma \equiv 1$ . We then have

$$r_0 = r \quad (14-126a)$$

$$ct_0(r, t) = ct - c^{-1} \int_0^r v(r', t) dr' \quad (14-126b)$$

Equation (14-126a) states that space increments will be judged to be the same by observers in both frames (i.e., no Lorentz contraction). Equation (14-126b) accounts for the finite propagation velocity of light and accounts for the classical retardation effect. [The significance of this term can be understood more fully by the following thought-experiment. Suppose clocks at a number of stations around some point  $r_1$  in the rest frame are initially synchronized.

Then suppose that at some time  $t_1$  all these stations simultaneously emit pulses of light received by (a) an observer at rest at  $r_1$ , and (b) an observer at  $r_1$  moving with velocity  $v$ . Observer (a) will receive the pulses synchronously, while observer (b) receives pulses from directions  $r > r_1$  sooner than from  $r < r_1$ . He thus concludes that the emission times ( $t_0$ ) were earlier for  $r > r_1$  than for  $r < r_1$ , as is shown by equation (14-126b) (for simplicity consider the case of  $v = \text{constant}$ ).] The retardation effect is, in one sense, *not* a relativistic term, but *merely acknowledges a finite light-propagation speed*; its significance from a relativistic viewpoint is, of course, profound.

To evaluate the derivatives in equations (14-125) the chain rule is applied.

$$\begin{aligned} \left( \frac{\partial}{\partial r} \right) &\equiv \left( \frac{\partial}{\partial r} \right)_{\mu v t} = \left( \frac{\partial r_0}{\partial r} \right)_{\mu v t} \frac{\partial}{\partial r_0} + \left( \frac{\partial \mu_0}{\partial r} \right)_{\mu v t} \frac{\partial}{\partial \mu_0} \\ &\quad + \left( \frac{\partial v_0}{\partial r} \right)_{\mu v t} \frac{\partial}{\partial v_0} + \left( \frac{\partial t_0}{\partial r} \right)_{\mu v t} \frac{\partial}{\partial t_0} \end{aligned} \quad (14-127a)$$

$$\begin{aligned} \left( \frac{\partial}{\partial \mu} \right) &\equiv \left( \frac{\partial}{\partial \mu} \right)_{r v t} = \left( \frac{\partial r_0}{\partial \mu} \right)_{r v t} \frac{\partial}{\partial r_0} + \left( \frac{\partial \mu_0}{\partial \mu} \right)_{r v t} \frac{\partial}{\partial \mu_0} \\ &\quad + \left( \frac{\partial v_0}{\partial \mu} \right)_{r v t} \frac{\partial}{\partial v_0} + \left( \frac{\partial t_0}{\partial \mu} \right)_{r v t} \frac{\partial}{\partial t_0} \end{aligned} \quad (14-127b)$$

$$\begin{aligned} \left( \frac{\partial}{\partial t} \right) &\equiv \left( \frac{\partial}{\partial t} \right)_{r \mu v} = \left( \frac{\partial r_0}{\partial t} \right)_{r \mu v} \frac{\partial}{\partial r_0} + \left( \frac{\partial \mu_0}{\partial t} \right)_{r \mu v} \frac{\partial}{\partial \mu_0} \\ &\quad + \left( \frac{\partial v_0}{\partial t} \right)_{r \mu v} \frac{\partial}{\partial v_0} + \left( \frac{\partial t_0}{\partial t} \right)_{r \mu v} \frac{\partial}{\partial t_0} \end{aligned} \quad (14-127c)$$

We use the first-order expressions  $(v/v_0) = 1 + \beta \mu_0$ ,  $(v_0/v) = 1 - \beta \mu$ ,  $\mu_0 = (\mu - \beta)(1 - \beta \mu)^{-1}$ , and  $\mu = (\mu_0 + \beta)(1 + \beta \mu_0)^{-1}$ , and make the additional approximation that fluid accelerations (which are identically zero for steady flow) are so small that the change in any velocity during the time of a photon flight, over a mean-free-path, is negligible compared to the velocity itself. We then neglect  $(\partial v/\partial t)$  and derivatives of the form  $(\partial x_0/\partial t)$  for  $x_0 = r_0, \mu_0$ , or  $v_0$ , and retain only  $(\partial t_0/\partial t) \equiv 1$ . The remaining coefficients in equations (14-127), to  $O(v/c)$ , are easily derived from equations (14-126) and the first-order relations written above. One finds

$$\left( \frac{\partial}{\partial r} \right)_{\mu v t} (r_0, \mu_0, v_0, t_0) = [1, c^{-1}(\mu_0^2 - 1)(\partial v/\partial r_0), -c^{-1}\mu_0 v_0(\partial v/\partial r_0), -\beta/c] \quad (14-128a)$$

$$\left( \frac{\partial}{\partial \mu} \right)_{r v t} (r_0, \mu_0, v_0, t_0) = [0, (1 + 2\mu_0\beta), -v_0\beta, 0] \quad (14-128b)$$

Starting with equation (14-125a), rewritten with the approximation mentioned above as

$$\begin{aligned} \{ (v/v_0) [c^{-1}(\partial/\partial t) + \mu(\partial/\partial r)] + 3\mu[\partial(v/v_0)/\partial r] \} I^0(r_0, \mu_0, v_0, t_0) \\ = \eta^0(v_0) - \chi^0(v_0) I^0(r_0, \mu_0, v_0, t_0), \end{aligned}$$

substituting from equations (14-127) and (14-128) and the first-order expressions for  $(v/v_0)$ , etc., and retaining only terms of first-order in  $(v/c)$ , one obtains:

$$\begin{aligned} &\left[ \frac{1}{c} \frac{\partial}{\partial t_0} + \left( \mu_0 + \frac{v}{c} \right) \frac{\partial}{\partial r_0} + \frac{\mu_0(\mu_0^2 - 1)}{c} \left( \frac{\partial v}{\partial r_0} \right) \frac{\partial}{\partial \mu_0} \right. \\ &\quad \left. - \frac{v_0 \mu_0^2}{c} \left( \frac{\partial v}{\partial r_0} \right) \frac{\partial}{\partial v_0} + \frac{3\mu_0^2}{c} \left( \frac{\partial v}{\partial r_0} \right) \right] I^0(r_0, \mu_0, v_0, t_0) \\ &= \eta^0(v_0) - \chi^0(v_0) I^0(r_0, \mu_0, v_0, t_0) \end{aligned} \quad (14-129)$$

For spherical geometry we have the additional term

$$\begin{aligned} (v_0/v)^2 r^{-1} (1 - \mu^2) (\partial/\partial \mu) [(v/v_0)^3 I^0] \\ = (v/v_0) r^{-1} (1 - \mu^2) (\partial I^0/\partial \mu) + 3r^{-1} (1 - \mu^2) [\partial(v/v_0)/\partial \mu] I^0 \end{aligned}$$

Again expanding to first order in  $(v/c)$ , and using the result from equation (14-107) that  $v^2(1 - \mu^2) = v_0^2(1 - \mu_0^2)$ , and also  $[\partial(v/v_0)/\partial \mu] = (v/c)$ , we obtain for these additional terms

$$r_0^{-1} (1 - \mu_0^2) \{ [(1 + \beta \mu_0)(\partial/\partial \mu_0) - \beta v_0(\partial/\partial v_0)] + 3\beta \} I^0$$

Thus the comoving-frame transfer equation to order  $O(v/c)$  in spherical geometry is

$$\begin{aligned} &\left[ \frac{1}{c} \frac{\partial}{\partial t_0} + \left( \mu_0 + \frac{v}{c} \right) \frac{\partial}{\partial r_0} + \frac{(1 - \mu_0^2)}{r_0} \left[ 1 + \frac{\mu_0 v}{c} \left( 1 - \frac{d \ln v}{d \ln r_0} \right) \right] \frac{\partial}{\partial \mu_0} \right. \\ &\quad \left. - \left( \frac{v_0 v}{c r_0} \right) \left[ 1 - \mu_0^2 \left( 1 - \frac{d \ln v}{d \ln r_0} \right) \right] \frac{\partial}{\partial v_0} \right. \\ &\quad \left. + \left( \frac{3v}{c r_0} \right) \left[ 1 - \mu_0^2 \left( 1 - \frac{d \ln v}{d \ln r_0} \right) \right] \right] I^0(r_0, \mu_0, v_0, t_0) \\ &= \eta^0(v_0) - \chi^0(v_0) I^0(r_0, \mu_0, v_0, t_0) \end{aligned} \quad (14-130)$$

*Exercise 14-10:* Verify equations (14-129) and (14-130) in detail.

Equations (14-129) and (14-130) are the comoving-frame equations including all terms of  $O(v/c)$ , and were first derived consistently by Castor (135). The time-derivative written in these equations is, in essence, still in the fixed frame (though it allows for retardation); the Lagrangian time derivative, which follows the motion of a fluid element (cf. §15-1) consists of the two terms  $(D/Dt) = (\partial/\partial t) + (v/c)(\partial/\partial r)$ , the second term being the advection term. For steady flows, the terms in  $(\partial/\partial t)$  are identically zero. The equations just derived are obviously fairly complicated. As we shall see, it is important to retain all of the terms in the moment equations. However, for a solution of the transfer equation itself, it is sufficient for most astrophysical flows [as verified by a detailed calculation (446)] to retain only the frequency-derivative terms because of the effective amplification of these terms by  $(c/v_{th})$ , as discussed earlier. In this limit, equation (14-129) for steady flow reduces to equation (14-99), while equation (14-130) reduces to (14-100). We shall describe a numerical method for solving equation (14-100) in the next subsection.

For problems of radiative transfer involving partial redistribution, it is useful to derive frequency-dependent moment equations from equations (14-129) and (14-130). For spherical geometry we obtain

$$\begin{aligned} \frac{1}{c} \frac{\partial J_v^0}{\partial t} + \frac{v}{c} \frac{\partial J_v^0}{\partial r} + \frac{1}{r^2} \frac{\partial(r^2 H_v^0)}{\partial r} + \left( \frac{v}{cr} \right) (3J_v^0 - K_v^0) + \frac{1}{c} (J_v^0 + K_v^0) \frac{\partial v}{\partial r} \\ + \left( \frac{v}{cr} \right) \frac{\partial}{\partial v_0} [v_0 (3K_v^0 - J_v^0)] - \frac{1}{c} \left( \frac{2v}{r} + \frac{\partial v}{\partial r} \right) \frac{\partial(v_0 K_v^0)}{\partial v_0} \\ = \eta^0(v_0) - \chi^0(v_0) J_v^0 \end{aligned} \quad (14-131a)$$

for the zero-order moment, and for the first-order moment

$$\begin{aligned} \frac{1}{c} \frac{\partial H_v^0}{\partial t} + \frac{v}{c} \frac{\partial H_v^0}{\partial r} + \frac{\partial K_v^0}{\partial r} + \frac{1}{r} (3K_v^0 - J_v^0) + \frac{2}{c} \left( \frac{v}{r} + \frac{\partial v}{\partial r} \right) H_v^0 \\ + \left( \frac{v}{cr} \right) \frac{\partial}{\partial v_0} [v_0 (3N_v^0 - H_v^0)] - \frac{1}{c} \left( \frac{2v}{r} + \frac{\partial v}{\partial r} \right) \frac{\partial(v_0 N_v^0)}{\partial v_0} = -\chi^0(v_0) H_v^0 \end{aligned} \quad (14-131b)$$

where

$$N_v^0 \equiv \frac{1}{2} \int_{-1}^1 I^0(r, \mu_0, v_0, t) \mu_0^3 d\mu_0 \quad (14-132)$$

and, for brevity, we have written  $J_v^0 \equiv J^0(r, v_0, t)$ , etc., and suppressed the suffix "0" on  $r$  and  $t$ . Again, for practical transfer calculations with steady

### 14-3 The Transfer Equation in the Fluid Frame

flow, it is sufficient to replace equations (14-131a) and (14-131b) with

$$r^{-2} [\partial(r^2 H_v^0)/\partial r] - a [\partial(J_v^0 - K_v^0)/\partial v_0 + b(\partial K_v^0/\partial v_0)] = \eta^0(v_0) - \chi^0(v_0) J_v^0 \quad (14-133a)$$

$$\begin{aligned} \text{and } (\partial K_v^0/\partial r) + r^{-1} (3K_v^0 - J_v^0) - a [\partial(H_v^0 - N_v^0)/\partial v_0 + b(\partial N_v^0/\partial v_0)] \\ = -\chi^0(v_0) H_v^0 \end{aligned} \quad (14-133b)$$

where  $a \equiv (v_0 v / cr)$  and  $b \equiv (d \ln v / d \ln r)$  [see (447)].

For problems of radiation hydrodynamics we require the frequency-integrated moment equations, which follow immediately from equations (14-131):

$$\begin{aligned} (\partial E_R^0/\partial t) + v(\partial E_R^0/\partial r) + r^{-2} [\partial(r^2 \mathcal{F}^0)/\partial r] \\ + (v/r)(3E_R^0 - p_R^0) + (\partial v/\partial r)(E_R^0 + p_R^0) \\ = 4\pi \int_0^\infty [\eta^0(v_0) - \chi^0(v_0) J_v^0] dv_0 \end{aligned} \quad (14-134a)$$

$$\begin{aligned} c^{-2} (\partial \mathcal{F}^0/\partial t) + (v/c^2)(\partial \mathcal{F}^0/\partial r) + (\partial p_R^0/\partial r) + (3p_R^0 - E_R^0)/r \\ + (2v/c^2 r)[1 + (d \ln v / d \ln r)] \mathcal{F}^0 = -c^{-1} \int_0^\infty \chi^0(v_0) \mathcal{F}_v^0 dv_0 \end{aligned} \quad (14-134b)$$

where  $E_R^0 = (4\pi/c) \int J^0(v_0) dv_0 \equiv (4\pi/c) J^0$  and  $p_R^0 \equiv (4\pi/c) K^0$ . In planar geometry, equations completely analogous to (14-131) through (14-134) can also be written down. Equations (14-134) contain additional velocity-dependent terms on the lefthand side compared to their counterparts [cf. equations (14-117)] in the fixed frame. But this is more than adequately compensated by the tremendous simplification of the righthand side, where the isotropy of the opacity and emissivity in the comoving frame allows the integrals to be expressed in terms of the moments themselves, instead of as double integrals over the specific intensity. The only question remaining to be faced is: "How do we actually solve the comoving-frame transfer equation for  $I^0(r, \mu_0, v_0)$  and its moments?"

#### SOLUTION FOR SPHERICALLY SYMMETRIC FLOWS

Let us now consider methods for solving the comoving-frame transfer equations in the limit that only Doppler shifts are taken into account—i.e., equations of the form of (14-99) and (14-100). As was mentioned earlier, the transfer equation in the comoving frame is a *partial differential equation*, which was first obtained by McCrea and Mitra (414). Chandrasekhar (156; 157) obtained solutions of these equations for planar geometry, with a linear

velocity law, a two-stream description of the radiation field, and strictly coherent scattering; generalizations of this approach are given in (1; 2; 3; 276, 199). Lucy (403) solved the equations in planar geometry, with coherent scattering, in the high-velocity limit, by ignoring the *spatial* derivative and treating the equation as an ordinary differential equation in frequency alone. An integral-equation method for planar geometries has also been devised (574); this method is restricted to linear velocity laws and hence is not useful for realistic models. A general and flexible numerical method developed by Noerdlinger and Rybicki (478) solves the equations in planar geometry using a Feautrier-type elimination scheme; this method can treat problems involving partial redistribution. In a ray-by-ray solution for spherical geometry, the number of angles must be of the same order as the number of depth-points, and a Feautrier-type solution becomes costly. If *complete redistribution* is assumed, we can construct an efficient Rybicki-type solution (444), as will be described here; for partial redistribution we use moment equations [e.g., equations (14-133)], thereby eliminating the angle-variable, in which case a Feautrier-type solution again becomes practical (447).

In spherical geometry we adopt the  $(p, z)$  coordinate system introduced in §7-6. Then, along a ray specified by constant  $p$ , equation (14-100) becomes

$$\pm [\partial I^\pm(z, p, v)/\partial z] - \tilde{\gamma}(z, p)[\partial I^\pm(z, p, v)/\partial v] = \eta(r, v) - \chi(r, v)I^\pm(z, p, v) \quad (14-135)$$

where  $\tilde{\gamma}(z, p) \equiv [vv(r)/cr][(1 - \mu^2) + \mu^2(d \ln v/d \ln r)]$  (14-136)

and  $r \equiv (p^2 + z^2)^{1/2}$ ,  $\mu \equiv (z/r)$ . In equations (14-135) and (14-136) we have suppressed the suffix “0” for notational simplicity (and continue to do so henceforth in this chapter), but it is to be stressed that all quantities are evaluated in the comoving frame. Now introducing the optical depth along the ray,  $d\tau(z, p, v) = -\chi(z, p, v) dz$ , and the variables

$$u(z, p, v) \equiv \frac{1}{2}[I^+(z, p, v) + I^-(z, p, v)] \quad (14-137)$$

and  $v(z, p, v) \equiv \frac{1}{2}[I^+(z, p, v) - I^-(z, p, v)]$  (14-138)

we can obtain from equation (14-135) the system

$$[\partial u(z, p, v)/\partial \tau(z, p, v)] + \gamma(z, p, v)[\partial v(z, p, v)/\partial v] = v(z, p, v) \quad (14-139)$$

and  $[\partial v(z, p, v)/\partial \tau(z, p, v)] + \gamma(z, p, v)[\partial u(z, p, v)/\partial v] = u(z, p, v) - S(z, p, v)$  (14-140)

where  $\gamma(z, p, v) \equiv \tilde{\gamma}(z, p)/\chi(z, p, v)$ , and the source function is assumed to have the form for an equivalent-two-level-atom with complete redistribution—i.e.,  $S(z, p, v) = S[r(z, p), v] = \alpha(r, v)J(r) + \beta(r)$ . The coefficients  $\alpha$  and  $\beta$  contain the thermalization parameter  $\epsilon$ , the opacity ratio  $\chi_c/\chi_i$ , and the profile function, while

$$J(r) \equiv \int_{v_{\min}}^{v_{\max}} dv \phi(v) \int_0^1 d\mu u[z(r, \mu), p(r, \mu), v] \quad (14-141)$$

In equation (14-141),  $v_{\min}$  and  $v_{\max}$  are chosen to contain the whole line profile as seen in the comoving frame. Note particularly in equations (14-137) and (14-138) that, because we are working in the comoving frame, we can now average  $I^+$  and  $I^-$  at a given value of  $v$ , in contrast to the situation in an observer's-frame formulation [cf. equations (14-23) and (14-24)].

Spatial boundary conditions are now required. At the outer radius  $r = R$   $I^- \equiv 0$ ; therefore  $u \equiv v$ , hence

$$[\partial u(z, p, v)/\partial \tau(z, p, v)]_{z_{\max}} + \gamma(z_{\max}, p, v)[\partial u(z_{\max}, p, v)/\partial v] = u(z_{\max}, p, v) \quad (14-142)$$

At the plane of symmetry  $z = 0$ , we can now write  $v(0, p, v) \equiv 0$ , hence for rays that do not intersect the core,

$$[\partial u(z, p, v)/\partial \tau(z, p, v)]_{z=0} = 0 \quad (14-143)$$

For rays that intersect the core (i.e.,  $p \leq r_c$ ) we (a) apply the diffusion approximation for an *opaque* core (stellar surface), which specifies  $v$ , or (b) set  $v \equiv 0$  (by symmetry) for a *hollow* core (nebular case).

In addition, an *initial condition in frequency* is required. For an *expanding* atmosphere [i.e., one in which  $v > 0$  and  $(dv/dr) > 0$ ], it is obvious that the high-frequency edge of the line profile (in the comoving frame) cannot intercept *line* photons from any other point in the atmosphere, because they will all be systematically red-shifted; any photon incident at the high-frequency edge must be a *continuum* photon. To specify the required initial condition we may therefore either (a) solve equations (14-139) and (14-140) in the continuum, omitting the frequency-derivative terms (which yields the standard second-order system) to obtain  $u(z, p, v_{\max}) = u_{\text{continuum}}$ , or (b) fix the derivative  $(\partial u/\partial v)_{v_{\max}}$  to any prespecified value given by the slope of the continuum; in particular, the choice  $(\partial u/\partial v) \equiv 0$  leads to equations identical to option (a) just mentioned.

The system is now discretized using the same grids  $\{r_d\}$ ,  $\{p_i\}$ ,  $\{z_{d_i}\}$  as were employed in §7-6 and §14-1. We now choose the frequency grid  $\{v_n\}$  ( $n = 1, \dots, N$ ) in order of *decreasing values* ( $v_1 > v_2 > \dots > v_N$ ) because the initial condition is posed at the highest frequency. We replace equation

(14-141) with a quadrature sum

$$J(r_d) = \sum_{n=1}^N w_n \sum_{i=1}^{I_d} a_{di} \phi(r_d, v_n) u[z(r_d, p_i), p_i, v_n] \quad (14-144)$$

Equations (14-139) and (14-140) are replaced with difference approximations

$$(u_{d+1, in} - u_{din})/\Delta\tau_{d+\frac{1}{2}, in} = v_{d+\frac{1}{2}, in} + \delta_{d+\frac{1}{2}, i, n-\frac{1}{2}}(v_{d+\frac{1}{2}, in} - v_{d+\frac{1}{2}, i, n-1}) \quad (14-145)$$

and  $(v_{d+\frac{1}{2}, in} - v_{d-\frac{1}{2}, in})/\Delta\tau_{din} = u_{din} - S_{din} + \delta_{di, n-\frac{1}{2}}(u_{din} - u_{di, n-1}) \quad (14-146)$

where  $u$  is presumed to be defined on the mesh-points  $z_d = z(r_d, p_i)$ , and  $u_{din} \equiv u(z_d, p_i, v_n)$ , while  $v$  is presumed to be defined on the interstices  $z_{d\pm\frac{1}{2}} \equiv \frac{1}{2}(z_d + z_{d\pm1})$  and  $v_{d\pm\frac{1}{2}, in} \equiv v(z_{d\pm\frac{1}{2}}, p_i, v_n)$ . Further, we have defined

$$\chi_{d\pm\frac{1}{2}, in} \equiv \frac{1}{2}(\chi_{d\pm1, in} + \chi_{din}) \quad (14-147)$$

$$\Delta\tau_{d\pm\frac{1}{2}, i, n} \equiv \chi_{d\pm\frac{1}{2}, in} |z_d - z_{d\pm1}| \quad (14-148)$$

$$\Delta\tau_{din} \equiv \frac{1}{2}(\Delta\tau_{d+\frac{1}{2}, in} + \Delta\tau_{d-\frac{1}{2}, in}) \quad (14-149)$$

and

$$\delta_{di, n-\frac{1}{2}} \equiv \gamma_{din}/(v_{n-1} - v_n) \quad (14-150)$$

Similar difference equations may be written to represent the boundary conditions (444). In equations (14-145) and (14-146), an *implicit* frequency differencing is used to assure stability (444; 462; 530).

Equation (14-145) can be solved analytically for  $v_{d+\frac{1}{2}, in}$  to yield

$$v_{d+\frac{1}{2}, in} = \{(u_{d+1, in} - u_{din})/\Delta\tau_{d+\frac{1}{2}, in} + \delta_{d+\frac{1}{2}, i, n-\frac{1}{2}} v_{d+\frac{1}{2}, i, n-1}\}/(1 + \delta_{d+\frac{1}{2}, i, n-\frac{1}{2}}) \quad (14-151)$$

Organizing the solution into vectors that specify the depth-variation along a particular ray at a given frequency—i.e.,

$$\mathbf{u}_{in} \equiv (u_{1in}, u_{2in}, \dots, u_{D_{in}in})^T \quad (14-152a)$$

and  $\mathbf{v}_{in} \equiv (v_{\frac{1}{2}, in}, \dots, v_{D_{in}-\frac{1}{2}, in})^T \quad (14-152b)$

equation (14-151) can be written in the form

$$\mathbf{v}_{in} = \mathbf{G}_{in}\mathbf{u}_{in} + \mathbf{H}_{in}\mathbf{v}_{i, n-1} \quad (14-153)$$

where  $\mathbf{G}$  is bidiagonal and  $\mathbf{H}$  is diagonal. Equations (14-151) can be used to eliminate  $v_{d\pm\frac{1}{2}, in}$  from (14-146); we then obtain a set of second-order equations for  $u_{din}$ , namely

$$\begin{aligned} & \{(u_{d+1, in} - u_{din})/\Delta\tau_{d+\frac{1}{2}, in}(1 + \delta_{d+\frac{1}{2}, i, n-\frac{1}{2}}) \\ & \quad - (u_{din} - u_{d-1, in})/\Delta\tau_{d-\frac{1}{2}, in}(1 + \delta_{d-\frac{1}{2}, i, n-\frac{1}{2}})\}/\Delta\tau_{din} \\ & = (1 + \delta_{di, n-\frac{1}{2}})u_{din} - S_{din} - \delta_{di, n-\frac{1}{2}}u_{di, n-1} \\ & \quad + [\delta_{d-\frac{1}{2}, i, n-\frac{1}{2}}(1 + \delta_{d-\frac{1}{2}, i, n-\frac{1}{2}})^{-1}v_{d-\frac{1}{2}, i, n-1} \\ & \quad - \delta_{d+\frac{1}{2}, i, n-\frac{1}{2}}(1 + \delta_{d+\frac{1}{2}, i, n-\frac{1}{2}})^{-1}v_{d+\frac{1}{2}, i, n-1}]/\Delta\tau_{din} \end{aligned} \quad (14-154)$$

Adding the boundary conditions to equation (14-154) we obtain the system

$$\mathbf{T}_{in}\mathbf{u}_{in} + \mathbf{U}_{in}\mathbf{u}_{i, n-1} + \mathbf{V}_{in}\mathbf{v}_{i, n-1} + \mathbf{W}_{in}\mathbf{J} = \mathbf{X}_{in} \quad (14-155)$$

where  $\mathbf{T}_{in}$  is tridiagonal,  $\mathbf{U}_{in}$  and  $\mathbf{W}_{in}$  are diagonal,  $\mathbf{V}_{in}$  is bidiagonal, and  $\mathbf{X}_{in}$  is a vector.

*Exercise 14-11:* Verify equations (14-151) and (14-154), and sketch the forms of the  $\mathbf{G}$ ,  $\mathbf{U}$ , and  $\mathbf{V}$  matrices.

To solve the complete system, we choose a definite ray, specified by a given  $p_i$ , and carry out a frequency-by-frequency integration procedure, with  $n$  ranging from 1 to  $N$ . This is effected by noting that the initial condition in frequency implies that  $\mathbf{U}_{i1}$ ,  $\mathbf{V}_{i1}$  and  $\mathbf{H}_{i1}$  are all exactly zero; thus we can obtain expressions of the form  $\mathbf{u}_{i1} = \mathbf{A}_{i1} - \mathbf{B}_{i1}\mathbf{J}$  and  $\mathbf{v}_{i1} = \mathbf{C}_{i1} - \mathbf{D}_{i1}\mathbf{J}$ , where  $\mathbf{A}_{i1} = \mathbf{T}_{i1}^{-1}\mathbf{X}_{i1}$  is a vector,  $\mathbf{B}_{i1} = \mathbf{T}_{i1}^{-1}\mathbf{W}_{i1}$  is a matrix,  $\mathbf{C}_{i1} = \mathbf{G}_{i1}\mathbf{A}_{i1}$ , and  $\mathbf{D}_{i1} = \mathbf{G}_{i1}\mathbf{B}_{i1}$ . Similar substitutions are carried out for successive values of  $n$ , to yield

$$\mathbf{u}_{in} = \mathbf{A}_{in} - \mathbf{B}_{in}\mathbf{J} \quad (14-156)$$

and  $\mathbf{v}_{in} = \mathbf{C}_{in} - \mathbf{D}_{in}\mathbf{J} \quad (14-157)$

where  $\mathbf{A}_{in} = \mathbf{T}_{in}^{-1}(\mathbf{X}_{in} - \mathbf{U}_{in}\mathbf{A}_{i, n-1} - \mathbf{V}_{in}\mathbf{C}_{i, n-1}) \quad (14-158)$

$$\mathbf{B}_{in} = \mathbf{T}_{in}^{-1}(\mathbf{W}_{in} - \mathbf{U}_{in}\mathbf{B}_{i, n-1} - \mathbf{V}_{in}\mathbf{D}_{i, n-1}) \quad (14-159)$$

$$\mathbf{C}_{in} = \mathbf{G}_{in}\mathbf{A}_{in} + \mathbf{H}_{in}\mathbf{C}_{i, n-1} \quad (14-160)$$

and  $\mathbf{D}_{in} = \mathbf{G}_{in}\mathbf{B}_{in} + \mathbf{H}_{in}\mathbf{D}_{i, n-1} \quad (14-161)$

Each result, of the form of equation (14-156), for every frequency  $v_n$ , along every ray  $p_i$ , is substituted into equation (14-144) to obtain a final system for  $J$  of the form

$$\left( \mathbf{I} + \sum_{l,n} \mathbf{F}_{ln} \mathbf{B}_{ln} \right) \mathbf{J} = \sum_{l,n} \mathbf{F}_{ln} \mathbf{A}_{ln} \quad (14-162)$$

where the  $\mathbf{F}$ 's contain the quadrature weights. The solution of this final system yields  $\mathbf{J}$ , and hence  $S(r, v)$ , and  $u(z, p, v)$  and  $v(z, p, v)$  from equations (14-156) and (14-157). Knowledge of  $u(z, p, v)$  implies knowledge of  $u(r, \mu, v)$ , so it is clear that we can calculate  $J^0(r, v)$  and  $K^0(r, v)$  in the comoving frame; similarly we can calculate the flux  $H^0(r, v)$  from  $v(r, \mu, v)$ . Thus we obtain a complete solution for the radiation field and its moments in the comoving frame.

The number of operations required to obtain  $\mathbf{A}_{ln}$  and  $\mathbf{B}_{ln}$  in equation (14-156) is proportional to  $D_l^2$ , so summing over all frequencies on all rays one obtains  $T_s = cN D^3 + c' D^3$  as an estimate of the computing time required. Note that this time is *linear* in the number of frequencies. A similar formulation can be written down for planar geometry; in this case we dispense with the rays and use  $M$  fixed angles  $\{\mu_i\}$ . In planar geometry the computing time required for the solution is  $T_p = cNM D^2 + c' D^3$ . For partial redistribution in spherical geometry one would use a Feautrier solution of the moment equations (447), obtaining the Eddington factors from a ray-by-ray formal solution with a given estimate of the source function. For partial redistribution in planar geometry the method of Noerdlinger and Rybicki (478) is applicable.

**Exercise 14-12:** Consider flows with monotonic velocity fields [i.e.,  $(dv/dr)$  everywhere  $\geq 0$  or everywhere  $\leq 0$ ]. (a) In *planar* geometry show that the choice of the initial condition in frequency is unique and depends only on the *sign* of  $(dv/dr)$  [cf. (451) for a discussion of non-monotonic velocity fields]. (b) In *spherical* geometry show that unique conditions can be found only if  $[v > 0, (dv/dr) > 0]$  or  $[v < 0, (dv/dr) < 0]$ , and that, owing to projection effects along a ray at the plane of symmetry ( $z = 0$ ), velocity distributions of the form  $[v > 0, (dv/dr) < 0]$  or  $[v < 0, (dv/dr) > 0]$ , though monotone in the *radial* direction, produce non-monotonic fields along tangent rays.

The method outlined above has been used to calculate source functions and line profiles in idealized model atmospheres (444). Each atmosphere is characterized by an outer radius  $R$  (in units of  $r_c = 1$ ), a continuum optical depth  $T_c$  (at  $r = r_c$ ), a static line optical depth  $T_l$ , opacities  $\chi_L \propto r^{-2}$  and  $\chi_c \propto r^{-2}$ , and constant Planck function  $B = 1$ . The two-level-atom thermalization parameter was set to  $\epsilon = 2/T_l$ . The velocity field was chosen to be either (a)  $dv/dr = \text{constant}$ , or (b)  $v(r) = v_0 [\tan^{-1}(ar + b) - \tan^{-1}(a + b)]$ , which gives a sharp rise at the point  $r_v = -(b/a)$ , and has constant terminal

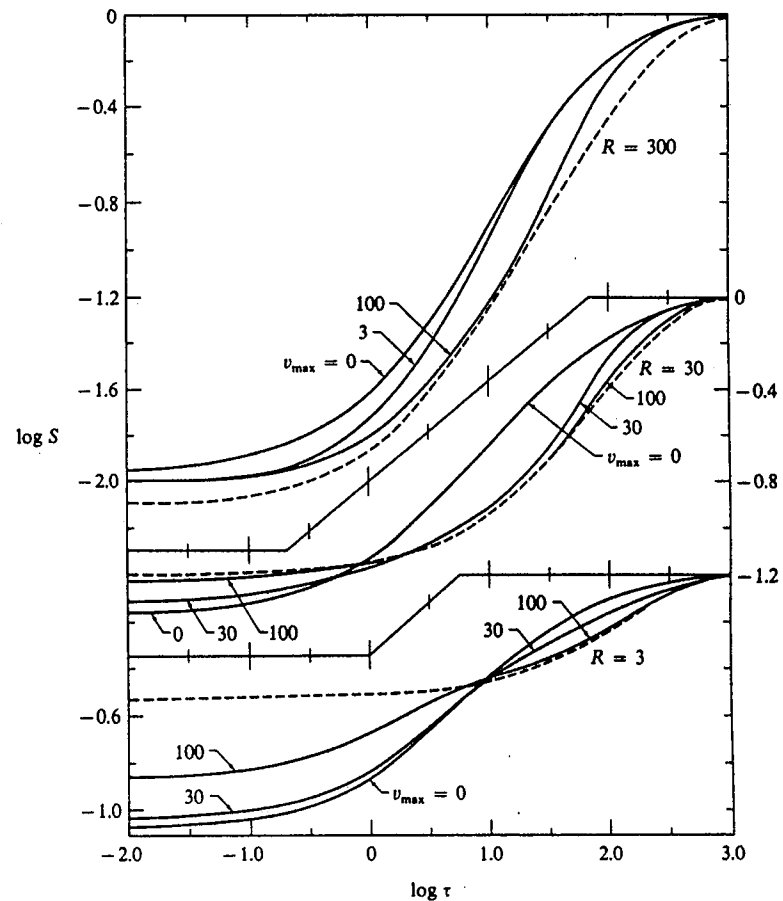
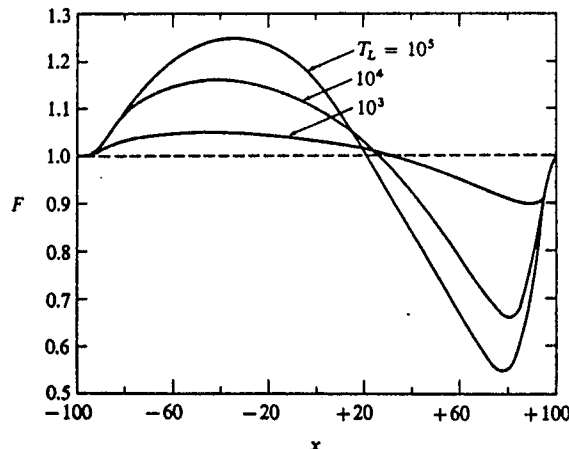


FIGURE 14-11  
Line source functions in expanding atmospheres for various values of outer radius  $R$  (in units of  $r_c$ ), and terminal velocity  $v_{\max}$  (in thermal velocity units). For all models  $T_c = 2$ ,  $T_l = 10^3$ ,  $B = 1$ , and  $\epsilon = 2 \times 10^{-3}$ . Abscissa: log of static line optical depth. The dashed line gives the mean intensity in the continuum. The curves are labeled with  $v_{\max} = v(R)$ . From (444), by permission.

velocity at large  $r$ . Form (b) is a caricature of stellar-wind solutions. Results for the source function in several models are shown in Figure 14-11; for these models  $T_l = 10^3$ ,  $T_c = 2$ ,  $r_v = (R + 1)/2$ ,  $B = 1$ , and  $\epsilon = 2 \times 10^{-3}$ . We see that the basic effect of the velocity gradient at depth is to increase the escape probability; hence the source function drops below its static value and, for large values of  $v_{\max}$ ,  $S_l$  approaches  $J_c$ , the mean intensity

## Stellar Winds



**FIGURE 14-12**  
Line profiles (emergent fluxes integrated over the disk) from expanding spherical atmospheres. Ordinate: flux relative to continuum flux. Abscissa:  $\Delta v/\Delta v_D$ . For all models,  $R = 300$ ,  $T_c = 2$ ,  $B = 1$ ,  $\epsilon = 2/T_L$ , and  $(dv/d\tau_1) = -100/T_L$ . From (444), by permission.

in the continuum (dashed line). Near the surface, the enhanced escape probability competes with interception of continuum radiation by the Doppler-shifted line. In planar geometries the latter effect dominates, and produces an *increase* in  $S_i$ ; in very extended atmospheres the former effect dominates, and  $S_i$  decreases. Flux profiles, as seen by an external observer, are shown in Figure 14-12 for models with parameters specified in the figure caption. Characteristic P-Cygni profiles are obtained with both the emission intensity and the absorption depth increasing with increasing optical depth.

The solution of the comoving-frame transfer equation by the method described above is convenient, efficient, and easily generalized to realistic stellar models. The method can also be extended to apply to multilevel atoms, and should permit the computation of line spectra for realistic model atoms in expanding atmospheres. Accurate theoretical spectra, when compared with observation, should assist in the determination of the physical structure of the atmospheres of stars with expanding envelopes and stellar winds.

The outermost atmospheric layers of many stars are in a state of continuous rapid expansion, and the material lost from a star in such a flow is called a *stellar wind*. These winds have a wide range of properties. At one extreme are very massive flows (mass-loss rate  $\sim 10^{-5} M_\odot/\text{year}$ ) that are optically thick in spectral lines (and even in some continua) and produce emission lines and P-Cygni profiles; at the other are relatively tenuous flows such as that of the Sun, which is optically thin and inconsequential in terms of mass-loss ( $10^{-14} M_\odot/\text{year}$ ), but still of great importance to the solar angular momentum balance. In Chapter 14 we discussed the problem of spectrum formation in a *given* flow; here we shall examine the *dynamics* of the wind and analyze questions of momentum and energy balance. We shall find that there are two primary mechanisms for producing stellar winds. (1) In stars with hydrogen convection zones (such as the Sun), the outer atmosphere is a mechanically-heated *corona* of very high temperature. Here we find that the corona cannot establish a static pressure balance with the interstellar medium, but must inevitably expand supersonically, driving the flow by tapping the thermal energy of the gas. (2) In early-type high-luminosity stars, the radiation field is so intense that momentum imparted to the gas by photons drives

the material in a transsonic flow. (There is also some observational evidence that there may be a corona near the surface of these stars, and our theoretical models for their winds are only *preliminary*.)

Stellar winds have important implications for many astrophysical problems. In some cases, the mass-loss rate is so large as to produce a significant change in the star's mass on a thermonuclear-evolution time-scale, and hence directly to affect the star's evolution track. In other cases, the possibility of noncatastrophic mass-loss over its entire lifetime may permit a star to evolve to a white-dwarf configuration without becoming a supernova. Stellar winds act as brakes on stellar rotation, and hence strongly influence the angular momentum content of stars. Further, stellar winds represent important sources of mass- and energy-input into the interstellar medium, and thus help to determine its composition and thermodynamic state. In this book we shall consider only winds from *single, isolated, stars*. Stellar winds can also occur in *binaries*, where they may induce *rapid mass-exchange* that radically alters the course of stellar evolution, or, in some cases, produce exotic objects such as *X-ray sources*; although space does not permit a discussion of these phenomena, the material presented here is basic to a study of the more complex cases just mentioned, and provides a background for an approach to the literature.

### 15-1 The Equations of Hydrodynamics for an Ideal Compressible Fluid

In this section we shall develop briefly the equations of hydrodynamics for an ideal (nonviscous) compressible fluid, which is taken to be a perfect gas. We shall ignore ionization effects, and assume that the material is already essentially completely ionized. No attempt will be made to discuss the equations in great depth, as numerous excellent texts and monographs on the subject of hydrodynamics are readily available (385; 692; 104; 490). For expository convenience, the equations will be derived in Cartesian coordinates when explicit reference to a coordinate system is required, then restated in vector-tensor notation, and finally rewritten in spherical coordinates (assuming spherical symmetry) for application to the stellar wind problem.

#### KINEMATICS

Let us first consider some of the basic kinematic properties of the fluid. We consider the gas to consist of a mixture of particles of different species (e.g., protons, electrons, heavy ions). Each species  $k$  has a mass  $m_k$ , and a space and velocity distribution function  $f_k(\mathbf{r}, \mathbf{V}, t)$ , defined such that  $f_k dx_1$

$dx_2 dx_3 dV_1 dV_2 dV_3$  gives the number of particles of type  $k$  in the volume element  $(\mathbf{r}, \mathbf{r} + d\mathbf{r}) = [(x_1, x_1 + dx_1), (x_2, x_2 + dx_2), (x_3, x_3 + dx_3)]$ , with velocities on the range

$$(\mathbf{V}, \mathbf{V} + d\mathbf{V}) = [(V_1, V_1 + dV_1), (V_2, V_2 + dV_2), (V_3, V_3 + dV_3)]$$

at time  $t$ . The plasma is assumed to be chemically homogeneous, so that the relative numbers of particles of different species are the same throughout the gas. The velocity distribution is characterized physically in terms of *macroscopic flow velocities* and a *microscopic thermal distribution*; the former describe the *average* motions of particles (and hence the bulk fluid motion) as seen in a fixed laboratory frame, while the latter gives the *random* individual particle motions relative to the average. We assume that the Coulomb collision rate in the plasma is so large that (a) there is *no drift* of any species relative to any other, and (b) on the microscopic level there is perfect equipartition of energy at each point, so that *all species have the same thermal distribution* specified by a *unique temperature*  $T(\mathbf{r})$ . Further, the microscopic velocity distribution is assumed to be *isotropic*.

The *number density* ( $\text{cm}^{-3}$ ) of particles of species  $k$  is given by

$$n_k(\mathbf{r}, t) \equiv \int_{-\infty}^{\infty} dV_1 \int_{-\infty}^{\infty} dV_2 \int_{-\infty}^{\infty} dV_3 f_k(\mathbf{r}, \mathbf{V}, t) \quad (15-1)$$

The *mass density* of species  $k$  is  $m_k n_k(\mathbf{r}, t)$ , and the *total density* ( $\text{gm cm}^{-3}$ ) is

$$\rho(\mathbf{r}, t) = \sum_k m_k n_k(\mathbf{r}, t) \quad (15-2)$$

The *average velocity* (i.e., the *fluid-flow velocity*) in the  $i$ th direction is

$$\langle V_i \rangle_k \equiv \int_{-\infty}^{\infty} dV_1 \int_{-\infty}^{\infty} dV_2 \int_{-\infty}^{\infty} dV_3 f_k(\mathbf{r}, \mathbf{V}, t) V_i \quad (15-3)$$

As mentioned above,  $\langle V_i \rangle_k$  is taken to be the same for all species, hence the subscript may be omitted. The full velocity component  $V_i$  of any particular particle may now be written as  $V_i = \langle V_i \rangle + V'_i$ , where  $V'_i$  is the random thermal velocity in the  $i$ th direction. Clearly  $\langle V'_i \rangle \equiv 0$ . The complete *fluid velocity* is

$$\begin{aligned} v(\mathbf{r}, t) &= \langle V_1 \rangle \mathbf{i} + \langle V_2 \rangle \mathbf{j} + \langle V_3 \rangle \mathbf{k} \\ &\equiv v_1(\mathbf{r}, t) \mathbf{i} + v_2(\mathbf{r}, t) \mathbf{j} + v_3(\mathbf{r}, t) \mathbf{k} \end{aligned} \quad (15-4)$$

The motion of the fluid results in mass transport and the *mass flux* is given by

$$\sum_k m_k n_k (\langle V_1 \rangle \mathbf{i} + \langle V_2 \rangle \mathbf{j} + \langle V_3 \rangle \mathbf{k}) = \left( \sum_k m_k n_k \right) \mathbf{v} = \rho \mathbf{v} \quad (15-5)$$

Similarly, the particles carry momentum, and the rate of transport of the  $i$ th component of momentum, across a surface oriented perpendicular to the  $j$ th direction, by particles of species  $k$ , is

$$\begin{aligned}\Pi_{ij}^k(\mathbf{r}, t) &= m_k \int_{-\infty}^{\infty} dV_1 \int_{-\infty}^{\infty} dV_2 \int_{-\infty}^{\infty} dV_3 f_k(\mathbf{r}, \mathbf{v}, t) V_i V_j \\ &= m_k \int_{-\infty}^{\infty} dV_1 \int_{-\infty}^{\infty} dV_2 \int_{-\infty}^{\infty} dV_3 f_k(\mathbf{r}, \mathbf{v}, t) (v_i + V_i)(v_j + V_j) \\ &= m_k n_k(\mathbf{r}, t) (v_i v_j + v_i \langle V_j \rangle_k + v_j \langle V_i \rangle_k + \langle V_i V_j \rangle_k) \\ &= m_k n_k(\mathbf{r}, t) (v_i v_j + \langle V_i V_j \rangle_k)\end{aligned}\quad (15-6)$$

The quantity  $\langle V_i V_j \rangle_k$  is the average of the  $i$ th and  $j$ th components of the random thermal velocity, and because the thermal distribution is isotropic and the individual components are uncorrelated,

$$\langle V_i V_j \rangle_k = \langle (V_i)^2 \rangle_k \delta_{ij} = (kT/m_k) \delta_{ij} \quad (15-7)$$

Hence

$$\Pi_{ij}^k = m_k n_k v_i v_j + (n_k kT) \delta_{ij} = m_k n_k v_i v_j + p_k \delta_{ij} \quad (15-8)$$

where  $p_k$  is the *partial pressure* from species  $k$ . Summing over all species, the total *momentum flux tensor* is given by

$$\Pi_{ij} = \left( \sum_k m_k n_k \right) v_i v_j + \left( \sum_k p_k \right) \delta_{ij} = \rho v_i v_j + p \delta_{ij} \quad (15-9)$$

where  $p$  is the *total gas pressure*.

Finally, there are two useful (and conceptually rather different) schemes for describing the changes that occur in the fluid as a result of material motions. As an external observer views the fluid, the natural description of its properties will be to write  $\alpha(x_1, x_2, x_3, t)$  for any property  $\alpha$ . The variation of  $\alpha$ , as a function of time and position, is described in terms of a time derivative  $(\partial/\partial t)$  computed at *fixed*  $(x_1, x_2, x_3)$ , and space derivatives  $(\partial/\partial x_i)$  evaluated at a *fixed*  $t$ . This system is called the *Eulerian description*. Alternatively, imagine that we *follow the motion* of a fluid element, consisting of a definite sample of material; this system is called the *Lagrangian description*. The time variation of the properties of a Lagrangian fluid element is described in terms of the *fluid-frame* time derivative  $(D/Dt)$  (also known as the "Lagrangian", "total", or "substantial" derivative). The relationship of the Lagrangian derivative to derivatives in the Eulerian frame may be obtained as follows. The derivative  $(D\alpha/Dt)$  is defined as the limit, as  $\Delta t \rightarrow 0$ , of  $[\alpha(t + \Delta t) - \alpha(t)]/\Delta t$ , where  $\alpha$  is measured in the fluid frame at times  $t$  and  $t + \Delta t$ , at (in general) two different positions:  $\mathbf{r}$ , and  $\mathbf{r} + \Delta \mathbf{r} = \mathbf{r} + \mathbf{v} \Delta t$ . Allowing for the change in

position of the fluid element we have

$$\begin{aligned}\alpha(t + \Delta t) &= \alpha(\mathbf{r}, t) + \Delta t \left[ (\partial\alpha/\partial t)_r + \sum_i (\partial\alpha/\partial x_i)_r v_i \right] \\ &= \alpha(\mathbf{r}, t) + \Delta t [(\partial\alpha/\partial t)_r + (\mathbf{v} \cdot \nabla)\alpha]\end{aligned}$$

It thus follows that for any  $\alpha$  (scalar or vector)

$$(D\alpha/Dt) = (\partial\alpha/\partial t) + (\mathbf{v} \cdot \nabla)\alpha \quad (15-10)$$

The Lagrangian system is particularly advantageous for time-dependent *one-dimensional* (planar or spherically symmetric) flows, while the Eulerian system has advantages in complicated geometries. For *steady flows* [i.e., all properties constant in time as viewed by an external observer, so that  $(\partial/\partial t) \equiv 0$ ], one usually employs the Eulerian system.

#### THE EQUATION OF CONTINUITY

Consider a fixed volume element  $d\tau$  in the fluid. If we demand overall *mass conservation*, then the rate of decrease of the mass in  $d\tau$  is given by the net mass flux out of the element through the surface  $S$  enclosing the element. That is,

$$\frac{\partial}{\partial t} \int \rho d\tau = - \oint_S (\rho \mathbf{v}) \cdot d\mathbf{S} = - \int \nabla \cdot (\rho \mathbf{v}) d\tau \quad (15-11)$$

where the second equality follows from the divergence theorem. The equation written above is true for an *arbitrary* element  $d\tau$ , and hence the integrands must be equal; therefore we have the *equation of continuity*

$$(\partial\rho/\partial t) + \nabla \cdot (\rho \mathbf{v}) = 0 \quad (15-12)$$

or, in view of equation (15-10),

$$(D\rho/Dt) + \rho \nabla \cdot \mathbf{v} = 0 \quad (15-13)$$

Equation (15-12) was also derived in §5-4 from the non-LTE rate equations [cf. equation (5-50)]. For *steady flow*,  $(\partial/\partial t) \equiv 0$ , hence

$$\nabla \cdot (\rho \mathbf{v}) = 0 \quad (15-14)$$

For a one-dimensional spherical flow, equation (15-12) becomes

$$(\partial\rho/\partial r) + r^{-2} [\partial(r^2 \rho v)/\partial r] = 0 \quad (15-15)$$

which, for steady flow implies

$$4\pi r^2 \rho v = \text{constant} = \dot{M} \quad (15-16)$$

Here  $\dot{M}$  is the *mass-loss rate* through an entire spherical surface and  $v$  denotes the velocity in the radial direction.

*Exercise 15-1:* Show that for any physical variable  $\alpha$  (scalar or vector) the equation of continuity implies that

$$\rho(D\alpha/Dt) = \partial(\rho\alpha)/\partial t + \nabla \cdot (\rho\alpha v) \quad (15-17)$$

#### MOMENTUM EQUATIONS

The *momentum density* (i.e., momentum per unit volume) in the flow is  $\rho v$ . If we again consider a fixed volume element  $d\tau$ , we may equate the time rate of change of the momentum in  $d\tau$  to the sum of the losses from the *momentum flux* through the surface  $S$  enclosing  $d\tau$ , and the gains from the *force per unit volume*  $f$  acting on the material in  $d\tau$ . That is,

$$\begin{aligned} \frac{\partial}{\partial t} \left( \int \rho v \, d\tau \right) &= - \oint_S \Pi \cdot dS + \int f \, d\tau \\ &= \int (f - \nabla \cdot \Pi) \, d\tau \end{aligned} \quad (15-18)$$

where the divergence theorem has again been employed. As the element  $d\tau$  is arbitrary, we conclude that

$$\partial(\rho v)/\partial t = -\nabla \cdot \Pi + f \quad (15-19)$$

Substituting for  $\Pi$  from equation (15-9) we have

$$[\partial(\rho v)/\partial t] + \nabla \cdot (\rho v v) = -\nabla p + f \quad (15-20)$$

In view of equation (15-17), we can rewrite equation (15-20) to obtain the equations of motion

$$\rho(Dv/Dt) = \rho[(\partial v/\partial t) + (v \cdot \nabla)v] = -\nabla p + f \quad (15-21)$$

For a spherically symmetric one-dimensional flow with a gravity force  $f_r = -(G\dot{M}\rho/r^2)$ , equation (15-21) becomes

$$\rho(\partial v/\partial t) + \rho v(\partial v/\partial r) = -(\partial p/\partial r) - (G\dot{M}\rho/r^2) \quad (15-22)$$

For steady flow the first term of equation (15-22) vanishes.

#### ENERGY EQUATION

The statement of *energy conservation* for an element of gas is conveniently given by the *first law of thermodynamics*, which equates the change in the specific (i.e., per unit mass) internal energy,  $de$ , plus the work done by the gas pressure  $p$  when the specific volume changes by an amount  $d(1/\rho)$ , to the amount of heat per unit mass added to the element,  $dq$ . That is,

$$de + p d(1/\rho) = dq \quad (15-23)$$

Imagine that these changes occur as we follow the motion of a Lagrangian fluid element for a time  $\Delta t$ , and assume that heat exchange with the surroundings occurs by means of *conduction* only (other sources and sinks—e.g., radiation and mechanical energy dissipation—being neglected) with a *conductive flux*  $q_c$ , which yields a rate of energy loss per unit mass of  $(1/\rho) \nabla \cdot q_c$ . Then equation (15-23) yields the *gas energy equation*

$$\rho \{ (De/Dt) + p[D(1/\rho)/Dt] \} = -\nabla \cdot q_c \quad (15-24)$$

Normally the conductive flux is written as  $q_c = -\kappa(\nabla T)$  where  $\kappa$  is the *thermal conductivity* of the material.

From the equation of continuity, one sees that  $\rho[D(1/\rho)/Dt] = \nabla \cdot v$ ; hence equation (15-24) can be written in the alternative form

$$\rho(De/Dt) + p(\nabla \cdot v) = -\nabla \cdot q_c \quad (15-25)$$

Now, from the momentum equation, a statement of *mechanical energy conservation* can be derived by taking the dot product of equation (15-21) with  $v$ , to find

$$\rho[D(\frac{1}{2}v^2)/Dt] + (v \cdot \nabla)p = v \cdot f \quad (15-26)$$

Adding equations (15-25) and (15-26), and noting that  $\nabla \cdot (ab) = (b \cdot \nabla)a + a(\nabla \cdot b)$ , we find a *total energy equation*

$$\rho[D(\frac{1}{2}v^2 + e)/Dt] + \nabla \cdot (pv) = v \cdot f - \nabla \cdot q_c \quad (15-27)$$

Applying equation (15-17) we may write instead

$$[\partial(\frac{1}{2}\rho v^2 + \rho e)/\partial t] + \nabla \cdot [(\frac{1}{2}\rho v^2 + \rho e + p)v + q_c] = v \cdot f \quad (15-28)$$

For one-dimensional *spherically-symmetric* flow equation (15-28) becomes

$$\frac{\partial}{\partial t} (\frac{1}{2}\rho v^2 + \rho e) + \frac{1}{r^2} \frac{\partial}{\partial r} \left[ r^2 \rho v \left( \frac{1}{2}v^2 + e + \frac{p}{\rho} \right) - r^2 \kappa \left( \frac{\partial T}{\partial r} \right) \right] = -\frac{G\dot{M}\rho v}{r^2} \quad (15-29)$$

For steady spherically symmetric flow

$$\frac{\partial}{\partial r} \left[ r^2 \rho v \left( \frac{1}{2} v^2 + h \right) - r^2 \kappa \left( \frac{\partial T}{\partial r} \right) \right] + (r^2 \rho v) (G \mathcal{M} / r^2) = 0 \quad (15-30)$$

where  $h \equiv e + (p/\rho)$  is the *specific enthalpy*. Recalling that  $(r^2 \rho v) = \text{constant}$ , we may integrate equation (15-30) to obtain the *total energy integral*

$$(4\pi r^2 \rho v) \left[ \frac{1}{2} v^2 + h - (G \mathcal{M} / r) \right] - (4\pi r^2) \kappa (\partial T / \partial r) = C \quad (15-31)$$

Equation (15-31) states that the total energy flux through a spherical surface (consisting of the flux of kinetic energy, gas enthalpy, potential energy, and heat conduction) is a constant in a steady flow.

#### SOUND WAVES

When a compressible fluid suffers a small impulsive disturbance, an oscillatory motion of small amplitude (consisting of alternating compressions and rarefactions) is generated and propagates through the medium. These oscillations are *sound waves*, and their characteristic speed is the *speed of sound*. Suppose the medium is planar and homogeneous, and originally at rest with an ambient density  $\rho_0$ , and pressure  $p_0$ . Write the perturbed values of density and pressure as  $\rho = \rho_0 + \rho_1$  and  $p = p_0 + p_1$ , respectively, where it is assumed that  $\rho_1 \ll \rho_0$  and  $p_1 \ll p_0$ ; further,  $v$ , the velocity of the disturbance, is to be regarded as a small quantity. Then substituting these expressions into the equation of continuity (15-12) and the momentum equation (15-21) (with the external force  $f \equiv 0$ ), expanding, and retaining only terms of the first order in the perturbations, we find

$$(\partial \rho_1 / \partial t) + \rho_0 (\partial v / \partial x) = 0 \quad (15-32)$$

and  $\rho_0 (\partial v / \partial t) + (\partial p_1 / \partial x) = 0 \quad (15-33)$

For an *ideal fluid* (i.e., no viscosity or conductivity), there is no thermal energy exchange from one fluid element to another, and the material behaves *adiabatically*. We may therefore write

$$(\partial p_1 / \partial x) = (\partial p / \partial \rho)_s (\partial \rho_1 / \partial x) \equiv a^2 (\partial \rho_1 / \partial x)$$

where  $(\partial p / \partial \rho)_s$  is the *isentropic derivative* of the pressure with respect to density. Now, differentiating equation (15-32) with respect to  $t$ , and (15-33) with respect to  $x$ , and eliminating the cross derivative  $(\partial^2 v / \partial t \partial x)$ , we obtain

$$(\partial^2 \rho_1 / \partial t^2) - a^2 (\partial^2 \rho_1 / \partial x^2) = 0 \quad (15-34)$$

Equation (15-34) is the *wave equation*, in which the wave velocity is  $a$ . We thus identify the *adiabatic speed of sound* as

$$a_s = [(\partial p / \partial \rho)_s]^{1/2} \quad (15-35)$$

For a perfect gas undergoing adiabatic changes,  $(p/p_0) = (\rho/\rho_0)^\gamma$ , where  $\gamma$  is the ratio of specific heats at constant pressure and constant volume ( $\gamma = \frac{5}{3}$  for an ideal monatomic gas); thus

$$a_s = (\gamma p / \rho)^{1/2} = (\gamma k T / \mu m_H)^{1/2} \quad (15-36)$$

where  $\mu$  is the number of atomic units per free particle. In certain situations there can be a very free exchange of energy between the wave and its surroundings via conduction or radiation; in this case the temperature fluctuations in the sound wave are destroyed (the wave is thereby damped), and the wave propagation proceeds isothermally. In this event  $p = \rho(kT_0/\mu m_H)$  and the *isothermal sound speed* is

$$a = (kT_0 / \mu m_H)^{1/2} \quad (15-37)$$

#### THE RANKINE-HUGONIOT RELATIONS FOR STATIONARY SHOCKS

The speed of sound determines the rate at which a disturbance propagates naturally in a compressible fluid. If the velocity of the flow exceeds the speed of sound, then the adjustments of the fluid state by sound waves cannot proceed quickly enough, and situations occur where the properties of the flow may change markedly over a rather small distance. This gives rise to almost discontinuous changes at a narrow interface called a *shock front*. Shocks may occur in a wide variety of circumstances. For example, in a pulsating star, a wave initiated at great depth will propagate with larger and larger velocities as it progresses upward in the atmosphere, because of the decrease in density; eventually it runs through the material at supersonic velocities, producing a shock front that travels outward into the upper layers of the atmosphere. Such shocks produce interesting spectroscopic phenomena in RR Lyrae and Cepheid variables, but we shall not be able to pursue this subject here. Alternatively, in a steady flow, a *stationary* shock front may be produced where the gas, in effect, encounters an obstacle (e.g., a constriction in a nozzle or flow channel or at the point where a stellar wind runs into the interstellar medium). For the purposes of this chapter, only stationary shocks will be considered.

The shock front itself has a structure whose properties are determined by dissipative processes involving viscosity, heat conduction, and radiation; furthermore, the downstream material may be forced out of equilibrium in

one or more degrees of freedom, depending on how long are the characteristic relaxation times that restore the equilibrium [see (692) for a detailed discussion of these phenomena]. These effects will be ignored here, and it will be assumed that the fluid is a perfect monatomic gas in equilibrium throughout, and that the shock is a discontinuity at an infinitely sharp interface. If we consider the flow of particles across an interface, it is clear that the flux of mass, momentum, and energy must be conserved. Using subscript 1 to denote *upstream* quantities (i.e., material flowing into the shock), and subscript 2 to denote *downstream* quantities (i.e., post-shock material), the conservation requirements just mentioned become (in planar geometry)

$$\rho_1 v_1 = \rho_2 v_2 \quad (15-38)$$

$$p_1 + \rho_1 v_1^2 = p_2 + \rho_2 v_2^2 \quad (15-39)$$

$$\text{and } \rho_1 v_1 [e_1 + (p_1/\rho_1) + \frac{1}{2}v_1^2] = \rho_2 v_2 [e_2 + (p_2/\rho_2) + \frac{1}{2}v_2^2] \quad (15-40)$$

The appropriate fluxes have been identified from equations (15-5), (15-9), and (15-28). In view of equation (15-38), and the results for a perfect gas that  $e = (p/\rho)/(y - 1)$  so that  $h = e + (p/\rho) = y(p/\rho)/(y - 1)$ , equation (15-40) can be rewritten as

$$[\gamma p_1 / (\gamma - 1) \rho_1] + \frac{1}{2} v_1^2 = [\gamma p_2 / (\gamma - 1) \rho_2] + \frac{1}{2} v_2^2 \quad (15-41)$$

If we eliminate  $v_2$  by means of equation (15-38), use the definition of the sound speed in equation (15-36), and define the *Mach number*  $M_1 \equiv v_1/a_s$ , then equations (15-39) and (15-41) may be rewritten as

$$(p_2/p_1) = 1 + \gamma M_1^2 [1 - (\rho_1/\rho_2)] \quad (15-42)$$

$$\text{and } 2[(\rho_1 p_2 / \rho_2 p_1) - 1] = (\gamma - 1) M_1^2 [1 - (\rho_1/\rho_2)^2] \quad (15-43)$$

which are known as the *Rankine-Hugoniot* relations. Equation (15-42) gives  $p_2$  as a function of  $\rho_2$  for given  $(\rho_1, p_1)$ . In principle, two solutions exist: (a)  $p_2 > p_1$  and  $\rho_2 > \rho_1$  and (b)  $p_2 < p_1$  and  $\rho_2 < \rho_1$ . However, it is found [see (385, §§82-84) or (692, §17)] that case (b) is excluded on the basis of the second law of thermodynamics and stability considerations, and that only *compression shocks* are physically possible.

Equations (15-42) and (15-43) can be solved simultaneously for  $(p_2/p_1)$  and  $(\rho_2/\rho_1)$ , yielding

$$(\rho_2/\rho_1) = (v_1/v_2) = (\gamma + 1) M_1^2 / [(\gamma - 1) M_1^2 + 2] \quad (15-44)$$

$$\text{and } (p_2/p_1) = [2\gamma M_1^2 - (\gamma - 1)] / (\gamma + 1) \quad (15-45)$$

Applying the perfect gas law we also may write

$$(T_2/T_1) = [2\gamma M_1^2 - (\gamma - 1)][(\gamma - 1) M_1^2 + 2] / M_1^2 (\gamma + 1)^2 \quad (15-46)$$

*Exercise 15-2:* (a) Verify equations (15-42) and (15-43). (b) Show that equation (15-43) can be rewritten in the customary forms

$$\begin{aligned} e_2 - e_1 &= \frac{1}{2}(\rho_1^{-1} - \rho_2^{-1})(p_1 + p_2) \\ \text{or} \quad h_2 - h_1 &= \frac{1}{2}(\rho_1^{-1} + \rho_2^{-1})(p_2 - p_1) \end{aligned}$$

*Exercise 15-3:* (a) Verify equations (15-44) through (15-46). (b) Show that the downstream Mach number is

$$M_2^2 = [(\gamma - 1)M_1^2 + 2] / [2\gamma M_1^2 - (\gamma - 1)]$$

and that this implies the downstream flow is always subsonic.

## 15-2 Coronal Winds

The outermost layers of the solar atmosphere comprise the *corona*, a tenuous (characteristic electron density  $\sim 4 \times 10^8 \text{ cm}^{-3}$ ), high-temperature ( $T \sim 1.5 \times 10^6 \text{ }^\circ\text{K}$ ) envelope which can be observed, at eclipses, to extend to several solar radii. As was described in §7-7, the high coronal temperature is a result of energy input from wave dissipation. The ultimate source of the waves providing this mechanical heating is the hydrogen convection zone, and we believe that all stars that have extensive convection zones should also have coronae.

For many years the corona was regarded as an essentially static envelope bound to the Sun, and although it was realized that particle bombardment of the Earth from energetic events (e.g., flares) on the Sun produced auroral and geomagnetic effects (164; 165), it was Biermann (91; 92; 93) who first advanced the idea of *continuous particle emission* ("corpuscular radiation") from the Sun. Realizing the importance, at coronal temperatures, of energy transport by conduction, Chapman (166) showed that the corona extended far out into interplanetary space and, in fact, enveloped the Earth in a low-density high-temperature medium. Subsequently Parker showed (496; 498) that any reasonable hydrostatic model of the corona, starting from known conditions near the Sun, led to such high pressures at large distances, as to preclude the possibility of containment by the pressure of the interstellar medium. Thus *static models are internally inconsistent*, and *large-scale coronal expansion must occur*. This expansion provides the source of the particle emission proposed by Biermann.

Parker developed a theoretical model indicating a flow with low velocities near the Sun, rising to very large supersonic values at large distances; he called this transsonic flow the *solar wind*, and made predictions of typical flow velocities, densities, and particle fluxes at the Earth's orbit. These predictions were supported by many bits of evidence [see the summaries of the fascinating historical growth of our conceptions of the solar wind in (107, Chap. 1) and (324, Chap. 1)], but an alternative model was proposed

by Chamberlain (147), which was everywhere subsonic and produced only a low-velocity *solar breeze* at the Earth's orbit. The ensuing debate in the literature, based almost entirely on theoretical considerations, led to a sharpening of the formulation of the theory (and makes interesting reading today because of the high standard of scientific argumentation it contains!). But the question of which picture really applied remained undecided until direct measurements from space vehicles provided conclusive evidence in favor of a high-speed wind.

Detailed measurements of solar-wind properties show that there is considerable fluctuation of all the physical variables; many of the variations correlate with a solar rotation period and hence reflect changes in the initial conditions of the flow at the corona, while others are the result of violent events such as flare-generated blast waves. Despite these variations, it is useful to consider the background low-speed "quiet" wind, whose characteristics must result from the conditions prevalent in the corona as a whole. A summary of quiet solar-wind properties measured at the Earth's orbit is given in Table 15-1. Although it must be emphasized that these data define only a high-order abstraction of the real solar wind, they nevertheless provide typical values against which theoretical results can be compared. From the data given, we see that the wind is a highly supersonic (Mach number  $\approx 8$ ), nearly-radial flow. It is easy to show (Exercise 15-4) that the effects of the mass-loss in the wind on the evolution of the Sun as a star are negligible. Moreover, the corona-wind ensemble is optically thin. Thus at first sight the flow seems to be of little significance from a stellar-astrophysical point of view. We shall see, however, that even this rather weak (see below) flow has implications of great consequence to the question of angular-momentum loss by the Sun.

TABLE 15-1  
*Properties of the Quiet Solar Wind at the Earth's Orbit*

Radial component of flow velocity	$300\text{--}325 \text{ km s}^{-1}$
Nonradial component of flow velocity	$8 \text{ km s}^{-1}$
Proton (or electron) density	$9 \text{ cm}^{-3}$
Average electron temperature	$1.5 \times 10^5 \text{ }^\circ\text{K}$
Average proton temperature	$4 \times 10^4 \text{ }^\circ\text{K}$
Magnetic field intensity	$5 \times 10^{-5} \text{ gauss}$
Proton flux	$2.4 \times 10^8 \text{ cm}^{-2} \text{ s}^{-1}$
Kinetic energy flux	$2.2 \times 10^{-1} \text{ erg cm}^{-2} \text{ s}^{-1}$
Enthalpy flux	$8 \times 10^{-3} \text{ erg cm}^{-2} \text{ s}^{-1}$
Gravitational flux	$4 \times 10^{-3} \text{ erg cm}^{-2} \text{ s}^{-1}$
Electron heat-conduction flux	$7 \times 10^{-3} \text{ erg cm}^{-2} \text{ s}^{-1}$

SOURCE: Adapted from (324, 44-45), by permission.

*Exercise 15-4:* Using the particle flux given in Table 15-1, show that the rate of mass-loss,  $\dot{M} = 4\pi r^2 n m v$ , where  $n$  is the particle density and  $m$  is a mean particle mass, is  $\sim 2 \times 10^{-14} M_\odot/\text{year}$ . Compare this with the thermonuclear mass-loss rate required to yield the solar luminosity.

As mentioned previously, we believe there should be coronae for all stars that have hydrogen convection zones (i.e., spectral types F and later); these stars should also have stellar winds. There is, in fact, direct observational evidence (e.g., P-Cygni line-profiles) for massive coronal winds in many late-type supergiants and giants. Thus estimates of mass-loss rates [see, e.g., (624, 238; 70, 246)] range from  $2 \times 10^{-10} M_\odot/\text{year}$  for K-giants to  $10^{-8} M_\odot/\text{year}$  for M-giants; and from  $10^{-7} M_\odot/\text{year}$  for G- and K-supergiants to  $10^{-6}$  or  $10^{-5} M_\odot/\text{year}$  for M-supergiants. All of these are coronal winds resulting mainly from the high temperature of the stellar corona (except possibly for the M-stars, where radiation pressure on grains may be important). Another class of massive winds ( $10^{-6}\text{--}10^{-5} M_\odot/\text{year}$ ) is found for early-type stars (OB supergiants and WR stars); these flows are driven by radiation pressure acting on the material (cf. §15.4).

In this section we shall examine the basic physics of coronal winds, using simplified and idealized descriptions, both of the material properties and of the nature of the flow. Our goal will be to gain insight into the overall nature of these winds, rather than to attempt detailed modeling. We shall repeatedly refer to the solar wind as an example, and as an indicator of what other processes need to be considered in an "ultimate" stellar-wind theory.

#### EXPANSION OF THE SOLAR CORONA

Suppose the corona is taken to be a fully-ionized pure-hydrogen plasma with  $T_0 \approx 1.5 \times 10^6 \text{ }^\circ\text{K}$  and  $n_0 \approx 4 \times 10^8 \text{ cm}^{-3}$ , where  $n_0$  denotes the density of protons or electrons ( $n_p = n_e$  for charge neutrality). At these high temperatures the electrons have large velocities, and can conduct energy efficiently, producing an energy flux  $q_c = -\kappa \nabla T$ , where the conductivity  $\kappa$  is given (598, 86) by  $\kappa = \kappa_0 T^4$  with  $\kappa_0 \approx 8 \times 10^{-7} \text{ ergs cm}^{-1} \text{ s}^{-1} \text{ deg}^{-1}$ . At  $10^6 \text{ }^\circ\text{K}$ , the conductivity of the plasma far exceeds ordinary laboratory conductors! If we assume that conduction is the dominant energy transport mechanism in the corona, then for equilibrium we must have  $\nabla \cdot q_c = 0$ , which implies that

$$r^{-2} d[r^2 \kappa_0 T^4 (dT/dr)]/dr = 0 \quad (15-47)$$

This equation can be integrated twice, and demanding that  $T \rightarrow 0$  as  $r \rightarrow \infty$ , we find

$$T(r) = T_0 (r_0/r)^{\frac{1}{3}} \quad (15-48)$$

where  $r_0$  denotes a suitable reference-level in the corona (which is of the order of  $R_\odot = 7 \times 10^{10} \text{ cm}$ ). The temperature fall-off implied by equation

(15-48) is extremely slow, and at the earth's orbit ( $r_{\oplus} = 1.5 \times 10^{13}$  cm) we find  $T \approx 3.3 \times 10^5$  °K for  $T_0 = 1.5 \times 10^6$  °K; thus *the earth is enveloped by high-temperature coronal material.*

If the corona were in hydrostatic equilibrium, we would have

$$(dp/dr) = -(G\mathcal{M}_{\odot}\rho/r^2) \quad (15-49)$$

The Debye length in the corona at the temperature and density quoted above is only about 0.3 cm [cf. equation (9-101)]. Hence the plasma is neutral except on the smallest scales, and we may write  $n_e = n_p \equiv n$  and  $\rho = n(m_p + m_e) = nm$ , where  $m$  denotes the mass of a hydrogen atom, and  $p = 2nkT$ . Then the hydrostatic equation becomes

$$d(nT)/dr = -(G\mathcal{M}_{\odot}m/2k)(n/r^2) \quad (15-50)$$

If  $T$  were constant, and we were to consider only distances  $r \approx r_0$ , we could approximate equation (15-50) with the usual planar limiting form  $d(\ln n)/dr = -(1/H)$ , where the scale-height  $H \equiv (G\mathcal{M}_{\odot}m/2kT_0r_0)^{-1} \approx 10^5$  km. As shown in Exercise 15-5, this scale-height is so large that the predicted particle density near the earth's orbit is quite large. We would then conclude that the Earth is immersed in a hot, fairly dense, extension of the corona. Actually the assumption that  $T \equiv T_0$  is too crude, and produces somewhat of an overestimate of  $n(r_{\oplus})$ . If, instead, we make use of equation (15-48), we may rewrite equation (15-50) as

which yields the solution

$$d[(r_0/r)^4 n]/d(r/r_0) = -(r_0/r)^2 n/H \quad (15-51)$$

$$n(r) = n_0(r/r_0)^4 \exp\{-7r_0[1 - (r_0/r)^4]/5H\} \quad (15-52)$$

from which we deduce  $n \sim 9 \times 10^4$  near the earth for  $n_0 = 4 \times 10^8$ .

*Exercise 15-5:* Assume the corona is isothermal,  $T \equiv T_0$ , but allow for the variation of the gravitational force to obtain an expression for  $n(r)$ . With  $n_0 \approx 4 \times 10^8$  cm<sup>-3</sup>, show that the particle density near the earth's orbit is about  $4 \times 10^5$  cm<sup>-3</sup>.

*Exercise 15-6:* Show that equation (15-52) yields a minimum for  $n$  at  $(r/r_0) = (7/4)(r_0/H)$ , and that  $n(r)$  increases outward beyond that point (formally this configuration would be unstable against a Rayleigh-Taylor instability).

Combining equations (15-48) and (15-52), we find that the pressure is

$$p(r) = p_0 \exp\{-7r_0[1 - (r_0/r)^4]/5H\} \quad (15-53)$$

Instead of vanishing at  $(r/r_0) = \infty$ , the pressure approaches a *finite* value. Adopting  $p_0 \approx 0.2$  dynes cm<sup>-2</sup>, we find  $p_{\infty} \approx 10^{-5}$  dynes cm<sup>-2</sup>. This pressure is to be compared with the pressure expected from the material and

magnetic fields in the interstellar medium. The average density of the medium is of the order of 1 cm<sup>-3</sup>; for an H I region,  $T \sim 10^2$  °K, while in a typical H II region  $T \sim 10^4$  °K, so that we expect pressures to range from  $1.4 \times 10^{-14}$  to  $3 \times 10^{-12}$  dynes cm<sup>-2</sup>. The magnetic field in the medium is of the order of  $10^{-5}$  gauss; hence the magnetic pressure ( $B^2/8\pi$ ) is of the order of  $4 \times 10^{-12}$  dynes cm<sup>-2</sup>. The pressure attributable to cosmic rays is estimated to be about  $2 \times 10^{-12}$  dynes cm<sup>-2</sup>; hence a reasonable upper bound of  $10^{-11}$  dynes cm<sup>-2</sup> can be assigned as the total interstellar pressure. This value is a factor of  $10^6$  smaller than that estimated for a hydrostatic corona, and we conclude that *the corona cannot be contained, but must undergo a steady expansion*. We therefore abandon the assumption of hydrostatic equilibrium and inquire into the hydrodynamics of coronal expansion.

#### ONE-FLUID MODELS OF STEADY, SPHERICALLY SYMMETRIC CORONAL WINDS

To simplify the treatment of the hydrodynamics of a coronal wind, the following assumptions are made: (1) the flow is taken to be *steady*; (2) the wind is spherically symmetric; (3) the gas is an ideal compressible fluid. Clearly all of these assumptions are idealizations, and they restrict the applicability of the results for, say, the real solar wind; nevertheless they provide a good basic physical model for general study.

The equations describing a steady flow are the *equation of continuity* (mass conservation)

$$r^{-2}d(r^2\rho v)/dr = 0 \quad (15-54)$$

the *momentum equation*

$$\rho v(dv/dr) = -(dp/dr) - \rho(G\mathcal{M}_{\odot}/r^2) \quad (15-55)$$

and the *energy equation* (including conductivity)

$$\frac{1}{r^2} \frac{d}{dr} \left[ r^2 \rho v \left( \frac{1}{2}v^2 + e + \frac{p}{\rho} \right) \right] = -\rho v \left( \frac{G\mathcal{M}_{\odot}}{r^2} \right) + \frac{1}{r^2} \frac{d}{dr} \left( r^2 \kappa \frac{dT}{dr} \right) \quad (15-56)$$

For a fully ionized gas of pure hydrogen,  $p = 2nkT$  and  $\rho = nm$ , where  $n = n_p = n_e$  and  $m$  is the mass of a hydrogen atom. The specific internal energy of the gas is  $2(\frac{3}{2}nkT)/(nm) = (3kT/m)$ , and  $(p/\rho) = (2nkT)/(nm) = (2kT/m)$ , so the specific enthalpy is  $h = e + (p/\rho) = (5kT/m)$ . Note that equation (15-56) does not include any terms representing radiative losses or mechanical energy deposition from dissipation of waves. The assumption made is that these processes occur in a relatively thin layer at the base of the corona, and that above some reference level only the kinetic, potential, thermal (enthalpy), and conductive terms need be taken into account.

The continuity equation can be integrated to give

$$4\pi r^2 nv = F = \text{constant} \quad (15-57)$$

where  $F$  denotes the particle flux, or

$$\dot{M} = mF = 4\pi r^2 nmv = \text{constant} \quad (15-58)$$

where  $\dot{M}$  denotes the rate of mass-loss. The energy equation can be integrated to give

$$(4\pi r^2 nv)[\frac{1}{2}mv^2 + 5kT - (G\dot{M}_\odot m/r)] - (4\pi r^2)\kappa(dT/dr) = E = \text{constant} \quad (15-59)$$

which states that the total energy flux through a spherical surface is a constant of the flow. Equations (15-57), (15-55), and (15-59) comprise a nonlinear system of two first-order differential equations, containing two constants of integration; two more constants will result from the integration of the system; hence a total of four conditions (boundary conditions or specifications of the nature of the solution) must, in general, be imposed. Before discussing this general problem, however, it is extremely instructive to consider the simple case of an isothermal corona.

If we demand that the flow be strictly isothermal, we need to specify only  $n$  and  $v$ , and hence we may omit the energy equation and employ only the momentum and continuity equations. [The ad hoc assumption  $T = \text{constant}$  is equivalent to invoking some unspecified mechanism to heat or cool the gas in just the right way as to yield the desired temperature.] Equation (15-55) becomes

$$nmv(dv/dr) = -2kT_0(dn/dr) - nm(G\dot{M}_\odot/r^2) \quad (15-60)$$

and using equation (15-57) to eliminate  $n$  we find

$$\frac{1}{2}[1 - (2kT_0/mv^2)](dv^2/dr) = -(G\dot{M}_\odot/r^2)[1 - (4kT_0r/G\dot{M}_\odot m)] \quad (15-61)$$

This equation yields several families of solutions that have substantially different mathematical behaviors and physical significance. For the solar corona,  $(4kT_0r_0/G\dot{M}_\odot m) \approx 0.3$ . Thus it is clear that the righthand side of equation (15-61) is negative for  $r < r_c$  and positive for  $r_c < r < \infty$ , where  $r_c$  is the critical radius

$$r_c \equiv (G\dot{M}_\odot m/4kT_0) \quad (15-62)$$

at which the righthand side is exactly zero. For the solar corona,  $(r_c/r_0) \approx 3.5$ . At  $r = r_c$ , the lefthand side of equation (15-61) must also be zero; this may occur in one of two ways. We may either have

$$(dv/dr)_{r_c} = 0 \quad (15-63)$$

or

$$v(r_c) = (2kT_0/\dot{m})^{1/2} \equiv v_c \quad (15-64)$$

The critical velocity  $v_c$  defined by equation (15-64) is equal to the isothermal sound speed.

We now restrict attention to solutions for which both  $v$  and  $(dv/dr)$  are single-valued and continuous. First, suppose that equation (15-63) is satisfied. We may then construct solutions for which  $1 - (2kT_0/mv^2)$  has the same sign for all  $r$ . If  $v(r_c) < v_c$  then  $v(r)$  will have a relative maximum at  $r_c$ ; this yields solutions of type 1 shown in Figure 15-1. These solutions are everywhere subsonic. On the other hand, if  $v(r_c) > v_c$ , then  $v(r)$  will have a relative

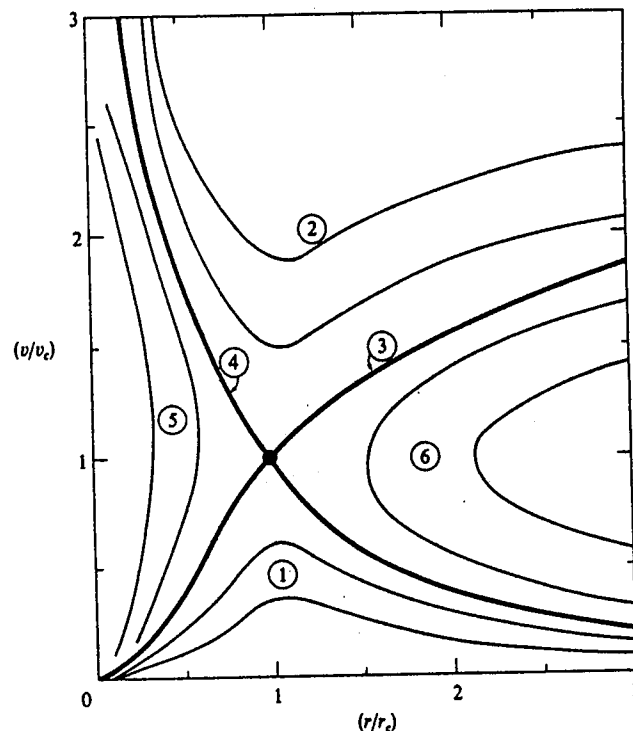


FIGURE 15-1  
Schematic variation of velocity in units of the critical velocity  $v_c$ , as a function of radial distance in units of the critical radius  $r_c$ , for stellar winds and breezes. Solutions of type 1 are the subsonic breezes. Solutions of type 2 are everywhere supersonic. Solutions 3 and 4 are the transonic critical solutions that pass through the critical point (heavy dot) continuously. Solutions of types 5 and 6 are double-valued, but are important for fitting shock transitions.

minimum at  $r_c$ , and will be everywhere supersonic; these are the type-2 solutions shown in Figure 15-1.

Alternatively, if equation (15-64) is satisfied, we obtain a *critical solution* (i.e.,  $v \equiv v_c$  at  $r = r_c$ ) that has a *finite slope* at  $r = r_c$ . Suppose that  $(dv/dr)_{r_c} > 0$ ; then we obtain a *unique transsonic solution* that is monotone increasing from subsonic speeds ( $v < v_c$ ) for  $r < r_c$  to supersonic velocities ( $v > v_c$ ) for  $r > r_c$ . This unique solution is shown as type 3 in Figure 15-1. If  $(dv/dr)_{r_c} < 0$ , then we obtain a unique solution in which  $v(r)$  is monotonically decreasing from supersonic speeds for  $r < r_c$  to subsonic speeds for  $r > r_c$ ; this is shown as type 4 in Figure 15-1.

Finally, there exist two families of solutions defined by the restrictions  $r \geq r_* > r_c$  or  $r \leq r_* < r_c$ , both of which have  $v(r_*) = v_c$  and  $(dv/dr)_{r_*} = \infty$ . These give rise to the double-valued solutions of types 5 and 6 shown in Figure 15-1. Initially we exclude consideration of these solutions because they are double-valued; we shall find later, however, that they may be used to provide *part* of a complete solution that includes a shock transition to match boundary conditions as  $r \rightarrow \infty$ .

To decide which solution to choose, we must now invoke physical boundary conditions. First, both the entire family of type-2 solutions and the unique type-4 solution can be excluded because they predict velocities  $v > v_c \approx 170 \text{ km s}^{-1}$  in the low corona, which is *not* observed. This leaves solutions of type 1 or the unique transsonic solution of type 3. We may make the choice on the basis of the behavior of the solution as  $r \rightarrow \infty$ . Equation (15-61) may be integrated straightaway to yield

$$(v/v_c)^2 - \ln(v/v_c)^2 = 4 \ln(r/r_c) + 4(r_c/r) + C \quad (15-65)$$

*Exercise 15-7:* (a) Verify equation (15-65). (b) Evaluate  $C$  for the critical solutions. (c) Evaluate  $C$  for solutions of types 1 and 2.

Consider first solutions of type 1 as  $r \rightarrow \infty$ . Here  $(v/v_c)$  is  $< 1$  and decreasing as  $r \rightarrow \infty$ , hence on the lefthand side the dominant term will be  $-2 \ln(v/v_c)$ , and on the righthand side it will be  $4 \ln(r/r_c)$ . Thus as  $r \rightarrow \infty$ , then  $v \propto r^{-2}$ , which implies (from the equation of continuity) that  $n$  remains *finite*. These solutions thus yield a pressure at  $r = \infty$  which greatly exceeds the ambient interstellar pressure, and therefore they can be rejected on the same grounds as the hydrostatic solution was. On the other hand, the critical solution has  $(v/v_c) > 1$  and increasing as  $r \rightarrow \infty$ , hence we find  $v \approx 2v_c[\ln(r/r_c)]^{\frac{1}{2}}$ . In this case  $n \propto r^{-2}v^{-1} \rightarrow 0$  as  $r \rightarrow \infty$ , and we conclude that this critical solution can indeed match the boundary condition at infinity.

Following a line of reasoning similar to that outlined above, Parker concluded (correctly!) that the solar corona must be undergoing a transsonic expansion into interplanetary and interstellar space (496), and that near

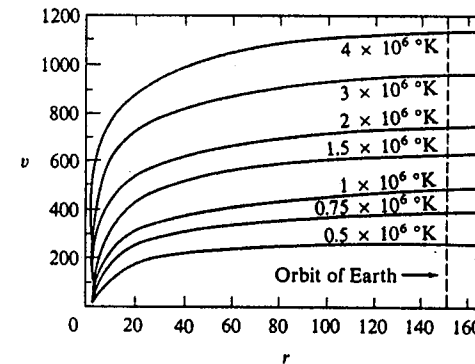


FIGURE 15-2  
Isothermal solar wind solutions; curves are labeled with coronal temperature. Ordinate: velocity in  $\text{km s}^{-1}$ ; abscissa: heliocentric distance in  $10^6 \text{ km}$ . From (496), by permission.

1273

the orbit of the Earth the *solar wind* has velocities of the order of a few hundred  $\text{km s}^{-1}$ . Several wind solutions for isothermal coronae at different temperatures are shown in Figure 15-2. The wind solution given above is not entirely satisfactory because  $(v/v_c)$  increases without limit as  $(r/r_c) \rightarrow \infty$ . This behavior is an artifact of the assumption that the corona is strictly isothermal. The corona is, in fact, nearly isothermal near the Sun because conduction is effective and distributes the heat deposited by wave dissipation very efficiently, thus obliterating large temperature gradients. At large distances, however, expansion of the gas must ultimately force it to cool; if we insist that  $T$  remain fixed, we have, in effect, introduced a (spurious) energy source to maintain the temperature. This effectively results in a continuous deposit of energy into the enthalpy of the gas, and this energy is available to do work to continue to accelerate the gas without limit. The problem is easily overcome, however, and Parker was able to produce satisfactory wind solutions by using either of two assumptions. (a) The corona is isothermal for  $r_\odot \leq r \leq r_*$ , and expands *adiabatically* for  $r > r_*$ . In this case, for  $r > r_*$  the pressure and density are related by a polytropic law of the form  $p = p_0(\rho/\rho_0)^\gamma$  with  $\gamma = \frac{5}{3}$  (ideal gas). (b) The corona is everywhere polytropic with a polytropic exponent  $\gamma < \frac{5}{3}$ . Both of these classes of solutions avoid an unphysical increase in  $v$  at large  $r$ , and one finds that  $v$  approaches a finite value  $v_\infty$  as  $r \rightarrow \infty$ .

The isothermal solutions described above reveal the broad outlines of the nature of coronal expansion into a supersonic wind, but clearly are inadequate for a detailed description of the flow. In particular, in solving the

problem, we wish to determine the temperature distribution  $T(r)$ . We must, therefore, turn to the full set of equations including energy balance, namely equations (15-55), (15-57), and (15-59). As before, there are two basic classes of solutions to be considered: (1) subsonic solutions, called *stellar breezes*, which resemble those of type 1 shown in Figure 15-1; (2) transsonic critical solutions, *stellar winds*, resembling the unique solution of type 3 shown in Figure 15-1. These two classes are distinguished from one another by the value of the total energy flux  $E$  in equation (15-59). The breeze solutions all have  $E = 0$ , while the wind solutions have  $E > 0$ .

Although we are primarily interested in *wind* solutions in the solar context, the *breeze* solutions, which have been studied extensively (147; 532), played an important role in the development of the theory, and it is worthwhile to consider them briefly here. In the breeze solutions, as  $r \rightarrow \infty$ , then  $u \rightarrow 0$ ,  $T \rightarrow 0$ , and  $p \rightarrow 0$ . There is a whole family of such solutions that are differentiated from one another by the limiting value of  $(mv^2/kT)$  as  $r \rightarrow \infty$  (532). Because a match to the interstellar pressure can now be achieved, we cannot exclude these solutions from the outset, as we could for an isothermal wind; indeed, Chamberlain (147) advocated this type of solution for the solar corona, in which case the velocity of the material near the Earth's orbit would be only  $20 \text{ km s}^{-1}$ . He argued that the correct hydrodynamic solution should be consistent with an evaporative model of the corona, in which individual particle motions are calculated assuming a critical level above which the density is so low that fast-moving particles suffer no further collisions, but escape. He found that in the evaporative model the mean speed of ions near  $r_\oplus$  would be about  $10 \text{ km s}^{-1}$ , and concluded that the breeze (rather than wind) solution was correct. The question was laid aside when direct observation proved the validity of the wind solution. But subsequent work (108; 339) has shown that the basic premise that the hydrodynamic and evaporative pictures should agree is, indeed, correct, and that the difficulty lay in the calculation of the original evaporative model. In particular, when account is taken of the fact that particles moving at different speeds escape from *different* levels, not from a *single* "critical" level (the faster particles escape from deeper, denser layers), and when a correct dynamic calculation is made of the electric field in the plasma that couples the electron and proton flows together, then the evaporative solutions yield  $n \approx 10 \text{ cm}^{-3}$ ,  $v \approx 300 \text{ km s}^{-1}$ , and  $T(\text{proton}) \approx 5 \times 10^4 \text{ °K}$ , in good agreement with the observed values. We would now conclude that the correct evaporative model supports the *solar wind* solution.

Let us now examine the wind solutions in greater detail. In all of these solutions, as  $r \rightarrow \infty$ , then  $v \rightarrow v_\infty$  (a nonzero value),  $n \rightarrow 0$ , and  $T \rightarrow 0$ . As mentioned above, four distinct conditions are required to specify the solution uniquely. Typically, these may be chosen to be values for the coronal density and temperature, and to meet the requirements that the solution pass

smoothly through the critical point, and that  $T(r) \rightarrow 0$  as  $r' \rightarrow \infty$ . The last of these conditions, however, is actually more complex than it seems, and it is now known that the nature of the variation of  $T$  with  $r$  depends upon the mechanism of heat transport at  $r = \infty$  [see (200; 201; 202; 532; 324, 47)]. Suppose first that the heat-conduction flux remains finite at  $r = \infty$ , with a value  $E_c(\infty)$ . From equation (15-59) it is clear that we will then find  $v_\infty = \{2[E - E_c(\infty)]/\mathcal{M}\}^{1/2}$ , and further, because  $[r^2 T^4 (dT/dr)]_\infty = \text{constant}$ , the temperature obeys the asymptotic law  $T \propto r^{-4}$ . This is the same law found by Chapman, and used by Parker (499) in his wind solutions. Next we might suppose that both a conduction flux and an enthalpy flux persist to  $r = \infty$ , and that the ratio  $(5kTv)/[r^2 T^4 (dT/dr)] \rightarrow \text{constant}$ . In this case both fluxes approach zero at  $r = \infty$ , and  $v_\infty = (2E/\mathcal{M})^{1/2}$ . Further, the special condition imposed on the ratio of the fluxes implies that  $T \propto r^{-4}$ , a solution first obtained by Whang and Chang (667). Finally, we might suppose that the conductive flux vanishes, as  $r \rightarrow \infty$ , *more rapidly* than the enthalpy flux. Again  $v_\infty = (2E/\mathcal{M})^{1/2}$ . In this case there is no energy exchange mechanism in the flow as  $r \rightarrow \infty$ , and the gas merely expands *adiabatically*. If the polytropic exponent is  $\gamma$ , then  $T \propto \rho^{(\gamma-1)}$ . But  $\rho \propto r^{-2}$ ; hence, as  $r \rightarrow \infty$ , then  $T \propto (r^{-2})^{(1/\gamma-1)}$  or  $T \propto r^{-4}$ , for  $\gamma$  equal to  $\frac{5}{3}$  (ideal gas).

The relationship of these solutions to one another was explained lucidly by Durney (200), who considered wind solutions that were all chosen to have the same value for  $T_0$ , but different values for  $n_0$ . For small values of  $n_0$ , the critical solutions yield large values for  $e(\infty) \equiv (E/F)$  which is the residual energy per particle at  $r = \infty$ , and they have  $T \propto r^{-4}$ . As  $n_0$  is increased, the conductive part of  $e(\infty)$ , say  $e_c(\infty)$ , becomes smaller, and at a particular value ( $n_0^*$ ),  $e_c(\infty) = 0$  and  $T \propto r^{-4}$  (i.e., this particular value gives the Whang and Chang solution). As  $n_0$  is increased further,  $e_c(\infty)$  remains equal to zero, and now  $e(\infty)$  decreases; here  $T \propto r^{-4}$ . Finally, when  $n_0$  increases still further, a limiting value is reached at which  $e(\infty) = 0$ , and a stellar breeze solution is obtained (see Figure 15-3). Physically, these results imply that, as  $n_0$  increases, more and more of the conductive flux at infinity is consumed by the expansion (the flow is more and more massive), until at some point  $e_c(\infty)$  vanishes. If we now add more material, the flow continues to be supersonic, but more and more thermal energy is consumed in the adiabatic expansion, and  $e(\infty)$  decreases. Eventually  $e(\infty)$  vanishes and the flow becomes subsonic.

In a systematic study of stellar wind solutions, it is very convenient to work with dimensionless variables. Chamberlain (147) suggested the transformations

$$\tau \equiv (T/T_0) \quad (15-66a)$$

$$\psi \equiv (v^2 \mu m/kT_0) \quad (15-66b)$$

$$\text{and} \quad \lambda \equiv (G\mathcal{M}_\odot \mu m/kT_0 r) \quad (15-66c)$$

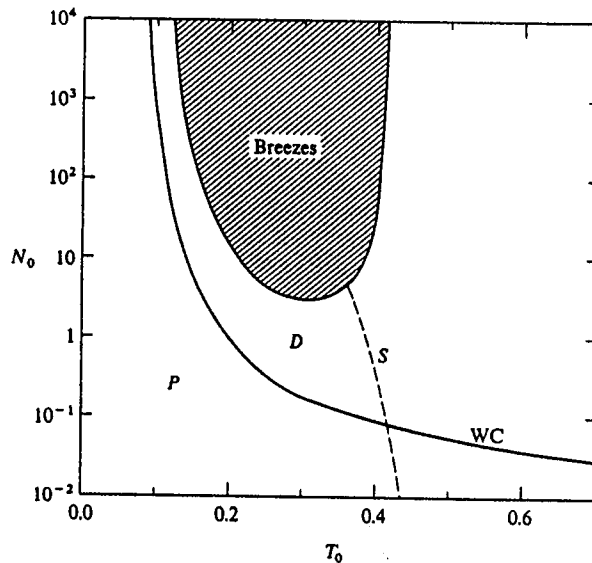


**FIGURE 15-3**  
Regions of stellar wind and breeze solutions as a function of coronal temperature  $T_0$  (in units of  $G\mathcal{M}_\odot \mu m/k r_0$ ) and density  $N_0$  [in units of  $2\kappa_0 k^{-1} (G\mathcal{M}_\odot r_0)^{-1}$ ]. Shaded area contains breeze solutions. The dotted curve marked  $S$  delimits the region (to the right) where the flow is already supersonic at the base of the corona ( $r = r_0$ ). The region  $P$  contains wind solutions with a Parker temperature law,  $T \propto r^{-1}$ , as  $r \rightarrow \infty$ ; these solutions have a nonzero conductive flux at infinity. The region  $D$  contains Durney temperature law ( $T \propto r^{-1}$ ) winds, which become adiabatic as  $r \rightarrow \infty$ . The curve marked WC gives the locus of solutions with a Whang-and-Chang temperature law,  $T \propto r^{-1}$  as  $r \rightarrow \infty$ ; these particular solutions occur just when the conductive flux at infinity first drops to zero. From (532).

where  $\mu$  is the number of atomic mass units per particle ( $=\frac{1}{2}$  for ionized hydrogen). In these units, equations (15-57), (15-55), and (15-59) become, respectively,

$$n\lambda^{-2}\psi^{\frac{1}{2}} = (kT_0/\mu m)^{\frac{1}{2}} F/(4\pi G^2 \mathcal{M}_\odot^2) \equiv C \quad (15-67)$$

$$\frac{1}{2}[1 - (\tau/\psi)](d\psi/d\lambda) = 1 - 2(\tau/\lambda) - (d\tau/d\lambda) \quad (15-68)$$

and

$$A\tau^{\frac{1}{2}}(d\tau/d\lambda) = \varepsilon_\infty - \frac{1}{2}\psi + \lambda - \frac{1}{2}\tau \quad (15-69)$$

where

$$\varepsilon_\infty \equiv \mu E/kT_0 F \quad (15-70)$$

is the residual energy per particle at infinity (in units of  $kT_0$ ), and

$$A \equiv 4\pi\kappa_0 G\mu^2 m \mathcal{M}_\odot T_0^{\frac{1}{2}} / (k^2 F) \quad (15-71)$$

In these equations we need specify only  $\varepsilon_\infty$  and  $A$  to perform the integration (imposing, of course, the requirements that a critical solution be obtained, and that  $\tau \rightarrow 0$  as  $\lambda \rightarrow 0$ ); by redimensionalization, one can obtain several solutions from a single dimensionless one. A further transformation (531) reduces the number of arbitrary constants to one (for winds only). Thus, write  $\tau_* \equiv \tau/\varepsilon_\infty$ ,  $\psi_* \equiv \psi/\varepsilon_\infty$ , and  $\lambda_* \equiv \lambda/\varepsilon_\infty$ . Then equation (15-68) has the same form in terms of the new variables, while equation (15-69) becomes

$$K\tau_*^{\frac{1}{2}}(d\tau_*/d\lambda_*) = 1 - \frac{1}{2}\psi_* + \lambda_* - \frac{1}{2}\tau_* \quad (15-72)$$

where  $K \equiv \varepsilon_\infty^{\frac{1}{2}} A$ . A large number of solutions for a wide range of the parameter  $K$  are given in (201), along with an example of how to recover a unique dimensional solution having specified, say,  $T_0$  and  $F$ . A detailed discussion of breeze solutions is given in (532).

*Exercise 15-8:* Carry out the transformation to dimensionless variables, and verify equations (15-67) through (15-72).

#### TRANSITION TO THE INTERSTELLAR MEDIUM

The solutions derived above all have pressures that vanish at  $r = \infty$ . Actually the interstellar medium does have a finite (if small!) pressure  $p_i \lesssim 10^{-11}$  dynes  $\text{cm}^{-2}$ . When the high-speed gas in the wind encounters the interstellar medium, a stationary shock front is formed (624, 306; 665) in which the flow speed suddenly diminishes to a small value, and the density and temperature rise. The solution jumps discontinuously from the critical solution (curve 3 in Figure 15-1) to one of the subsonic solutions of type 6 shown in Figure 15-1. Beyond the shock the material finally cools and recombines, and the velocity drops to zero [see, e.g., (106)].

At large distances from the star, the wind is highly supersonic, and the gas pressure is negligible compared to the kinetic energy density. Thus, balance with the interstellar pressure is achieved through the *impact pressure* of the material in the wind. We then have

$$mnv^2 \approx p_i \quad (15-73)$$

From the equation of continuity and the assumption that  $v$  is approximately constant, we know that  $n(r) = n_\oplus (r_\oplus/r)^2$ , and using this relation we may estimate the radius of the shock front in the solar wind as

$$(r_s/r_\oplus) = (mn_\oplus v^2/p_i)^{\frac{1}{2}} \quad (15-74)$$

Adopting  $n_{\oplus} \approx 10 \text{ cm}^{-3}$ ,  $v \approx 300 \text{ km s}^{-1}$ , and the upper limit on  $p_1$  given above, we find  $r_s \gtrsim 30 \text{ a.u.}$  (i.e., outside the orbit of Neptune). The physical conditions in the flow beyond the shock can be estimated by applying the Rankine-Hugoniot relations [equations (15-44) through (15-46)]. On the conservative assumption that the temperature falls as  $r^{-4}$ , the temperature in the preshock flow is of the order of  $4 \times 10^4 \text{ }^{\circ}\text{K}$ , which implies a sound speed in ionized hydrogen of about  $25 \text{ km s}^{-1}$ , so the Mach number is about 12. In the large Mach-number limit, the Rankine-Hugoniot relations reduce to

$$v_2 = v_1(\gamma - 1)/(\gamma + 1) \quad (15-75)$$

$$n_2 = n_1(\gamma + 1)/(\gamma - 1) \quad (15-76)$$

and

$$p_2 = 2n_1mv^2/(\gamma + 1) \quad (15-77)$$

where in deriving equation (15-77) we have written

$$p_1M_1^2 = (p_1/a_s^2)v_1^2 = (\rho_1/\gamma)v_1^2$$

Here the subscript 1 denotes preshock and 2 denotes postshock conditions. Combining equations (15-76) and (15-77) into a perfect gas law, we estimate the postshock temperature to be

$$T_2 = (\gamma - 1)mv^2/[(\gamma + 1)^2k] \quad (15-78)$$

where we have assumed that the material remains fully ionized, and that the proton and electron temperatures equalize. Assuming  $\gamma = \frac{5}{3}$ , we see that  $v_2 = \frac{1}{4}v_1 \approx 75 \text{ km s}^{-1}$  while  $T_2 = 3mv^2/(32k) \approx 10^6 \text{ }^{\circ}\text{K}$  [which shows that the postshock material is indeed subsonic, as expected from Exercise 15-3(b) for  $M_1 \gg 1$ ].

The injection of hot, high-velocity material from stellar winds has significant implications for the energy balance in the interstellar medium. The picture developed here is purposely quite simplified; more elaborate calculations have been made allowing for the effect of an "interstellar wind" (arising from the Sun's peculiar velocity with respect to the interstellar medium), magnetic fields, and thermal conduction [see, e.g., (498, Chap. IX)].

#### THE MAGNETIC FIELD AND BRAKING OF STELLAR ROTATION

From direct observation it is known that the Sun has a magnetic field. Because coronal material is completely ionized, it has an extremely high electrical (as well as thermal) conductivity, and thus magnetic fields are "frozen" into the material (i.e., the charged particles cannot diffuse readily across field lines). The large-scale expansion of the corona thus implies that there will be a transport of the solar magnetic field into interplanetary space. If the Sun did not rotate, the field lines would be drawn out radially. The Sun

does rotate, however, and the field lines must be considered to be anchored at the solar surface. Field lines from a particular point on the surface will be drawn out along the streamlines of fluid elements as seen by an observer in the rotating frame of the Sun; this yields a spiral pattern for the interplanetary field (496; 498, 137; 107, 67; 324, 11).

When the magnetic field is taken into account, the physics of the fluid flow in the wind becomes much more complicated, and considerable mathematical complexity results; we shall not pursue this problem here but merely refer the interested reader to the literature [e.g., (463; 659)]. It is of considerable interest, however, to calculate the angular momentum carried away in the wind, for this loss has important implications for stellar rotation. The magnetic field must satisfy Maxwell's equation  $\nabla \cdot \mathbf{B} = 0$ , from which it follows, in spherical coordinates, that  $B_r(r) = (r_0/r)^2 B_r(r_0)$ . The azimuthal component in the spiral pattern,  $B_\phi$ , can be computed in terms of  $B_r$ , and hence the total field can be calculated. We can then estimate the ratio of the energy density in the flow to the magnetic energy density—i.e.,  $\alpha = (\frac{1}{2}mnv^2)/(B^2/8\pi)$ ; one finds that  $\alpha \gg 1$  in the vicinity of the Earth's orbit, but  $\alpha$  is small at the base of the corona. This implies that—although the fluid motions will dominate the field at large distances, and will drag it along with the material—deeper in the flow, the magnetic field will dominate and will be able to drag the material along with the solar rotation as seen in a fixed frame. Thus there is a region with  $r \leq r_A$  in which the material is forced into *corotation* with the Sun, and a region  $r > r_A$  where the material streams essentially radially. Intuitively we would expect the transition to occur at the radius  $r_A$  where  $\alpha = 1$ , and detailed analysis [(463; 659; 324, §III.15; 107, §3.7)] shows this conjecture to be correct. The speed of the hydromagnetic *Alfvén waves* is  $v_A = (B^2/4\pi\rho)^{\frac{1}{2}}$ , hence  $\alpha$  is nothing more than the square of the *Alfvénic Mach-number*  $\alpha = (v/v_A)^2 = M_A^{-2}$ ; thus the flow corotates with the sun inside the *Alfvénic critical point*, and streams radially outside it. The Alfvén speed can be directly measured in the vicinity of the earth's orbit; using the equation of continuity and the inverse-square radial dependence of  $B$ , and demanding that  $M_A = 1$  at the Alfvénic critical point, we find

$$(r_A/r_{\oplus}) = v_A(r_{\oplus})/[v(r_A)v(r_{\oplus})]^{\frac{1}{2}} \quad (15-79)$$

We may obtain a lower bound for  $r_A$  by assuming  $v(r_A) \approx v(r_{\oplus})$ , and substituting numerical values we find  $r_A \approx 20 R_{\odot}$ . This region is large, and thus the effects of magnetic fields greatly increase the angular momentum contained in the material flowing in the wind.

*Exercise 15-9:* Verify equation (15-79) and the numerical estimate of  $r_A$ .

The angular momentum of a particle of unit mass at the equator of a star is  $l_0 = \omega r_A^2$ ; where  $\omega$  is the angular frequency of stellar rotation. Hence the

total angular momentum lost from the stellar surface as a whole is

$$(dL/dt) = -(4\pi r^2 n \nu m) l_0 \int_0^{\pi/2} \cos^3 \theta \, d\theta = -\frac{2}{3} \dot{M} l_0 \quad (15-80)$$

where we have accounted for the fact that (at latitude  $\theta$ )  $l(\theta) = l_0 \cos^2 \theta$ . This angular-momentum loss into the wind implies a *braking* of the star's rotation. We may estimate the rotational-braking decay-time  $\tau$  by writing  $(dL/dt) \approx -L/\tau$ , and expressing  $L$  as  $L = I\omega$ , where  $I$  is the moment of inertia, from which we find  $\tau = \frac{2}{3}I/(\dot{M}r_A^2)$ . For the Sun,  $I = 6 \times 10^{53}$  gm cm<sup>2</sup>, and using  $\dot{M} = 2 \times 10^{-14} M_\odot/\text{year}$  and  $r_A \approx 20 R_\odot$ , we find  $\tau \approx 10^{10}$  years, which is comparable to the thermonuclear-evolution time-scale for the Sun. That is, if the solar wind maintains its present properties, we expect the solar angular momentum to be significantly diminished during the main-sequence lifetime of the Sun.

One of the striking features of the statistics of stellar rotation is the marked drop in the observed average rotation speed  $\langle v \sin i \rangle$ , as a function of spectral type, for stars of spectral types F and later. Although it is possible that this decrease is associated with the formation of planetary systems (in the solar system the Sun has only 2 percent of the angular momentum), it is also extremely suggestive that this is precisely the point where stars develop deep hydrogen convection zones, and hence presumably have coronae and winds. It is thus very attractive to hypothesize (554) that all later-type stars lose their angular momentum via magnetic braking in stellar winds. Time-scales for such braking can be estimated by an examination of mean rotation speeds of stars in clusters whose ages can be determined from stellar-evolution considerations; when this is done, it is found that there is indeed a strong decrease with age (362), and that the braking times may be as short as  $5 \times 10^8$  years. Although the stellar time-scale appears much shorter than that derived from the *present* solar wind, it is known that chromospheric activity (and presumably also the activity of the corona-wind complex) decreases with age (675; 677); hence it is possible that in the early history of the Sun the wind was stronger, and provided more efficient braking. Actually this discussion provides a good example of the fruitful exchange of ideas that occurs when solar properties are used to develop detailed physical models of a particular phenomenon, which are then applied in a stellar context, where results of evolutionary significance on long time-scales can be inferred.

#### DETAILED PHYSICS OF THE SOLAR WIND

The study of the solar wind by means of direct measurements from satellites has greatly deepened our understanding of the physics of coronal flows. In an effort to fit the observations, numerous theoretical refinements have been introduced to extend the basic model described above, and to achieve greater realism. Space does not permit anything more than mere

mention of the many physical problems that have been addressed; for further details see, e.g., (324) or (107) and the references cited therein.

First we might ask how well a one-fluid conductive model fits the data; taking the model by Whang and Chang (667) as typical, one finds  $n = 8 \text{ cm}^{-3}$ ,  $v = 260 \text{ km s}^{-1}$ , and  $T = 1.6 \times 10^5 \text{ }^\circ\text{K}$  at the radius of the earth's orbit. Comparing with the observed values listed in Table 15-1, we see that the model gives good agreement for the density, and the one-fluid temperature agrees well with the electron temperature, but is a factor of four larger than the proton temperature; the velocity is about 20 percent too low. The fact that the protons and electrons can have different temperatures is explained by the very low densities, and hence collision rates, in the solar wind near  $r_\oplus$ ; these rates are so low that they cannot equilibrate the thermal energy in the two separate components (moreover, the thermal velocity distribution for both electrons and protons is observed to be anisotropic). Two-fluid models have been constructed (618; 282) in which electrons and protons are allowed to have distinct temperatures; an energy equation is written for each component, including an energy exchange term of the form  $\frac{2}{3}\nu k(T_p - T_e)$ , where  $\nu$  is a collision frequency calculated for Coulomb collisions of the charged particles. Typical models of this type yield  $n \approx 15 \text{ cm}^{-3}$ ,  $v \approx 250 \text{ km s}^{-1}$ ,  $T_e \approx 3.4 \times 10^5 \text{ }^\circ\text{K}$ , and  $T_p \approx 4.4 \times 10^3 \text{ }^\circ\text{K}$  at  $r = r_\oplus$ . The densities are about a factor of two too large, the velocity is 20 percent too low, the electron temperature is a factor of two too high, and the proton temperature is a factor of 10 too low. Although the basic concepts used in the two-fluid model do admit more physical realism than is inherent in a one fluid description, the quantitative results are not impressive; in particular it appears that the energy exchange between protons and electrons must proceed more efficiently than is predicted from Coulomb collisions alone. The exchange has been treated on the assumptions that the particle-velocity distributions are isotropic and Maxwellian, and that magnetic field effects may be ignored; possibly all of these assumptions are inadequate. However, most of the discrepancy seems to be removed when the effects of viscosity are taken into account.

Magnetic fields may play an important role in determining the nature of the solar-wind flow, through magnetic forces, by modification of transport coefficients such as the conductivity, and through energy transport and dissipation by hydromagnetic waves. Each of these effects leads to a significant increase in the complexity of the theory, and can appreciably alter the detailed results. Worse, allowing major sources of momentum of energy input into the wind throughout the flow (from *any* source, not just magnetic), changes the whole topology of permitted solutions of the equations, and introduces many possibilities beyond those shown in Figure 15-1 (307).

The models described above all omit the effects of viscosity. When viscous forces are included, the equations become of higher order, and the momentum

equation no longer possesses a singular or critical point (668). The earliest one-fluid viscous models (553; 668), using classical viscosity coefficients for a proton-electron plasma, were disappointing, for they yielded flow speeds and temperatures about a factor of two too small. A resolution of the difficulty is achieved when magnetic effects upon the viscous stress tensor are taken into account (660), and modern models including viscous terms (681) have the right velocities, and raise the proton temperature (from the spuriously low values found in the inviscid two-fluid models) to values close to those observed.

Even the most refined and accurate spherically symmetric models still represent only very high-order abstractions of the real solar wind, for it varies, on time-scales of days, over wide ranges of all the physical variables. Prominent individual features that appear are high-speed plasma streams; these often are observed to recur with a synodic solar-rotation period, and are, therefore, the result of specific conditions in localized regions of the corona. Further, there are energetic flare-produced shock waves that give rise to geomagnetic storms. These structures often interact in a complex way and, more and more, it seems that it is an oversimplification to view the solar wind as a smooth flow upon which "atypical" structural features are superposed; rather, these complex structures are, in some sense, the wind itself. Similarly we are coming to understand that the wind does not arise from a single smooth coronal condition, but that it may be produced in highly specific regions of markedly differing properties, and can be substantially modified by interaction with magnetic fields and by rapid (nonspherical) divergence from a limited initial volume. At some point the problem of the time-dependence of a full three-dimensional model must be solved; only for the solar wind do we have data that require (and, reciprocally, permit!) such solutions, but it is clear that the results will have important implications for stellar winds as well.

#### STELLAR CORONAE AND WINDS

As mentioned above, it is reasonable to suppose that all stars having hydrogen convection zones should also have coronae and winds. Further, many stars clearly have much more massive flows than the Sun, for the winds are sufficiently optically thick in some spectral lines to give rise to displaced lines or P-Cygni features. Needless to say, we know less about stellar winds than about the solar wind, and much work remains to be done in this rapidly developing field; nevertheless, a number of interesting results emerge even from very simplified calculations.

Parker emphasized (498, Chap. XV) that the amount of energy consumed by coronal expansion rises very rapidly with increasing coronal temperature; for example, for the Sun, the energy consumption ranges from  $10^{27}$  to  $3 \times$

$10^{30}$  ergs  $s^{-1}$  if  $T_0$  varies from  $10^6$  °K to  $4 \times 10^6$  °K. Thus a coronal wind acts as a very effective thermostat for controlling the coronal temperature. If a wind is present, we demand that the temperature be compatible with the flow—i.e.,  $T_0 \leq (GM_*m/4kR_*)$ . For the Sun, the numerical factor of 4 is replaced by 10, so one might expect

$$T_0 \approx 0.1(GM_*m/kR) \quad (15-81)$$

In main-sequence stars,  $(M_*/R_*)$  varies only by about a factor of two above or below the solar value, which suggests a similar restricted range for  $T_0$  (less than the variation of photospheric temperatures!). In contrast, the energy in the wind may vary widely (perhaps more so than the stellar luminosity). For a giant or supergiant,  $(M_*/R_*)$  is much smaller than in main-sequence stars and, accordingly,  $T_0$  should also be much smaller. For example, in an M-supergiant, equation (15-81) suggests  $T_0 \approx 4 \times 10^4$  °K. At such low temperatures conduction becomes ineffective, and one must invoke some mechanism to heat the corona as a whole (665; 666); quite possibly, significant wave dissipation occurs throughout the corona. Similarly, the velocity of the winds ultimately approach some significant fraction of the escape velocity, and thus we can expect

$$v_\infty \gtrsim (2GM_*/R_*) \quad (15-82)$$

Again this implies little variation along the main sequence, and implies that supergiants have quite low wind velocities. The picture developed above depends on the *assumption* that the wind is subsonic at the coronal temperature maximum. If, however, the critical point in the wind lies *below* this maximum, the run of temperature with distance is no longer monotonic and the properties of the flow may change substantially.

To construct detailed models or apply existing computations [e.g., (201)], we need to specify the relevant coronal conditions, such as  $n_0$  and  $T_0$ , from theoretical calculations—or to specify one of these quantities and a flow parameter such as the mass-loss rate, which can sometimes be determined observationally. The computation of coronal conditions is exceedingly difficult. The basic technique is to calculate the acoustic energy flux created in the convection zone [see, e.g., (394; 395; 525; 601)], compute the dissipation of this flux in the coronal material, and (taking into account losses by radiation and the energy transported by conduction) obtain a temperature-density structure in a model corona [see, e.g., (192; 377; 378; 630; 631; 632)]. Each of these steps requires use of an uncertain theory, and of necessity many approximations must be made, so a high degree of reliability cannot be assigned to the final results. In particular, a good fit is not obtained to observed solar coronal properties [see Fig. 21 of (192)] in all cases. But if we simply accept the calculations, however uncertain, at face value, it appears that for

main-sequence stars the maximum acoustic flux is found for stars near spectral types F0; for these stars  $T_0 \approx 4 \times 10^6 \text{ }^\circ\text{K}$  and  $n_0 \approx 3 \times 10^{10} \text{ cm}^{-3}$  (192). One would expect substantial coronal winds in these stars. If  $T_0$  and  $n_0$  are regarded as given, then the calculations cited previously can be used to derive wind models.

Consideration of the energetics of stellar coronae and winds is also quite instructive (290). A corona is heated by the mechanical flux  $F_m$  delivered to it, and loses energy via radiation and conduction, and in the kinetic energy of the wind. Analysis shows that, for a given coronal pressure, the rate of energy loss by mass-ejection and by conduction increases with rising temperature, while that by radiation decreases. Therefore, for a given pressure, a temperature exists at which the total energy loss from the corona is a minimum. Further, losses from all three processes increase with increasing pressure, so for minimum-flux coronae there is a monotone relation between coronal pressure and the energy flux required to maintain the corona and wind. This suggests that a given  $F_m$  determines a unique coronal temperature and pressure, and hence wind. (Actually it remains to be demonstrated that, if one has a given minimum-flux corona, and arbitrarily changes  $F_m$ , then the corona necessarily adjusts to a new minimum-flux configuration.) The competition among these processes establishes three basic classes of coronae. (1) For low values of  $F_m$  the main losses are by conduction and radiation. An example is the solar corona-wind complex where only about 10 percent of the mechanical flux delivered to the corona goes into the wind. (If the wind arises in geometrically localized regions of the corona—e.g., coronal holes—the local conversion efficiency may be much higher.) (2) At intermediate values of  $F_m$  the losses are mainly from radiation and mass ejection. An example is the wind in the A2 supergiant  $\alpha$  Cyg where losses into the wind are dominant, while those by radiation are significant, and those by conduction are negligible. (3) At very large values of  $F_m$ , mass loss totally dominates. For early-type stars the rate of mass ejection is as high as  $10^{-6}$  to  $10^{-5} M_\odot/\text{year}$ , and exceedingly high coronal temperatures (which appear to be excluded by the observations) would be required to drive the winds; here the winds are driven instead by radiation forces (see §15-4).

### 15-3 Radiation Hydrodynamics

In both the atmospheres and interiors of stars, there exist intense radiation fields that can influence heavily the momentum and energy gains and losses of the material, and hence its motions. To study the dynamics of a flow occurring in such a situation, it is fruitful to consider the fluid as consisting of both material particles and photons, and to calculate the contributions of both types of particles to the equations of motion and of energy conserva-

tion. In this way we obtain the equations of *radiation hydrodynamics*, which describe the coupled flow of the gas and radiation. In the applications of interest here, it will be assumed that the flow velocities  $v \ll c$ , so that the material particles can be treated nonrelativistically; in certain other contexts (e.g., in supernovae or thermonuclear explosions), this assumption may not be valid. Despite the restriction to  $v \ll c$ , the fact that the photons have velocity  $c$  leads to subtleties in the way the radiation and material terms interact, and it is a nontrivial task to obtain equations that describe the interaction fully consistently. In the end it is simplest and most reliable to develop them in a relativistically covariant form from the outset (621; 524; 664; 135). These equations may subsequently be simplified to retain only terms of order  $(v/c)$ , and to omit terms of  $O(v^2/c^2)$  and higher. It must again be noted that, as was true in our earlier treatment of the comoving-frame transfer equation, it is not sufficient to apply a unique Lorentz transformation, because the fluid velocity is, in general, a function of position and time. As before, we consider transformations from a set of uniformly-moving frames that instantaneously coincide with the moving fluid.

The radiative contributions to the equations can, in principle, be written in terms of either laboratory-frame or fluid-frame quantities. Although in some ways it is easier to write down the equations of radiation hydrodynamics in a stationary frame [see, e.g., (521; 551; 692)], they are actually of a simpler form when written in the comoving frame of the fluid, for the radiative terms are most easily evaluated in that frame (621; 135). In the past this approach was not widely employed, because one must be able to solve the comoving-frame transfer equation to calculate the necessary radiation-field quantities. As was shown in §14-3, the comoving-frame transfer equation is easily solved with present-day techniques (and is, in some ways, simpler than the fixed-frame equation, which is complicated by anisotropies in the absorption and emission coefficients arising from Doppler shifts). We shall, therefore, concentrate primarily on a comoving-frame formulation, but it will also be shown that these equations are consistent (to order  $v/c$ ) with the fixed-frame equations. Only one-dimensional spherically-symmetric flows will be treated in this book; an extensive collection of formulae for three-dimensional flows in various coordinate systems can be found in (521, Chap. 9).

#### THE MATERIAL STRESS-ENERGY TENSOR AND THE RADIATING-FLUID EQUATIONS OF MOTION

In the Cartesian coordinate system  $(x^1, x^2, x^3, x^4) \equiv (x, y, z, ict)$ , a covariant formulation of the equations of motion and of energy conservation for the material alone yields a system of equations of the form

$$(\partial T^{\alpha\beta}/\partial x^\beta) = F^\alpha, \quad (\alpha = 1, \dots, 4) \quad (15-83)$$

where  $F^\alpha$  is a four-vector force (the Minkowski force) and  $T^{\alpha\beta}$  is a tensor describing the momentum flux (stress), momentum density, and energy density of the material. Similar equations were written in §14-3 for the radiation [cf. equations (14-118) through (14-122)], and by analogy with equation (14-120) we might expect  $T^{\alpha\beta}$  to be of the form

$$T = \begin{pmatrix} \Pi & icG \\ icG & -E \end{pmatrix} \quad (15-84)$$

where  $\Pi$ ,  $G$ , and  $E$  are suitable covariant generalizations of the momentum flux tensor, the momentum density vector, and the total energy density of the material, respectively. We place three demands upon  $T$ : (1) that it be written in terms of scalar invariants and four-vectors, so that it is covariant; (2) that it reduce to the correct limit in the frame at rest with respect to the fluid; and (3) that it yield the correct nonrelativistic limit in the laboratory frame.

First, we may define the *proper time*, a four-scalar (invariant) as

$$(d\tau)^2 \equiv -(dx_\alpha dx^\alpha)/c^2 = dt^2 - c^{-2}(dx^2 + dy^2 + dz^2) \quad (15-85)$$

Clearly  $d\tau$  reduces to  $dt$  as  $v \rightarrow 0$ . Then we define the *contravariant four-velocity* as

$$V^\alpha \equiv (dx^\alpha/d\tau) \quad (15-86)$$

Noting from equation (15-85) that  $(dt/d\tau) = (1 - v^2/c^2)^{-\frac{1}{2}} \equiv \gamma$ , where  $v$  is the ordinary velocity  $v^2 \equiv [(dx/dt)^2 + (dy/dt)^2 + (dz/dt)^2]$ , we have

$$\begin{aligned} V^i &= (dx^i/dt)(dt/d\tau) = (1 - v^2/c^2)^{-\frac{1}{2}}(dx^i/dt) \\ &= \gamma v^i, \quad (i = 1, 2, 3) \end{aligned} \quad (15-87a)$$

$$V^4 = ic(dt/d\tau) = ic\gamma \quad (15-87b)$$

Note in passing that  $V_\alpha V^\alpha = -c^2$ , a world scalar (which is *invariant* under any arbitrary coordinate transformation, as can be readily shown from the transformation properties of covariant and contravariant vectors). Next, if  $\rho_0$ ,  $e$ , and  $p$  are the invariant mass density (i.e., the particle number density times rest-mass per particle), the specific internal energy, and the pressure measured in the rest-frame of the fluid, then the equivalent total mass density is

$$\rho_{00} = \rho_0(1 + e/c^2) \quad (15-88)$$

Also, following Thomas (621) we define

$$\rho_{000} = \rho_{00} + p/c^2 = \rho_0(1 + h/c^2) \quad (15-89)$$

Here  $h$  is the specific enthalpy of the gas, and  $(\rho_0 h/c^2)$  gives the mass equivalent (per unit volume) of the total energy contained in the microscopic motions of the gas.

Noting that in the nonrelativistic limit  $\Pi^{ij} = \rho v^i v^j + p \delta^{ij}$ , while  $G^i = \rho v^i$ , we may hypothesize, by analogy, that

$$T^{\alpha\beta} = \rho_{000} V^\alpha V^\beta + p \delta^{\alpha\beta} \quad (15-90)$$

where  $\delta^{\alpha\beta}$  denotes the standard Kronecker symbol. It is obvious that equation (15-90) satisfies requirement (1) stated above. The individual components may be written more specifically as

$$T^{ij} = \rho_{000} V^i V^j + p \delta^{ij} = \rho_1 v^i v^j + p \delta^{ij} \quad (15-91a)$$

$$T^{i4} = T^{4i} = ic\rho_{000} V^i = ic\rho_1 v^i \quad (15-91b)$$

$$\text{and } T^{44} = -c^2 \gamma^2 \rho_{000} + p = -c^2 \rho_1 + p \quad (15-91c)$$

where  $i = 1, 2, 3$ ,  $j = 1, 2, 3$ , and  $\rho_1 \equiv \gamma^2 \rho_{000}$ . Notice, now, that in the frame of the fluid itself, where  $v \equiv 0$ ,  $T$  becomes diagonal, with  $T^{ii} = p = (\Pi^{ii})_0$  and  $T^{44} = -(\rho_0 c^2 + \rho_0 e)$ ; this gives the correct static pressure and the correct energy per unit volume of the fluid (including the material rest-energy). Thus requirement (2) stated above is satisfied. Next, let us examine the nonrelativistic limit ( $v/c \ll 1$ ) of  $T$ . Note first that, if  $\rho_0$  is the mass density in the fluid frame, then [remembering that a volume element transforms as  $dV = \gamma^{-1} dV_0$  (Lorentz contraction)], the density seen in the laboratory frame will be  $\rho = \gamma \rho_0$ . Thus, expanding each element of  $T$ , and retaining only the leading terms, we see by inspection that  $T^{ij}$  and  $T^{i4}$  (or  $T^{4i}$ ) reduce to the correct momentum-flux tensor and momentum density, while

$$\begin{aligned} T^{44} &= -\gamma^2(\rho_0 c^2 + \rho_0 e + p v^2/c^2) \rightarrow -\gamma(\rho c^2 + \rho e) \\ &\approx -(\rho c^2 + \frac{1}{2}\rho v^2 + \rho e) \end{aligned} \quad (15-92)$$

which is the nonrelativistic energy density (including the rest-mass energy). Thus  $T$  satisfies requirement (3) stated above.

The action of external forces upon the fluid are expressed in terms of a *four-force* (per unit volume)  $F^\alpha$  whose spatial components give the rate of increase of the momentum of the matter per unit volume and whose time component specifies the rate of increase of energy per unit volume. The expression  $V_\alpha F^\alpha$  is a *scalar invariant*, and hence may be evaluated in any frame. In particular, we may evaluate it in the frame comoving with the fluid. In this frame

$$V_\alpha F^\alpha = (V_4 F^4)_0 = -c^2(d\rho_{00}/d\tau) \quad (15-93)$$

In the absence of general-relativistic effects, the derivative on the righthand side will be zero unless there is a change in the proper mass density arising from a chemical energy release or from a conversion of matter to energy by, say, a thermonuclear reaction. Thus  $V_a F^a = 0$ ; note that this relation implies that in the comoving frame  $(F^a)_0 = 0$ , a result that will be used below.

The equations of motion for the material alone are given by equation (15-83), where  $T^{ab}$  is defined by equation (15-90). If  $R^{ab}$  denotes the radiation stress-energy tensor [cf. equation (14-120)], then the equations of motion for the complete fluid (matter plus radiation) are

$$\partial(T^{ab} + R^{ab})/\partial x^b = F^a \quad (15-94)$$

or

$$(\partial T^{ab}/\partial x^b) = F^a + g^a \quad (15-95)$$

where  $g^a$  is given by equation (14-121). In addition, we may write an equation of continuity for the material particles alone (the photons are massless); demanding number conservation, we have

$$\partial(\rho_0 V^a)/\partial x^a = 0 \quad (15-96)$$

#### THE FLUID-FRAME ENERGY EQUATION

If we were to assume that the first law of thermodynamics remains valid for the combined material and radiation fluid in the comoving frame of the material, then the gas-energy equation [cf. equation (15-24)] would need to be modified only to account for gains and losses of energy (per unit volume per unit time) by the material from interaction with the radiation field. Thus we could write

$$\rho_0(De/Dt) - (p/\rho_0)(D\rho_0/Dt) = 4\pi \int_0^\infty (\chi_v^0 J_v^0 - \eta_v^0) dv \quad (15-97)$$

where  $(D/Dt)$  denotes the Lagrangian time-derivative, following the motion of the material, and  $\chi_v^0$ ,  $\eta_v^0$ , and  $J_v^0$  are evaluated in the *comoving frame*, which is at rest with respect to the gas. It will now be shown that this a priori expectation is right, and that equation (15-97) is rigorously correct (621; 135). Forming the dot product of the equations of motion (15-95) with  $-V_a$  [and using the explicit form for  $T^{ab}$  given by equation (15-90)] one finds

$$-(V_a V^a) \frac{\partial(\rho_{000} V^b)}{\partial x^b} - \rho_{000} V^b \left( V_a \frac{\partial V^a}{\partial x^b} \right) - V^a \frac{\partial p}{\partial x^a} = -V_a F^a - V_a g^a \quad (15-98)$$

But  $V_a V^a = -c^2$ , so  $V_a (\partial V^a / \partial x^b) = \partial(\frac{1}{2} V_a V^a) / \partial x^b = 0$  and, recalling that  $V_a F^a = 0$ , equation (15-98) becomes

$$c^2 \partial(\rho_{000} V^a) / \partial x^a - V^a (\partial p / \partial x^a) = -V_a g^a \quad (15-99)$$

Now, subtracting  $(c^2 + e + p/\rho_0)$  times equation (15-96) from equation (15-99) and writing  $(D/Dt) \equiv V^a (\partial/\partial x^a)$ , we obtain

$$\rho_0 (De/Dt) - (p/\rho_0) (D\rho_0/Dt) = -V_a g^a \quad (15-100)$$

*Exercise 15-10:* Fill in the missing steps between equations (15-99) and (15-100).

As the lefthand side of equation (15-100) is evaluated following the fluid flow, the righthand side can be evaluated in the comoving frame. In this frame  $V^i = 0$  ( $i = 1, 2, 3$ ), and  $V^4 = ic$  instantaneously, and from equation (14-121)

$$g^4 = (4\pi i/c) \int (\chi_v^0 J_v^0 - \eta_v^0) dv \quad (15-101)$$

where advantage has been taken of the isotropy of the absorption and emission coefficients in the comoving frame. It is thus clear that equation (15-100) reduces to equation (15-97), which is then, in fact, the correct gas-energy equation for the material as it interacts with the radiation field.

#### THE FLUID-FRAME MOMENTUM EQUATIONS

To obtain an equation of motion in the comoving fluid frame, one might argue that the forces exerted by the radiation field on the material should be added to the usual body forces exerted by, say, gravity. The net force exerted by the radiation, when calculated in the comoving frame, is given by [cf. equation (14-121)]

$$g_R^0 = c^{-1} \int \chi_v^0 \mathcal{F}_v^0 dv \quad (15-102)$$

where again  $\chi_v^0$  and  $\mathcal{F}_v^0$  are evaluated in the comoving frame, and advantage has been taken of the isotropy of  $\chi_v^0$  and  $\eta_v^0$ . Thus from equation (15-21) we expect that

$$\rho(Dv/Dt) = -\nabla p + \mathbf{F} + c^{-1} \int \chi_v^0 \mathcal{F}_v^0 dv \quad (15-103)$$

To verify equation (15-103) we examine the  $i$ th component of equation (15-95), which, using equations (15-91), may be written

$$[\partial(\rho_1 v^i v^j)/\partial x^j] + [\partial(\rho_1 v^i)/\partial t] + (\partial p/\partial x^i) = F^i + g^i \quad (15-104)$$

$$\text{or } \rho_1 \frac{\partial v^i}{\partial t} + \rho_1 v^j \frac{\partial v^i}{\partial x^j} + v^i \frac{\partial(\rho_1 v^j)}{\partial x^j} + v^i \frac{\partial \rho_1}{\partial t} + \frac{\partial p}{\partial x^i} = F^i + g^i \quad (15-105)$$

But the time-component of equation (15-95), multiplied by  $v^i$  is

$$v^i [\partial(\rho_1 v^j)/\partial x^j] + v^i [\partial(\rho_1 - c^{-2} p)/\partial t] = v^i (F^4 + g^4)/(ic) \quad (15-106)$$

Hence by subtraction

$$\rho_1 \frac{\partial v^i}{\partial t} + \rho_1 v^j \frac{\partial v^i}{\partial x^j} + \frac{\partial p}{\partial x^i} + \frac{v^i}{c^2} \frac{\partial p}{\partial t} = F^i + g^i - \frac{v^i}{ic} (F^4 + g^4) \quad (15-107)$$

Writing  $(D/Dt) = V^a (\partial/\partial x^a)$  and  $\rho = \gamma \rho_{000}$ , equation (15-107) becomes

$$\rho(Dv/Dt) = -\nabla p - (v/c^2)(\partial p/\partial t) + F + g - v(F^4 + g^4)/ic \quad (15-108)$$

Again, the lefthand side of the equation is evaluated following the fluid flow, so the righthand side can be evaluated in the comoving frame of the fluid (in which  $v$  is instantaneously zero). We then find equation (15-103), as expected, when  $g$  is evaluated using equation (14-121).

It is convenient to rewrite equation (15-108) with  $g^a$  replaced by  $-(\partial R^{ab}/\partial x^b)$  [cf. equation (14-120)] to obtain

$$\begin{aligned} \rho \frac{Dv}{Dt} + \nabla p + \left( \nabla \cdot P + \frac{1}{c^2} \frac{\partial \mathcal{F}}{\partial t} \right) - \frac{v}{c^2} \left( \frac{\partial E_R}{\partial t} + \nabla \cdot \mathcal{F} \right) \\ = F - \frac{v}{c^2} \left[ \left( \frac{\partial p}{\partial t} \right) + v \cdot F \right] \end{aligned} \quad (15-109)$$

where the rate of increase of material energy per unit volume has been written as  $F^4 = -(v \cdot F)/ic$ . In equation (15-109) the radiation-field quantities are now expressed in an arbitrary (laboratory) frame. Notice now that, if we are concerned with describing only a nonrelativistic fluid flow, the term from  $F^4$  is  $O(v^2/c^2)$  with respect to  $F$  and hence may be omitted. Likewise, if we compute the fluid flow (as opposed to the time-evolution of the photons), the characteristic times involved will be  $\Delta t \sim \Delta x/v$  where  $v$  is the fluid velocity, and the term in  $(\partial p/\partial t)$  is clearly  $O(v^2/c^2)$  compared to  $\nabla p$  and may be omitted. Finally,  $E_R \sim p_R$ ; hence  $(v/c^2)(\partial E_R/\partial t)$  is  $O(v^2/c^2)$  compared to  $\nabla \cdot P$  and may also be omitted. All of these terms will be dropped henceforth. Note that the term  $-v[(\partial E_R/\partial t) + \nabla \cdot \mathcal{F}]/c^2$  in equation (15-109) accounts for the rate of change of the proper mass density of the matter resulting from its interaction with the radiation field.

#### THE INERTIAL-FRAME EQUATIONS

Most treatments of radiation hydrodynamics formulate the equations in an inertial laboratory frame. Let us now show [working to  $O(v/c)$  only] that the inertial-frame and comoving-frame equations are consistent. This may be done by expressing the inertial-frame radiation-field quantities in terms of their comoving-frame counterparts via equation (14-124), i.e.

$$E_R = E_R^0 + 2c^{-2}v \cdot \mathcal{F}^0 \quad (15-110a)$$

$$\mathcal{F} = \mathcal{F}^0 + E_R^0 v + v \cdot P^0 \quad (15-110b)$$

$$P = P^0 + c^{-2}(v \mathcal{F}^0 + \mathcal{F}^0 v) \quad (15-110c)$$

Consider first the momentum equation (15-109), which for a spherically symmetric flow with a gravity force becomes

$$\rho \frac{Dv}{Dt} + \frac{\partial p}{\partial r} + \frac{1}{c^2} \frac{\partial \mathcal{F}}{\partial t} + \frac{\partial p_R}{\partial r} + \frac{(3p_R - E_R)}{r} - \frac{v}{c^2} \left( \frac{\partial \mathcal{F}}{\partial r} + \frac{2\mathcal{F}}{r} \right) = -\frac{G\mathcal{M}\rho}{r^2} \quad (15-111)$$

where use has been made of equation (1-43b) for  $\nabla \cdot P$ . To obtain an equation correct to  $O(v/c)$  the full transformations of equations (15-110a) and (15-110c) must be used. However, even in the free-flow limit,  $\mathcal{F}^0 \sim cE_R^0$  or  $cp_R^0$ ; hence it is clear that all of the terms in  $\mathcal{F}$  in equation (15-111) are already at most only  $O(v/c)$  (remembering that we consider  $\Delta t \sim \Delta x/v$ ). Thus the additional terms in  $v$  in equation (15-110b) will introduce terms of  $O(v^2/c^2)$  and can be omitted, so that it is sufficient to write  $\mathcal{F} = \mathcal{F}^0$ . Substituting for the inertial-frame radiation field as indicated, we thus obtain

$$\begin{aligned} \rho \frac{Dv}{Dt} + \frac{\partial p}{\partial r} + \left[ \frac{1}{c^2} \frac{\partial \mathcal{F}^0}{\partial t} + \frac{v}{c^2} \frac{\partial \mathcal{F}^0}{\partial r} + \frac{\partial p_R^0}{\partial r} \right. \\ \left. + \frac{(3p_R^0 - E_R^0)}{r} + \frac{2\mathcal{F}^0}{c^2} \left( \frac{\partial v}{\partial r} + \frac{v}{r} \right) \right] = -\frac{G\mathcal{M}\rho}{r^2} \end{aligned} \quad (15-112)$$

*Exercise 15-11:* Verify equation (15-112).

In view of the comoving-frame transfer equation (14-134b), all of the terms in the square brackets collapse to yield

$$\rho(Dv/Dt) + (\partial p/\partial r) = -(G\mathcal{M}\rho/r^2) + (4\pi/c) \int \chi_v^0 H_v^0 dv \quad (15-113)$$

It is thus apparent that the comoving-frame transfer equation derived in Chapter 14 renders the inertial-frame and fluid-frame equations of motion fully consistent to order  $(v/c)$ .

Let us now consider energy conservation (ignoring thermal conduction) as expressed by equation (15-28). The time derivative operates on the energy per unit volume, and to this term we should add  $E_R$ ; the divergence operates on the energy flux, and to this term we should add  $\mathcal{F}$ . Hence

$$[\partial(\rho e + \frac{1}{2}\rho v^2 + E_R)/\partial t] + \nabla \cdot [(\rho e + \frac{1}{2}\rho v^2 + p)v + \mathcal{F}] = v \cdot F \quad (15-114)$$

To obtain a gas-energy equation, we subtract out the mechanical work terms obtained by taking the dot product of  $v$  with the momentum equations (15-109). Note that the two terms in  $(v/c^2)$  will then become  $O(v^2/c^2)$ , as will  $c^{-2}v \cdot (\partial \mathcal{F}/\partial t)$  for time-intervals  $\Delta t \sim \Delta x/v$ ; hence

$$\rho[D(\frac{1}{2}v^2)/Dt] + (v \cdot \nabla)p + v \cdot (\nabla \cdot P) = v \cdot F \quad (15-115)$$

and by subtraction from equation (15-114) we find

$$[\partial(\rho e + E_R)/\partial t] + \nabla \cdot (\rho ev + \mathcal{F}) + p(\nabla \cdot v) - v \cdot (\nabla \cdot P) = 0 \quad (15-116)$$

In view of equations (15-17) and (15-13), equation (15-116) reduces to

$$\rho(De/Dt) - (p/\rho)(D\rho/Dt) + [(\partial E_R/\partial t) + \nabla \cdot \mathcal{F} - v \cdot (\nabla \cdot P)] = 0 \quad (15-117)$$

It is clear that, in transforming to comoving-frame quantities, we must now carry all three terms of equation (15-110b) for  $\mathcal{F}$ ; but manifestly the second terms of equations (15-110a) and (15-110c) will produce terms of  $O(v^2/c^2)$  in time-intervals characteristic of the fluid flow; hence these terms may be omitted. Thus we calculate  $\nabla \cdot \mathcal{F} = \nabla \cdot (\mathcal{F}^0 + E_R^0 v + v \cdot P^0)$ , and note that, for spherically symmetric flow,

$$\begin{aligned} \nabla \cdot (E_R^0 v) &= E_R^0 (\nabla \cdot v) + (v \cdot \nabla) E_R^0 \\ &= v \left( \frac{\partial E_R^0}{\partial r} \right) + E_R^0 \left( \frac{\partial v}{\partial r} + \frac{2v}{r} \right) \end{aligned} \quad (15-118a)$$

$$\begin{aligned} \nabla \cdot (v \cdot P^0) &= r^{-2} \partial(r^2 v p_R^0)/\partial r \\ &= v(\partial p_R^0/\partial r) + p_R^0[(\partial v/\partial r) + 2(v/r)] \end{aligned} \quad (15-118b)$$

Further,  $v \cdot (\nabla \cdot P^0) = v[(\partial p_R^0/\partial r) + (3p_R^0 - E_R^0)/r]$  (15-118c)

so, expanding the term in square brackets in equation (15-117), we have

$$\begin{aligned} \left( \frac{\partial E_R^0}{\partial t} \right) + \left( \frac{\partial \mathcal{F}^0}{\partial r} + \frac{2\mathcal{F}^0}{r} \right) + v \left( \frac{\partial E_R^0}{\partial r} \right) \\ + E_R^0 \left( \frac{\partial v}{\partial r} + \frac{2v}{r} \right) + p_R^0 \frac{\partial v}{\partial r} + (E_R^0 - p_R^0) \left( \frac{v}{r} \right) \\ = \left( \frac{\partial E_R^0}{\partial t} \right) + v \left( \frac{\partial E_R^0}{\partial r} \right) + \left( \frac{\partial \mathcal{F}^0}{\partial r} + \frac{2\mathcal{F}^0}{r} \right) \\ + (E_R^0 + p_R^0) \frac{\partial v}{\partial r} + (3E_R^0 - p_R^0) \left( \frac{v}{r} \right) \\ = 4\pi \int (\eta_v^0 - \chi_v^0 J_v^0) dv \end{aligned} \quad (15-119)$$

by virtue of equation (14-134a). Equation (15-117) is thus identical to the comoving-frame equation (15-97).

Finally, it is useful to combine the momentum and gas-energy equations into a total energy equation that displays the effects of radiative momentum and energy inputs in a transparent way. Let  $q_R$  be the rate of net gain of energy density by the material from the radiation, and let  $\mathbf{f}_R$  be the force per unit volume exerted by radiation. Then, from equations (15-97) and (15-13),

$$\rho(De/Dt) + p(\nabla \cdot v) = q_R \quad (15-120)$$

and from equation (15-103), by forming the scalar product with  $v$ ,

$$\rho[D(\frac{1}{2}v^2)/Dt] + (v \cdot \nabla)p = v \cdot (\mathbf{f} + \mathbf{f}_R) \quad (15-121)$$

By addition of equations (15-120) and (15-121), and use of equation (15-17),

$$\left[ \partial(\frac{1}{2}\rho v^2 + \rho e)/\partial t \right] + \nabla \cdot [(\frac{1}{2}\rho v^2 + \rho e + p)v] = q_R + v \cdot (\mathbf{f} + \mathbf{f}_R) \quad (15-122)$$

For a steady ( $\partial/\partial t \equiv 0$ ) spherically symmetric flow, integration of equation (15-122) with the usual gravity force gives

$$\begin{aligned} (4\pi r^2 \rho v) [\frac{1}{2}v^2 + e + (p/\rho) - (GM/r)] \\ + 4\pi \int_r^\infty (q_R + v \cdot \mathbf{f}_R) r^2 dr = E = \text{Constant} \end{aligned} \quad (15-123)$$

which is analogous to equation (15-59) with added radiative terms. For later work it will be convenient to denote the first set of terms by  $E_0$  and to write

$$E_0(r) + 4\pi \int_r^\infty (q_R + v \cdot \mathbf{f}_R) r^2 dr = E = \text{Constant} \quad (15-124)$$

## 15-4 Radiatively Driven Winds

Observational evidence gathered over the last decade has demonstrated compellingly that rapid mass loss via transsonic winds is ubiquitous throughout the high-temperature, high-luminosity portions of the Hertzsprung-Russell diagram. The basic theoretical framework within which such flows are explained involves winds driven by momentum input into the gas from the intense radiation fields of these luminous stars. Although the basic outlines of the theory seem fairly well established at present, this is a very active and rapidly developing field, and a number of important questions remain open, awaiting future study. We shall, therefore, confine attention to admittedly idealized models that illustrate the basic physics; detailed fitting of computed models to observed data is only beginning, and the reader should turn to the current research literature to follow these developments.

**OBSERVATIONAL EVIDENCE FOR TRANSSONIC WINDS  
IN EARLY-TYPE STARS**

A large number of characteristic features (e.g., P-Cygni profiles, emission lines, line asymmetries) in the visible spectra of many O and early B stars (particularly supergiants, Of, and WR stars) have long provided evidence that these objects have extensive envelopes, and that the material being observed in the lines is flowing outward from the stellar photosphere [see, e.g., (261, Chap. 10)]. The case for actual mass loss was not unequivocal, however, because the observed velocities measured from the short-wavelength edge of the absorption in P-Cygni features (typically  $200\text{--}400 \text{ km s}^{-1}$ ) did not exceed the surface escape velocity

$$v_{\text{esc}} = 620(\mathcal{M}/\mathcal{M}_\odot)^{\frac{1}{2}}(R/R_\odot)^{-\frac{1}{2}} \text{ km s}^{-1} \quad (15-125)$$

which is of the order of  $1000\text{--}1500 \text{ km s}^{-1}$  for a main-sequence O-star, and  $600\text{--}900 \text{ km s}^{-1}$  for an OB-supergiant. The data obtained from ground-based observations suffer from a fundamental limitation: all of the lines observed are *subordinate transitions* that arise from levels with *high excitation potentials*, and hence with small populations outside the regions of high temperature and density. The column density of absorbers in these lines is therefore quite small, and one observes only the *innermost* layers of the envelope, just outside the photosphere.

In contrast, complementary information is obtained from the ultraviolet region of the spectrum accessible to observation from space, which contains *resonance lines* arising from the *ground states* of the dominant ionization stages of abundant light elements. The column densities in these lines are so large that one may sample the *outermost* parts of the envelope. Decisive *direct* evidence of mass loss was thus first provided when Morton (467) discovered displacements corresponding to outflow velocities in the range  $1500\text{--}3000 \text{ km s}^{-1}$  in the P-Cygni profiles of the ultraviolet resonance lines of Si IV  $\lambda 1402.8 \text{ \AA}$  and C IV  $\lambda 1549.5 \text{ \AA}$  in spectra obtained from rockets [see also (468; 469; 470; 129; 600; 579; 580)]. Combining the ultraviolet and ground-based data, we infer a transsonic flow in the expanding envelope. The measured resonance-line velocities are, in fact, only lower limits on the actual terminal velocity of the flow, because variations in the ionization equilibrium may cause the absorbing ion to vanish at some level in the envelope (or the material may just become optically thin and produce features below the detection threshold). Recently, results of great accuracy and sensitivity have been obtained for ultraviolet OB spectra from the orbiting observatory *Copernicus* (589).

Further evidence for mass loss is provided by infrared and radio continuum observations (of several OB and WR stars), which are most readily interpreted in terms of free-free emission from an extended, optically-thick

envelope having a density profile consistent with steady outflow of the material (171; 241; 277; 685).

The ground-based data are of great importance for they, in principle, provide information in the region where the flow passes through the sonic velocity. The hydrogen  $H\alpha$  line and the He II  $\lambda 14686$  line are among the strongest lines in the visible spectrum of OB stars, and hence usually provide the first indications of atmospheric extension and expansion by coming into emission. Extensive observational surveys have been made of both lines.  $H\alpha$  is found (537) to show emission in luminous B-stars of all types from B0 to A3. There are well-defined lower limits to the luminosity at which  $H\alpha$  emission first becomes conspicuous, namely  $M_v \approx -5.8$  ( $M_{\text{bol}} \approx -8.8$ ) near spectral type B0, and  $M_v \approx -6.8$  ( $M_{\text{bol}} \approx -7.3$ ) near spectral type A0, and there is a definite relation between the net emission strength of  $H\alpha$  and the stellar luminosity. There is clear evidence for differential expansion of the atmosphere for stars about 0.5 mag less luminous than those that show conspicuous  $H\alpha$  emission. For the O-stars (177) there is generally a close correlation between the emission strength of He II  $\lambda 14686$  and that of  $H\alpha$ , and emission at either line is an indicator of an extensive envelope around the star. Further, it is found that the luminosity at which  $H\alpha$  weakens, or comes into emission, is  $M_v \approx -6$  ( $M_{\text{bol}} \approx -9$ ). The  $H\alpha$  profiles typically exhibit P-Cygni characteristics, or show an extended blueward absorption wing indicating expansion; typical velocity widths are of the order of  $\pm 600 \text{ km s}^{-1}$ . As the expanding envelope of an OB star becomes more extended and dense, a definite series of other spectroscopic effects are manifested, and a useful qualitative assessment of the state of the atmosphere can be obtained by an examination of the particular effects that do appear (328).

Measurements of the radial velocities (in the usual spectroscopic sense) indicated by different lines of various ions in Of spectra (326; 327), show some interesting features. (1) There is a *velocity progression* with line-series (e.g., the Balmer lines), with the strongest lines showing the largest velocities of approach; this indicates an *accelerating outward flow*, for the outermost layers are seen in the strongest lines. By theoretical fitting of the observed profiles it is possible, in principle, to infer the variation of velocity with radial distance from the star. If such information can be obtained reliably, it is of great value, for it can provide important constraints on possible theoretical models in the crucial transsonic flow regions. For one star (HD 152236), it was found (327) that the velocity rises sharply outward, from a value near the sound speed ( $\sim 25 \text{ km s}^{-1}$ ) to  $v \sim 300 \text{ km s}^{-1}$  in about 0.5 stellar radii above the photosphere; for two other stars this rise is much more gradual, with velocities of a few hundred  $\text{km s}^{-1}$  being attained at two or three stellar radii above the photosphere. We shall note the significance of these results later in this section. (2) There is a clear correlation of larger velocities with *smaller* lower-level excitation potentials for the lines. If the

excitation were presumed to be in LTE, this correlation would imply that the temperature decreases outward in the envelope (as would be expected if the envelope is in radiative equilibrium, or is expanding adiabatically). Of course, LTE is not likely, and probably the correlation reflects increasing dilution of the radiation field (hence lower radiative excitation rates) or decreasing densities (hence lower collisional excitation rates). Both sets of results mentioned here urgently need to be refined with trustworthy diagnostics, based on careful solutions of the coupled transfer and statistical equilibrium equations, for various flow models. Finally, it should be mentioned that broad, faint emission features have been observed (678) underlying the relatively narrow, bright, emission lines of He II  $\lambda 4686$ , C III  $\lambda 5696$ , and N III  $\lambda 4634-40$  in some O spectra. These features have total velocity widths up to  $4000 \text{ km s}^{-1}$ , and if real (they are not seen by all observers) could possibly result from emission originating in the extensive, rapidly-expanding outer envelope of the star.

A large body of ultraviolet data has now been accumulated, thanks to the possibility of making long-term observations from the satellite *Copernicus* (589). Because the observed resonance lines are intrinsically strong and easily detected, they provide extremely sensitive indicators of stellar winds. From an examination of ultraviolet spectra of 47 O-, B-, and A-stars (see Figure 15-4 for an example), it is found that mass loss occurs over a much wider range of temperature and luminosity than indicated by effects seen in the spectrum visible from the ground. Essentially all stars with luminosities greater than  $3 \times 10^4 L_\odot$  (a reduction of a factor of 15 relative to the ground-based limit) are found to show mass loss. The observed terminal velocities

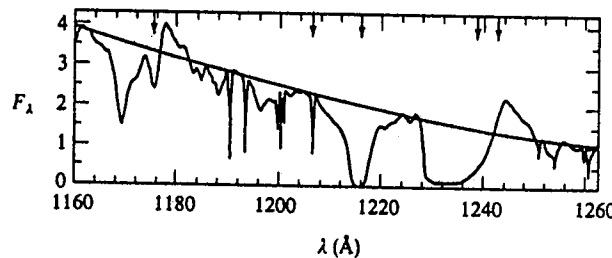


FIGURE 15-4  
Far-ultraviolet scan of the spectrum of  $\zeta$  Pup (O5f) obtained from the satellite *Copernicus*. Ordinate gives flux (in arbitrary units), and abscissa gives wavelength in Å. The positions of the C III  $\lambda 1175.7$ , Si III  $\lambda 1206.5$ , H I  $\lambda 1216$ , and N V  $\lambda 1238.8$ , 1242.8 lines are marked with vertical arrows. The smooth upper curve is an estimated "continuum" level, drawn for illustrative purposes only; note the marked P-Cygni character of the C III and N V lines. From (589), by permission.

are all clearly larger than the surface escape velocity (and hence much larger than  $v_{\text{esc}}$  at great distance from the star), and range from  $300 \text{ km s}^{-1}$  to  $3500 \text{ km s}^{-1}$ . There does not appear to be a significant correlation of  $v_\infty$  with stellar temperature, luminosity, gravity, or rotation velocity.

A wide variety of ions are observed, ranging from Mg II and C II in the coolest stars, through C IV, Si IV, and N V in the hotter stars. Lines arising from excited states (e.g., N IV  $\lambda 1718.5$  at 16.1 eV, or He II  $\lambda 1640$  at 40.6 eV) show lower velocities (470), again indicating decreasing excitation with increasing distance from the star; as noted above, this probably reflects decreasing densities and radiation fields. In several stars the O VI  $\lambda 1032$  and  $\lambda 1038$  lines are observed (533; 589). These lines are unexpectedly strong, and indicate a higher density of  $O^{5+}$  than would be estimated from the color temperature of the stellar radiation field. If it is assumed that the ionization equilibrium is established by collisions (coronal case), the temperature derived is about  $2 \times 10^5 \text{ °K}$ , which is taken as evidence for coronal heating in these stars. On the other hand, an upper bound of about  $3 \times 10^5 \text{ °K}$  on  $T$  follows from observations of lower ionization stages (e.g., C III and N III) in the flow, and from comparisons of upper limits of X-ray fluxes to H $\alpha$  emission strengths (145). We shall see below that temperatures in this range are too low to drive the flow by a coronal-wind mechanism and produce terminal speeds in the observed range.

Mass-loss rates have been estimated from the observed line-strengths (468) and profiles (329) for the Orion supergiants  $\delta$ ,  $\epsilon$ , and  $\zeta$  Ori, yielding values of about 1 to  $2 \times 10^{-6} M_\odot/\text{year}$ . Detailed fits to line profiles for  $\zeta$  Pup (O5f) yield a mass-loss rate of  $7 (\pm 3) \times 10^{-6} M_\odot/\text{year}$  (383).

#### BASIC DYNAMICS OF RADIATION-DRIVEN WINDS

The first question that arises is whether the flows observed in early-type stars can result from coronal expansion of the kind considered in §15-2. As recognized by Lucy and Solomon (404), the answer to this question is probably negative. To begin, the OB stars are thought not to have extensive convection zones, and are not expected a priori to have coronae. But even if they did have coronae for some reason, then equations (15-59), (15-62), and (15-64) imply that the critical-point temperature  $T_c$  required to drive the flow must satisfy the relation  $2kT_c \approx \frac{1}{2}mv_\infty^2$ . Adopting  $v_\infty \sim 3 \times 10^3 \text{ km s}^{-1}$ , we find  $T_c \sim 3 \times 10^7 \text{ °K}$ , a value that is completely excluded by (a) the absence of soft X-ray emission from the stars, and (b) the presence of lines from ions such as C IV, N V, and Si IV (observed to exist in the flow at velocities from  $\sim \frac{1}{2}v_\infty$  to  $v_\infty$ ), which would be destroyed by collisional ionization at temperatures greater than about  $3 \times 10^5 \text{ °K}$ .

We must therefore seek an alternate mechanism to drive the wind. Lucy and Solomon (404) suggested that this mechanism is direct momentum input

into the gas through the absorption of radiation by the strong resonance lines observed in the ultraviolet spectrum. The momentum input results when photons are absorbed by certain ions from the stellar radiation field, which is strongly outward-directed, and then scattered *isotropically*. Because the emission process is isotropic, it produces zero net change in the momentum of the material; hence there is a net gain of outward momentum from the incident radiation field. The absorbing ions are thus accelerated radially, and they then suffer collisions with all other particles in the medium; in this way the momentum gained by the particular ions absorbing the radiation is shared with the other atoms in the gas, and accelerates the material as a whole. The outward acceleration experienced by the gas is then

$$g_R = (4\pi/c\rho) \int_0^\infty \chi_v^0 H_v^0 dv \quad (15-126)$$

where  $\chi_v^0$  denotes the absorption coefficient per unit volume from all sources (continua, electron scattering, and lines);  $H_v^0$  is the incident flux.

The outward radiative acceleration is to be compared with the inward acceleration of gravity,  $g = (GM/r^2)$ ; if  $g$  is everywhere greater than  $g_R$ , then the atmosphere remains in hydrostatic equilibrium and does not expand. We therefore must investigate the circumstances under which  $g_R$  will exceed  $g$ ; for convenience we shall define

$$\Gamma \equiv (g_R/g) \quad (15-127)$$

In O-stars the continuous opacity is dominated by electron scattering in those spectral regions where most of the flux emerges. Pure Thomson scattering is frequency independent, and the resulting  $\Gamma$  can be written immediately as

$$\Gamma_e = (s_e L / 4\pi c G M) \quad (15-128)$$

where  $s_e = (n_e \sigma_e / \rho)$  is the electron-scattering coefficient per gram. Recalling the results of Exercise 7-1,  $\Gamma_e \approx 2.5 \times 10^{-5} (L/L_\odot)(M_\odot/M)$ ; for an O-star ( $L/L_\odot \approx 10^6$ ,  $M/M_\odot \approx 60$ , and  $\Gamma_e \approx 0.4$ ). It is thus clear that *continuum absorption alone cannot produce a force that exceeds gravity*. (We shall see below that it is essential for a transsonic wind that it does not!). We must therefore look to the spectral lines to produce the required force.

At great depth in the atmosphere the diffusion approximation is valid, and  $H_v \propto \chi_v^{-1}$  [cf. equation (2-91)]; in this limit the product  $\chi_v H_v$  appearing in equation (15-126) is independent of the value of  $\chi_v$ ; i.e., *in the diffusion limit the lines are no more effective than the continuum in delivering momentum to the gas*. Thus at depth,  $\Gamma$  remains essentially equal to  $\Gamma_e$  as given by equation (15-128). On the other hand, at the surface of the atmosphere  $H_v$  may rise far above its diffusion-approximation value, because intense radiation emerges from the material below, and none is incident from above. To estimate

the *maximum* force that can result from a single line, we assume that the line intercepts *unattenuated* continuum radiation—i.e.,  $F_v = F_c = B_v(T_{\text{eff}})$ . Then an upper limit to the acceleration of the material by a single line of an atom of chemical species  $k$ , in excitation state  $i$ , of ionization stage  $j$ , is

$$g_R^0 = (\pi^2 e^2 / mc^2) f_{ii} B_v(T_{\text{eff}}) (n_{ijk}/N_{jk}) (N_{jk}/N_k) (\alpha_k X/m_H) \quad (15-129)$$

where  $n_{ijk}$  is the population of the particular level,  $N_{jk}$  is the total number of atoms in all excitation states of ionization stage  $j$ ,  $N_k$  is the total number of all atoms and ions of species  $k$ ,  $\alpha_k$  is the abundance of species  $k$  relative to hydrogen, and  $X$  is the mass fraction of the stellar material that is hydrogen. Lucy and Solomon considered the C IV line at  $\lambda 1548 \text{ \AA}$ , and adopting  $f = 0.2$ ,  $T_{\text{eff}} = 25,000^\circ\text{K}$  (to maximize  $B_v$ ),  $\alpha_C = 3 \times 10^{-4}$ ,  $X = 1$ , and  $(n_{ijC}/N_{jC}) = 1$ , they found

$$\log(g_R^0)_{\lambda 1548} = 5.47 + \log(N_{jC}/N_C) \quad (15-130)$$

For a typical O-supergiant,  $\log g \approx 3$ ; hence the upper limit on the force (obtained when  $N_{jC}/N_C = 1$ ) from even this one line *exceeds the force of gravity by a factor of 300*.

Of course, the estimate just derived is (purposely) a gross upper limit, because the carbon atoms in the photosphere of the star produce a dark absorption line in which  $F_v \ll F_c$ . To account for this, Lucy and Solomon solved the transfer equation approximately, and found that above a certain critical level in the atmosphere the radiation force, computed using equation (15-126) for the C IV  $\lambda 1548$  line, still exceeded gravity. [Interestingly, similar results had also been found in standard plane-parallel, static, model-atmosphere calculations (7; 298). For early-type stars, the radiation force on a realistic line spectrum exceeded gravity at the surface of the model; but this was regarded as “nonphysical” for the purposes of model construction and was suppressed in the calculation!] In summary, one finds that, for O-stars, the forces obtained when the atmosphere is assumed to be static are incompatible with that assumption; hence *hydrostatic equilibrium in the outermost layers is not possible, and an outflow of material must occur*.

Once the uppermost layer begins to move, the lines will be Doppler-shifted away from their rest positions and will begin to intercept the intense flux in the adjacent continuum; this enhances the momentum input to the material and hence increases the acceleration. The underlying layers must expand to fill the rarefaction left by acceleration of the upper layers. Furthermore, the lines in these lower layers become unsaturated (because the absorption lines in the upper layer have been Doppler-shifted); hence these underlying layers also begin to experience a radiative force that exceeds gravity. In this manner, a flow can be initiated; it remains to be shown that (a) the *amount* of mass loss produced is significant, and (b) the variation of the radiation force

with depth is *consistent* with transsonic flow. Let us consider the latter point first.

To obtain a transsonic flow, certain conditions at the sonic point must be met (408; 132), as is the case for coronal winds. For steady flow, mass conservation is expressed by equation (15-16), while the momentum equation (15-103) can be written, using equation (15-127), as

$$v(dv/dr) + \rho^{-1}(dp/dr) = -G\mathcal{M}(1 - \Gamma)/r^2 \quad (15-131)$$

Here  $\Gamma$  is assumed to be a given function of the radius  $r$ . The pressure may be expressed in terms of the density and isothermal sound speed  $a$  [cf. equation (15-37)] as  $p = a^2\rho$ ;  $a$  is assumed to be a function of the radius  $r$ . Then using the equation of continuity (15-14), we find

$$\rho^{-1}(dp/dr) = (da^2/dr) - (2a^2/r) - (a^2/v)(dv/dr) \quad (15-132)$$

Substituting equation (15-132) into equation (15-131), we obtain

$$\frac{1}{2}[1 - (a^2/v^2)](dv^2/dr) = (2a^2/r) - (da^2/dr) - G\mathcal{M}(1 - \Gamma)/r^2 \quad (15-133)$$

For simplicity, assume the envelope is isothermal (a good approximation), so that the term in  $(da^2/dr)$  may be omitted. Then it is clear that, if we are to obtain a smooth transition from subsonic flow at small  $r$  to supersonic flow at large  $r$ , the righthand side of equation (15-133) must (1) *vanish* at some critical radius  $r = r_c$ , where  $v = a$ ; (2) be *negative* for  $r < r_c$ ; and (3) be *positive* for  $r > r_c$ . The condition for  $r < r_c$  can be met only if  $\Gamma < 1$  in that region; i.e., in the subsonic-flow region the radiation force must be *less* than that of gravity. If  $\Gamma$  is greater than unity everywhere (which implies that the *whole star* is unstable), transsonic flow becomes *impossible*, and one has either an initially *subsonic* flow that *decelerates*, or a *supersonic* flow that *accelerates*. For  $r > r_c$  in transsonic flows,  $\Gamma$  may become arbitrarily large; indeed the larger it is, the greater is the momentum input into the gas, and the larger  $(dv/dr)$  will be. This is, of course, of great interest for early-type stellar winds, for we have seen that  $\Gamma$  can become very large in the supersonic-flow region, where the lines are sufficiently displaced from their rest frequencies that they absorb continuum radiation; indeed it is just these large values of  $\Gamma$  that lead to the high values of  $v_\infty$  that are observed. Because the flow is already supersonic where  $\Gamma$  exceeds unity, information about the momentum input cannot propagate back upstream, and the flow at the sonic point itself is essentially unaffected.

It is important to recognize that the radiation force on the continuum and on spectrum lines has precisely the right properties, as delineated above, to produce the desired transsonic wind. That is,  $\Gamma$  is less than unity inside the star where the diffusion approximation is valid, approaches unity as the lines desaturate, becomes greater than one when the lines are optically thin, and

reaches very large values when the lines shift into the continuum. We shall find below that, to a good approximation, the force depends upon a power of the velocity gradient; this dependence allows the force, and the flow it produces, to accommodate to one another, so that a steady transsonic wind can be obtained.

Before leaving the question of how the flow is achieved, it is worthwhile to comment on some other points that have been made in the literature. Cassinelli and Castor (132) studied the problem of energy input into an optically thin flow with continuum opacity only. They reached several important conclusions. (a) A flow can be driven by thermal energy-input from radiation into the gas via *true absorption* processes near the critical point. Such a mechanism deposits energy in an extended region, analogous to the solar corona, with radiation now playing the role conduction has at coronal temperatures. It was noted that the term  $E_0$  in equation (15-124) is negative near the star, but must become positive at large distances for finite  $v_\infty$ . It was argued that this change must be brought about by the integrated absorptive energy input ( $q_R$ ), and was concluded that true absorption is *essential* to effect the transition from subsonic to supersonic flow. This conclusion, however, is too restrictive (307), for it is clear from equation (15-124) that, although appropriate thermal energy input can drive the flow, the work done by radiative forces can serve equally well. In fact, it is precisely this work that drives the winds calculated by Lucy and Solomon (who assumed that the lines *scatter* the radiation conservatively, so that  $q_R \equiv 0$ ), as well as those described later in this section. (b) In the event that the wind is driven by true absorption, then virtually every early-type star has a wind, but in most cases the sonic point is so far from the stellar surface that the mass-flux is minuscule (the density continues to fall with an essentially hydrostatic scale-height inside the sonic point). Only if unrealistically large values for the absorption coefficient and the parameter  $\Gamma$  (assumed constant) are adopted do significant winds result. These difficulties are overcome entirely when a realistic representation of the radiative force on lines is used (see below). (c) The time required by the material to gain and lose energy radiatively is short compared to the time a fluid element requires to move through a density scale-height. Therefore, to a high degree of approximation, the energy balance is given by radiative equilibrium; this result is exploited in the models described later.

The first successful radiatively-driven wind models for O-stars were constructed by Lucy and Solomon (404). They assumed (1) *planar* geometry (adequate for the flow inside the sonic point); (2) constant temperature; (3) and ionization equilibrium fixed by equation (5-46) with  $W = \frac{1}{2}$ , and  $T_c$  and  $T_e$  equal to  $0.7T_{eff}$  (the effective temperature of the model photosphere); and (4) that the radiation force is dominated by absorption in resonance lines of a few ions (C III, C IV, N III, N V, Si IV, S III, S IV, and

S VI). The momentum equation was written as

$$\frac{1}{2}[1 - (a/v)^2](dv^2/dr) = -g_{\text{eff}} \quad (15-134)$$

where  $g_{\text{eff}} \equiv g_* - g_{R,l}$ ;  $g_* \equiv g - (\pi F s_e/c)$ , which allows for the radiation force from electron scattering; and  $g_{R,l}$  is the radiation force on the lines. To calculate  $g_{R,l}$ , the lines were treated as pure scatterers, illuminated from below by a photospheric intensity

$$I_v(0, \mu) = \sigma B_v(T_{\text{eff}})/[\sigma + \chi_l(v)] \quad (15-135)$$

where  $\sigma = n_e \sigma_e$ , the electron scattering coefficient per unit volume. Equation (15-135) gives a rough representation of the emergent intensity in the profile of a pure scattering line formed in the photosphere. In calculating the intensity higher in the envelope, re-emissions were ignored because, on the average, they contribute nothing to the force exerted by radiation on the material. In this case  $I_v(\tau_v)$  decays exponentially, and we can write  $I_v(\tau_v) = I_v(0) \exp(-\tau_v/\mu)$ , where  $\tau_v$  is the optical depth, at frequency  $v$ , from the base of the envelope to the test point, allowing for Doppler shifting of the line profile along the path. Then

$$g_{R,l} = (2\pi/c\rho) \sum_l \int_0^1 d\mu \int_0^\infty dv \chi_l(v) I_v(0) \mu e^{-\tau_v/\mu} \quad (15-136)$$

where the sum extends over all lines.

The density  $\rho_0$  at the base of the envelope is taken from a model atmosphere. Then a trial value is chosen for the velocity  $v_0$ ; this fixes the mass-flux  $J = \rho_0 v_0$ . The mass-flux is an eigenvalue of the problem: if too large a value is chosen, then at the sonic point, where  $v = a$ , the radiation force will be too small [essentially because  $\tau_v$  in equation (15-136) will be too large], and  $g_{\text{eff}}$  will be  $> 0$ , making a continuous transition to supersonic flow impossible. Likewise, if  $J$  is chosen too small,  $g_{\text{eff}}$  at the sonic point will be  $< 0$ . For precisely the right value of  $J$ , the condition  $g_{\text{eff}} = 0$  will be met, and transsonic flow is possible. A large number of solutions, for a range of stellar parameters, were obtained in this way, and it was found that they gave mass-loss rates of the order of  $10^{-8} M_\odot/\text{year}$  (or less), which is about a factor of 100 smaller than the observed values, despite the fact that reasonable terminal velocities,  $v_\infty \approx 3300 \text{ km s}^{-1}$ , were obtained.

Let us now inquire: "How large a mass-flux can be driven by radiation from a star?" Suppose that the spectrum contains a large number of lines, each of which totally removes the momentum from the radiation field at each frequency where it absorbs. Assume that the material is accelerated from  $v = 0$  to  $v = v_\infty$  in the process, so that a line at frequency  $v_l$  is spread over a frequency range  $\Delta v_l = (v_l v/c)$ . Then the maximum mass-loss that can be driven is obtained by putting the material momentum-flux equal to the

radiative momentum absorbed in the lines (assuming perfect efficiency); i.e.,

$$\dot{M} v_\infty = (4\pi^2 r^2/c) \sum_l F(v_l) \Delta v_l \quad (15-137)$$

where the sum extends over all lines. Lucy and Solomon argued that the sum would be dominated by a single line located near the maximum of the flux distribution, and wrote  $\dot{M} v_\infty = (4\pi^2 r^2/c) \cdot F_{\max}(v_{\max} v_\infty/c)$ , or

$$\dot{M} = (4\pi^2 r^2/c^2) F_{\max} v_{\max} \approx (4\pi^2 r^2/c^2) F = (L/c^2),$$

where  $F$  denotes the integrated flux, and  $L$  is the stellar luminosity. This yields  $\dot{M} = 7 \times 10^{-14} (L/L_\odot) M_\odot/\text{year}$ , or about  $7 \times 10^{-8} M_\odot/\text{year}$  for  $L = 10^6 L_\odot$ . Lucy and Solomon considered this result to be an upper limit to the mass loss; actually it is more nearly a lower limit (627), for in essence it is obtained by accelerating a single line across the entire spectrum, to drive the material (formally) to the speed of light. A better estimate (132) is obtained by replacing  $(4\pi^2 r^2) \sum F(v_l) \Delta v_l$  in equation (15-137) with  $L$ ; then

$$\dot{M} \leq (L/v_\infty c) = 7 \times 10^{-12} (L/L_\odot) (3000/v_\infty) M_\odot/\text{year} \quad (15-138)$$

where  $v_\infty$  is expressed in  $\text{km s}^{-1}$ . For  $L = 10^6 L_\odot$ ,  $v_\infty = 3000 \text{ km s}^{-1}$ ,  $\dot{M} = 7 \times 10^{-6} M_\odot/\text{year}$ , which is the observed value for  $\zeta$  Pup. This result presumes that all the momentum carried by stellar photons is converted into mass-loss in a single scattering; in actuality only some fraction  $\epsilon$  will be so converted, but observations indicate that  $\epsilon$  may be substantial, perhaps as large as 0.5. Thus it appears that adequate mass-loss rates can be obtained, if (and only if) enough lines are included in the calculation of  $g_R$  [see also the discussion in (145)]. A still larger bound on  $\dot{M}$  may be obtained when account is taken of the possibility that some photons may scatter several times in the envelope, passing back and forth to regions on opposite sides of the central star between successive scatterings. Quantitative estimates of the importance of this effect have yet to be made.

#### LINE-DRIVEN WINDS IN Of STARS

The most complete and internally consistent theory for radiatively driven stellar winds at present is that of Castor, Abbott, and Klein (138; 145). The physical parameters employed make this theory applicable to Of stars. The flow is assumed to be time-independent and spherically symmetric; the gas is taken to be a single fluid; and conduction and viscosity are neglected. The gas is assumed to absorb momentum from the radiation field in spectral lines according to a particular force law discussed below.

The single-fluid approximation can be justified (145) by a comparison of the fluid-flow velocity to the drift velocity of the ions absorbing the radiative

momentum (relative to the remainder of the material with which they suffer Coulomb collisions). For a representative electron density of  $n_e \sim 10^{11}$  and temperature  $T \sim 40,000^\circ\text{K}$ , the drift velocity of  $\text{C}^{+3}$  ions is found to be  $0.7 \text{ km s}^{-1}$ , which is clearly negligible in a medium with a flow velocity of  $1000 \text{ km s}^{-1}$ . Also the lines of all chemical species are observed to span the same velocity range, indicating that there is no systematic separation of the material, and supporting the single-fluid picture. To justify the neglect of viscosity, one computes the *Reynolds number*  $\mathcal{R} \equiv (v/l)/\nu$ , where  $l$  is a characteristic length-scale in the flow at density  $\rho$  and velocity  $v$ , for a fluid with kinematic viscosity  $\nu$ . The Reynolds number essentially gives the ratio of inertial to viscous forces (490, 19; 385, 62); at very large values of  $\mathcal{R}$ , the fluid may be regarded as inviscid. In an Of wind the minimum calculated value of  $\mathcal{R}$  is found (145) to be of the order of  $10^{10}$ , which assures that viscosity can be neglected. Finally, because the temperature of the material is not extremely high, the thermal conductivity is low; and further, because the mass flux is large ( $10^8$  times the solar wind), the conductive flux is found (145) to be about eight orders of magnitude smaller than heat transport by bulk motions, and hence it can be ignored.

Let us now consider how to calculate the force exerted by the radiation on the material; the essential point is to account for saturation of the lines, so that the transition between the optically thick and thin limits is handled correctly. This problem has been treated in detail by Castor (137); his analysis leads to a simple result, for which a heuristic argument that contains the essence of the physics will be presented here. Suppose that the absorbing lines are confined to a discrete layer overlying the photosphere. Let the continuum flux incident from below be  $\pi F_c$ , and approximate the momentum absorbed (per unit mass) from the unattenuated continuum, by a line of opacity  $\chi_l$  and width  $\Delta v_D$ , as  $g_{R,l}(0) = (\pi F_c \chi_l \Delta v_D / c\rho)$ . To account for attenuation we note that (as only the net momentum input is needed) re-emissions, which are presumed to be isotropic, can be ignored. In this case the incident flux decays as  $e^{-\tau_l}$  where  $\tau_l$  is the line optical depth computed allowing for Doppler shifts. Thus the average rate of momentum input into the layer is

$$\tau_l \langle g_{R,l} \rangle = g_{R,l}(0) \int_0^{\tau_l} e^{-\tau'} d\tau' \quad (15-139)$$

or  $\langle g_{R,l} \rangle = (\pi F_c \chi_l \Delta v_D / c\rho)(1 - e^{-\tau_l})/\tau_l$  (15-140)

In their work, Castor, Abott, and Klein replace the term  $\tau_l^{-1}(1 - e^{-\tau_l})$  with  $\min(1, \tau_l^{-1})$ , which provides an adequate approximation.

At a given observer's-frame frequency, the effective optical thickness  $\tau_l$  will be limited by (a) the amount of material in the line-layer if the medium is static, in which case

$$\tau_l = \int_R^\infty \chi_l dr \quad (15-141a)$$

where  $R$  is the photospheric radius, or (b) by the velocity gradient (which Doppler-shifts the line from its rest frequency) in a moving medium, in which case

$$\tau_l \approx \chi_l v_{th} (dv/dr)^{-1} \quad (15-141b)$$

where  $v_{th}$  is the thermal velocity of the absorbing atoms. Equation (15-141b) is derived from considerations similar to those employed in development of the Sobolev approximation, and is the planar equivalent of equations (14-61) and (14-62).

It is more convenient to have a depth-scale that is independent of line-strength, so we introduce  $\beta_l \equiv (\chi_l/\sigma)$ , and calculate an equivalent electron optical depth scale  $t \equiv \tau_l/\beta_l$ , which for an expanding atmosphere is defined to be

$$t = \sigma v_{th} (dv/dr)^{-1} \quad (15-142)$$

We shall use equation (15-142) throughout the wind, even though it becomes invalid in the stellar photosphere, for the radiation force on the lines becomes negligible there anyway. The total line force is obtained by summing equation (15-140) over all lines, and can be written

$$g_{R,I} = (\pi F \sigma / c\rho) M(t) = (s_e L / 4\pi c r^2) M(t) \quad (15-143)$$

where  $M(t) \equiv F^{-1} \sum_l F_c(v_l) \Delta v_{D,l} \min(\beta_l, t^{-1})$  (15-144)

is the *radiation-force multiplier*. The calculation of the radiation force is thus reduced to the evaluation of  $M(t)$ , which is a function of only one parameter ( $t$ ).

Castor, Abott, and Klein evaluated  $M(t)$  on the assumption that the line spectrum is the same as that of C III (for which an extensive set of  $f$ -values was available), and by assigning a total abundance of  $\text{C}^{+3}$  relative to hydrogen of  $10^{-3}$  (which is the total abundance of C, N, and O taken together). The occupation numbers were computed using LTE. Although these assumptions are somewhat rough, the results are certainly qualitatively correct. The numerical values of  $M(t)$  are found to be well fitted by the formula  $M(t) = kt^{-\alpha}$ , with  $k \approx \frac{1}{30}$  and  $\alpha = 0.7$ . In more recent work (145), all elements from H through Ni are included, and the coefficients  $k$  and  $\alpha$  are allowed to depend on the relevant physical variables (but these refinements will not be considered further here). Using equations (15-142) and (15-143), and the formula for  $M(t)$ , we find finally

$$g_{R,I} = \left( \frac{s_e L k}{4\pi c r^2} \right) \left( \frac{1}{\sigma v_{th}} \frac{dv}{dr} \right)^\alpha = \frac{C}{r^2} \left( r^2 v \frac{dv}{dr} \right)^\alpha \quad (15-145)$$

where the equation of continuity has been invoked, and the constant  $C$  is

$$C = (s_e L k / 4\pi c) [4\pi / (s_e v_{th} M)]^\alpha \quad (15-146)$$

Using equation (15-145) for the line contribution to the radiation force, the equation of motion [cf. equation (15-133)] becomes

$$\frac{1}{2} \left(1 - \frac{a^2}{v^2}\right) \frac{dv^2}{dr} = \frac{2a^2}{r} - \frac{da^2}{dr} - \frac{G\mathcal{M}(1 - \Gamma_e)}{r^2} + \frac{C}{r^2} \left(r^2 v \frac{dv}{dr}\right)^{\alpha} \quad (15-147)$$

Or, defining the new variables  $w \equiv \frac{1}{2}v^2$  and  $u \equiv -r^{-1}$ , equation (15-147) is equivalent to

$$F(u, w, w') \equiv (1 - \frac{1}{2}a^2w^{-1})w' - h(u) - C(w')^{\alpha} = 0 \quad (15-148)$$

where  $w' \equiv (dw/du)$ , and

$$h(u) \equiv -G\mathcal{M}(1 - \Gamma_e) - 2a^2u^{-1} - (da^2/du) \quad (15-149)$$

Equation (15-147) [or equation (15-148)] has a *singular point* at which solutions terminate, have cusps, or show other discontinuities; this point is *not* the sonic point. At the sonic point, where  $r = a$ , it is easily seen that the lefthand side of equation (15-147) vanishes, and that the righthand side can be made to vanish as well with a suitable choice of  $(dv/dr)$ , which need not be infinite or discontinuous. This difference from standard coronal-wind theory results from the force depending on  $(dv/dr)$  instead of just  $r$  itself. The critical-point analysis is relatively complicated, compared to the theory described in §15-2, because the equation is *nonlinear* in  $(dv/dr)$ . Detailed study (138) of the situation shows that the *locus of singular points* is specified by

$$[\partial F(u, w, w')/\partial w'] = (1 - \frac{1}{2}a^2w^{-1}) - \alpha C(w')^{\alpha-1} = 0 \quad (15-150)$$

But not every point on this locus yields an acceptable solution; if  $w'$  is to be *continuous* the additional condition

$$(\partial F/\partial u) + w'(\partial F/\partial w) = 0 \quad (15-151)$$

must also be satisfied. Equations (15-148), (15-150), and (15-151) determine  $(u, w,$  and  $w')$  if  $C$  is given, or  $(w, w',$  and  $C)$  if  $u$  is given. Analytical expressions can then be obtained for the rate of mass-loss, the velocity law, and the acceleration  $(dv/dr)$ . In the limit  $v \gg a$  these are quite simple:

$$\dot{\mathcal{M}} = \left(\frac{4\pi G\mathcal{M}}{s_e v_{th}}\right) \alpha \left(\frac{1 - \alpha}{1 - \Gamma_e}\right)^{(1-\alpha)/\alpha} (k\Gamma_e)^{(1/\alpha)} \quad (15-152)$$

$$v^2 = [2G\mathcal{M}(1 - \Gamma_e)\alpha/(1 - \alpha)][(1/r_s) - (1/r)] \quad (15-153)$$

and  $(r_c/r_s) = 1 + \{-\frac{1}{2}n + [\frac{1}{4}n^2 + 4 - 2n(n+1)]^{\frac{1}{2}}\}^{-1}$  (15-154)

where  $r_s$  is the sonic radius (essentially equal to  $R$ , the photospheric radius), and  $r_c$  is the critical radius. Equation (15-154) is based on the assumption that  $T \propto r^{-n}$ ; likely values for  $n$  lie between 0 (isothermal) and  $\frac{1}{2}$  (radiative equilibrium), which implies that  $1.5 \lesssim (r_c/r_s) \lesssim 1.74$ .

The stellar model is parameterized by a choice of  $L, \mathcal{M}$ , and  $R$ , and by an assumed relation for  $T(r)$  [or  $a^2(r)$ ]. The mass-loss rate is fixed almost entirely by  $\mathcal{M}$  and  $L$  (via  $\Gamma_e$ ); the characteristic temperature  $T_{eff}$  also enters into  $v_{th}$ . In practice, the model is determined by guessing a value for  $r_c$  from equation (15-154) with  $r_s = R$ ; equation (15-147) is then solved numerically, and the exact relation between radius and optical depth is computed. The value of  $r_c$  is then adjusted until a reasonable photospheric optical depth ( $\approx \frac{2}{3}$ ) is attained at  $r = R$ . Having constructed a dynamical model, one may use the resulting density structure in a spherical model-atmosphere code to adjust the temperature structure in such a way as to satisfy the requirement of radiative equilibrium. The new temperature structure is then employed to reconstruct a new dynamical model, and the process is iterated. In practice the dynamics—and hence the velocity, density structure, and mass-loss rate—is insensitive to the temperature structure, and the iteration process converges rapidly.

Castor, Abbott, and Klein have published (138) a solution for parameters appropriate to an O5 star:  $\mathcal{M} = 60\mathcal{M}_\odot$ ,  $L = 9.7 \times 10^5 L_\odot$ ,  $R = 9.6 \times 10^{11}$  cm =  $13.8R_\odot$ ,  $T_{eff} = 49,300^\circ K$ ,  $\log g = 3.94$ ,  $\Gamma_e = 0.4$ . The resulting mass-loss rate is  $\dot{\mathcal{M}} = 6.6 \times 10^{-6} \mathcal{M}_\odot/\text{year}$ , a value appropriate to a star like ζ Pup. The terminal velocity is  $v_\infty = 1500 \text{ km s}^{-1}$ , so  $\dot{\mathcal{M}} \approx \frac{1}{2}(L/v_\infty c)$ , which shows that about one half of the momentum originally carried by radiation has been transferred to the matter. Furthermore, about one-half of the continuum radiation field is blocked by the lines; this value appears to be in good agreement with observation (304). Standard stellar evolution theory (606) gives main-sequence lifetimes at this mass of about  $3 \times 10^6$  years, which implies a total mass-loss of about  $\frac{1}{3}$  the original mass; it thus appears that the stellar winds of these stars will have very significant effects on their evolution.

The density and velocity structures of the model described above are shown in Figures 15-5 and 15-6; the letters P, S, and C designate the photosphere, sonic point, and critical point respectively. The striking characteristic of the solution is the “core-halo” nature of the density structure: inside the sonic point the model has a nearly hydrostatic density gradient, while outside the critical point,  $\rho \propto r^{-2}$ . The model inside  $r_c$  is essentially planar. The velocity rise outside  $r_s$  is abrupt and, in fact, the predicted gradient is much steeper than those inferred observationally for some Of stars (326; 327); however, these empirical analyses are rather rough, and a much more accurate study is urgently needed. The velocity variation is, of course, fundamental to

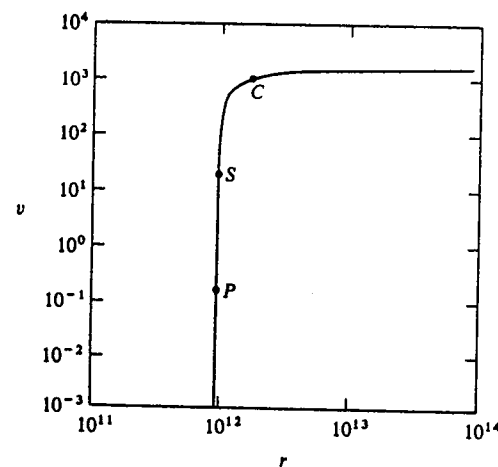


FIGURE 15-5  
Variation of velocity (in  $\text{km s}^{-1}$ ) with radius (in cm) in an Of stellar-wind model. From (138), by permission.

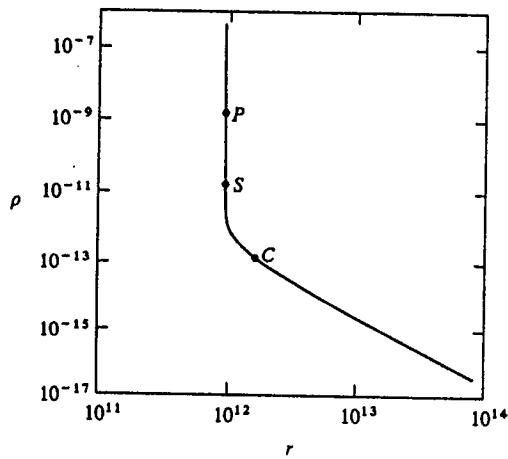


FIGURE 15-6  
Variation of density (in  $\text{gm cm}^{-3}$ ) with radius (in cm) in an Of stellar-wind model. From (138), by permission.

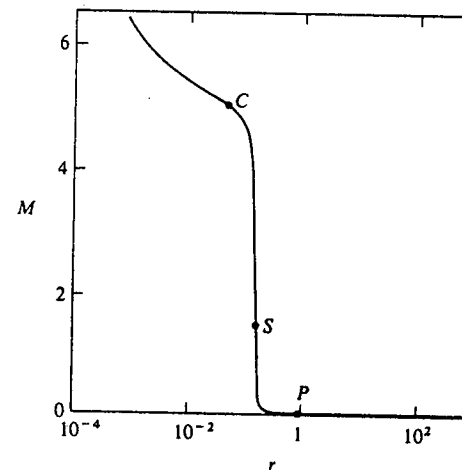


FIGURE 15-7  
Variation of radiation force multiplier  $M$  with continuum optical depth in an Of stellar-wind model. From (138), by permission.

the dynamics, and its empirical determination strongly merits any efforts necessary to yield accurate results.

The variation of the radiation-force multiplier is shown in Figure 15-7. There one sees that in the outer envelope  $M \approx 5$ , which implies that the radiation force on the lines is about twice the force of gravity; adding the acceleration from electron scattering (and subtracting the force of gravity), we see that the material experiences a net outward acceleration of about 1.4 times gravity.

The emergent *relative* flux distribution from the wind model is almost identical to that from a *planar* static model with  $T_{\text{eff}} \approx 50,000^{\circ}\text{K}$ . However, the outer envelope has an electron-scattering optical depth of about 0.16, and this layer (which scatters conservatively and hence does not affect the relative energy distribution) increases somewhat the observed radius of the star (measured interferometrically), and thus reduces the *absolute* flux. A critical discussion (304) of both the visible and ultraviolet data for  $\zeta$  Pup (allowing for interstellar reddening effects and line-blanketing) shows that, if both the observational data and the theoretical models are pushed to the allowable limits, agreement is obtained with the Castor–Abbott–Klein model. Earlier work had suggested the need to consider sphericity effects in an extended atmosphere to fit the flux distribution.

Finally, a calculation of the  $H\alpha$  and  $\text{He II } \lambda 4686$  line profiles from the wind model yields profiles of shape similar to those observed, and with emission